TRIPTYCENE- AND BIPHENYLENE-BASED BIFUNCTIONAL LEWIS ACIDS AS ANION RECEPTORS

A Dissertation

by

CHANG-HONG CHEN

Submitted to the Office of Graduate and Professional Studies of
Texas A&M University
in partial fulfillment of the requirements for the degree of

DOCTOR OF PHILOSOPHY

Chair of Committee,	François P. Gabbaï
Committee Members,	Michael B. Hall
	Oleg V. Ozerov
	Melissa A. Grunlan
Head of Department,	Simon W. North

August 2018

Major Subject: Chemistry

ABSTRACT

The chemistry of main group-based polydentate Lewis acids has drawn considerable attention over the past few decades, owing to application in anion sensing, anion transport, small molecule activation and catalysis. Bidentate Lewis acids featuring the rigid 1,8-naphthalenediyl or *ortho*-phenylene backbones are the most studied examples of such systems. Owing to the short spacing of the two Lewis acidic sites, these derivatives can only chelate monoatomic anions or polyatomic anions amenable to μ(1,1) ligation. Bearing in mind that this limitation could be overcome through modification of the backbone architecture, we have recently become interested in bidentate Lewis acids with an increased separation between the Lewis acidic centers. It occurred to us that triptycene and biphenylene backbones may offer extended separation between Lewis acidic centers, which may facilitate the selective complexation of larger anions.

In this thesis, we report on the chemistry of triptycene- and biphenylene-based diboranes as large-bite bidentate Lewis acids for the μ(1,2) complexation of the cyanide anion as well as hydrazine. The results demonstrate that the biphenylene platform can be used as a support for hybrid ditopic Lewis acids containing both borane and borinic acid moieties. An investigation of this unusual bifunctional Lewis acid reveals that this is well for the complexation of the fluoride anion in aqueous media. Finally, this thesis shows that these platforms can also be incorporated in antimony-based bifunctional derivatives. The most interesting results have been obtained with a triptycene-based distiborane which shows a remarkable affinity for fluoride anions. Altogether, these results indicate that

changes in the nature of the backbone have a defining influence on the binding selectivity of bidentate Lewis acids. These results may also define new directions in the chemistry of these main group compounds with applications in molecular recognition, sensing as well as in the mitigation of toxic chemicals.

DEDICATION

For Mom, Dad and Pei-Shih

ACKNOWLEDGEMENTS

First, I would like to thank my parents who always support me in both of my personal and professional life. It is impossible for me to make this far without their love and encouragement. I also want to thank my wife, Pei-Shih, who dedicates precious efforts to support my Ph.D. career and make our family beloved.

I am deeply thankful to the members of the Gabbaï group. Dr. Baofei Pan, Dr. Kewei Huang, Dr. Boris Vabre, Dr. Daniel Tofan, Dr. Guillaume Bélanger-Chabot, Dr. Sumit Sahu, Dr. Kantapat Chansaenpak, Dr. Haifeng Yang, Dr. Masato Hirai, Dr. James (Stuart) Jones, Dr. Anna Marie Christianson, Ahmed Ali, Mengxi Yang, Elham Tabei, Ying-Hao Lo, Di You, Kevin Jack, Mohammadjavad Karimi and Gyeong-Jin Park. Very special thanks go to Masato and Stuart for their mentorship and guidance during the early years of my Ph.D. I would also like to thank my committee. Dr. Oleg Ozerov, Dr. Michael Hall and Dr. Melissa Grunlan, who provide guidance through my Ph.D. career.

Finally, my greatest thanks go to my research advisor, Prof. François Gabbaï. I am grateful to him for giving me the opportunity to join his research lab and enduring patience, as well as the great efforts he spent on my projects. François is an excellent scientist as well as a great educator, I have learned tremendously from him during this five years.

CONTRIBUTORS AND FUNDING SOURCES

Contributors

This work was supervised by a dissertation committee consisting of Professor François P. Gabbaï (advisor), Professor Oleg V. Ozerov and Prof. Michael B. Hall of the Department of Chemistry and Professor Melissa A. Grunlan of the Department of Biomedical Engineering, Department of Materials Science & Engineering and Department of Chemistry.

The software and computational resources for computational studies were supported by the Laboratory for Molecular Simulation at Texas A&M University.

All other work conducted for dissertation was completed by the student independently.

Funding Sources

This graduate work was supported by the American Chemical Society Petroleum Research Fund for partial support of this research (Grant 56871-ND3), Welch Foundation (Grant A-1423) and Texas A&M University (Arthur E. Martell Chair of Chemistry).

TABLE OF CONTENTS

Page

LIST OF FIGURES

Page

LIST OF TABLES

Page

CHAPTER I

INTRODUCTION TO MAIN-GROUP POLYFUNCTIONAL LEWIS ACIDS

1.1 Molecular recognition by main-group polyfunctional Lewis acids

Owing to their inherent Lewis acidity, three-coordinate organoboron compounds have received increasing attention as powerful anion receptors.[1-4] Although neutral monofunctional boranes are widely known to efficiently capture small anions in organic solvents, available studies indicate that their effectiveness drastically declines in the presence of water. For instance, while tris(9-anthryl)borane forms a stable fluoroborate complex in tetrahydrofuran (THF), the resulting fluoroborate dissociates to the starting triaryl borane and fluoride anion in the presence of water.[5] This observation clearly suggests that the application of neutral monofunctional boranes in anion sensing chemistry is largely limited, especially in aqueous media. One of the successful strategies to resolve this issue is by aligning multiple receptor sites in close proximity to stabilize the guest anion via chelation. A prototypical example of such anion chelators is 1,8-bis(dimethylborane)naphthalene (**1**). This compound, in which the lowest unoccupied molecular orbital (LUMO) consists of large contribution from the vacant p orbitals of the two boron centers. Reaction of **1** hydride, fluoride or hydroxide anions afforded the corresponding anionic μ-complexes in aprotic solvents (Figure 1).[6-7] In our group, we have previously demonstrated that 1,8-bis(boryl)napthalenes **2** and **3** are strong Lewis acids that can overcome the high hydration energy of fluoride in aqueous media.[8-9] Indeed, these diboranes feature higher fluoride binding constants than those of monofunctional borane

analogs and the resulting fluoroborates exhibit higher stability in aqueous media (Figure 2).[3, 10] This view is also supported by the results from the computational studies, in which the bidentate systems display higher fluoride ion affinity (FIA) than the monofunctional boranes.[10]

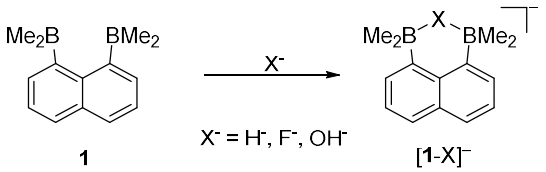

Figure 1. Reaction of 1,8-bis(dimethylboryl)naphthalene with F^-, H^- and OH^-.

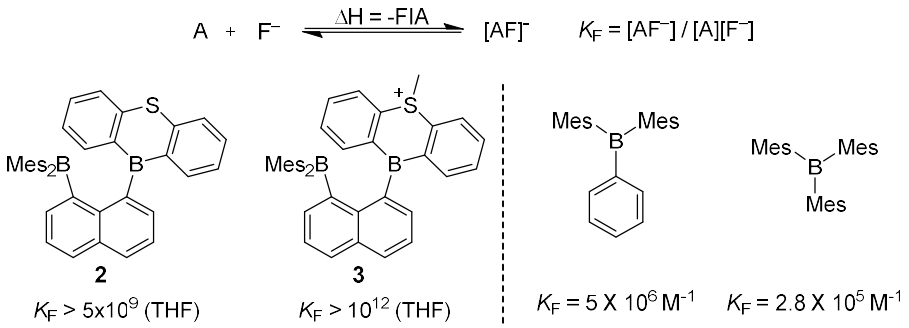

Figure 2. Comparison of the fluoride binding constants (K_F) of diboranes **2** and **3** and common monofunctional boranes.

The scope of backbones supporting multidentate Lewis acids is not limited to naphthalene. Other common platforms, such as *ortho*-phenylene[11-13] and ferrocene[14] have also been utilized to support multiple Lewis acidic functionalities (Figure 3). In addition to the diboranes which may bind anions between two Lewis acidic boron centers, placing boranes and other Lewis acidic main-group moieties in close proximity is an alternate approach to probe the efficacy of bifunctional systems. For example, the borane/mercury,[15-16] borane/tellurium,[17] borane/stibonium,[18-19] borane/phosphonium[20-21]

and borane/sulfonium systems shown in Figure 3[17, 22] all display higher anion affinities than their monofunctional analogues, which clearly illustrates the impact of chelation in these multifunctional Lewis acids.

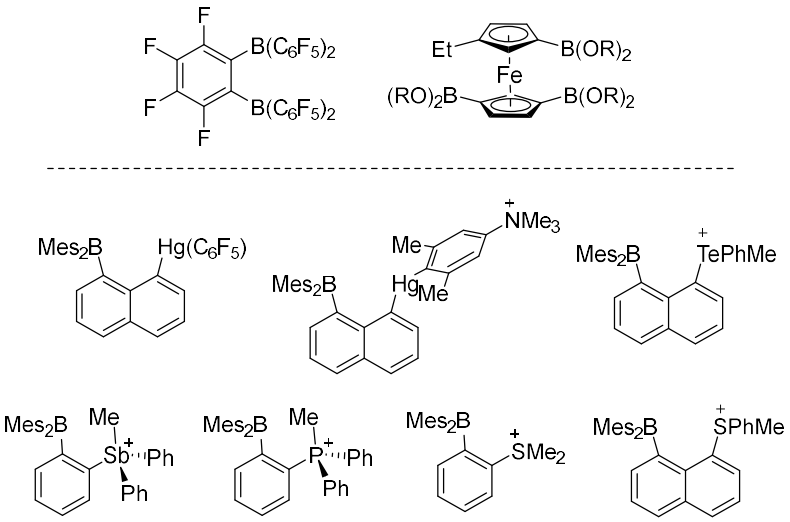

Figure 3. Examples of *ortho*-phenylene and ferrocene-based multidentate boranes (top) and hybrid borane/main-group element bidentate Lewis acids.

Recently, we have become interested in antimony-based Lewis acids due to their superior Lewis acidity toward small anions, such as fluoride, and their remarkable stability in aqueous media.[23-27] Hoping to take advantage of chelation effects, we previously designed a distiborane based on a 9,9-dimethylxanthene scaffold (**4**) (Figure 4).[28] Computational studies show that the preorganized orientation of the two stiborane units of **4** results in a highly electropositive pocket between the two antimony centers. Gratifyingly, compound **4** sequesters fluoride anions in a water/THF (v/v = 0.95/0.05) mixture with a binding constant of 700 M^{-1} to form a stable fluoroantimonate containing an Sb–F–Sb bridging moiety, as confirmed by X-ray analysis. To our knowledge,

compound **4** is the earliest example of a neutral main-group Lewis acid able to capture fluoride anions in water. By comparison, the monofunctional stiborane (**5**) does not bind fluoride anions under the same reaction condition (Figure 4), pointing to the effective chelation of fluoride by **4**. It is noteworthy that compound **4** selectively binds fluoride anions in aqueous media and produced no noticeable response to other common anions, such as $Cl^–$, $Br^–$ $HCO_3^–$, $HSO_4^–$ and $H_2PO_4^–$.

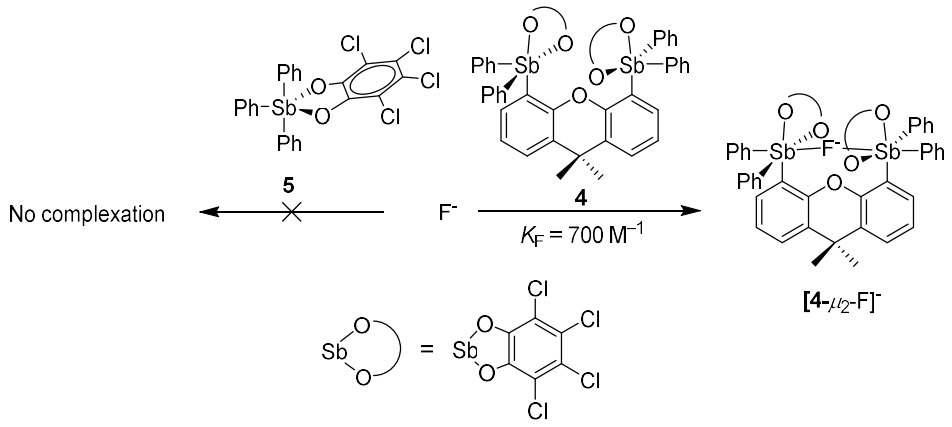

Figure 4. The reaction of distiborane **4** and stiborane **5** with fluoride anion in H_2O/THF (v/v = 0.95/0.05) mixture.

In addition to multifunctional Lewis acids with rigid frameworks, Lewis acidic units can also be incorporate in flexible backbones. For instance, Chen and Jäkle reported the synthesis and the anion affinity of the hexameric bora-cyclophane (**6**) in which each boron atom is connected with 9,9-dimethylfluorene linkers (Figure 5).[29] Because the spacing between each Lewis acidic unit is large, the borane units in **6** can be treated as individual monofunctional boranes. Indeed, compound **6** can be converted into the corresponding hexaborate species ([**6**–X_6]$^{6–}$, X = F, CN) which were confirmed by solution studies. The formation of fluoride or cyanide complexes is accompanied by a

turn-off response of the parent compound's blue fluorescence due to occupation of boron p-orbitals, which breaks the π-conjugation of the system. In addition to cyclic multifunctional Lewis acids, the same group also reported linear borazine oligomers featuring three or four repeating triarylborane functionalities (**7**) (Figure 5) which show response to cyanide anions.[30] In these donor-acceptor-donor-type conjugated borazine oligomers, free borane acceptor sites allow for effective intramolecular charge transfer (ICT) from the diarylamino donor moieties. Complexation of cyanide results in disruption of the aforementioned ICT character and thus dramatically changes both fluorescence and absorbance spectra.

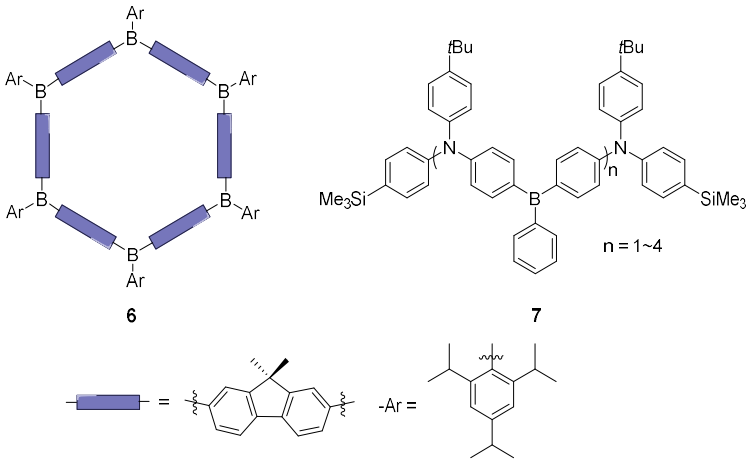

Figure 5. Schematic representations of compound **6** and **7**.

1.2 Anion transport by main-group polyfunctional Lewis acids

Ion transport in biological systems is often achieved by large proteins with multiple binding sites. This process regulates the ions and pH across the membranes. Dysregulations of ion transport, also referred as channelopathies, may lead to severe diseases such as cystic fibrosis (CF).[31] In this regard, synthetic carriers incorporating anion binding sites have received a great deal of attention for their potential in the treatment of such diseases.[32]

Specifically, main-group Lewis acids have been tested as synthetic carriers to transport anions across the membranes owing to their reversible anion binding nature. An early example of such a compound is the silicon-based macrocyclic compound (**8**) reported by Jung and Xia, which was discovered to effectively transport anions across phases in U-tube experiments (Figure 6).[33] In U-tube experiments, a solution of **8** in CH_2Cl_2 was sandwiched between a saturated aqueous solution of tetramethylammonium halide ([TMA][X], X = F, Cl, Br and I) and pure water. The results from these experiments revealed that compound **8** productively transports Cl^- and Br^- across the organic layer to equilibrate Cl^- and Br^- concentrations (Figure 6).

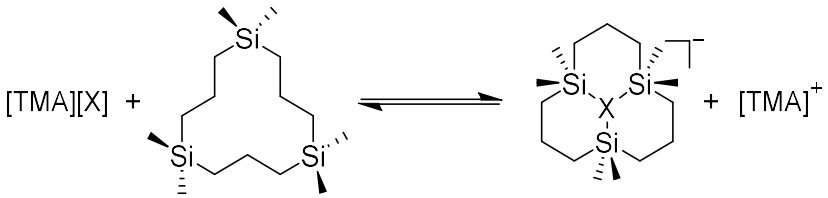

8

Figure 6. Compound **8** and proposed anionic complex formation.

Other successful examples include macrocyclic organomercury compounds.[34-35] By integrating multiple mercury centers with electron-withdrawing substituents in preorganized frameworks, these compounds can be utilized as selective anion carriers in anion electrodes. For example, trimeric perfluoro-*ortho*-phenylenemercury (**9**), which contains three mercury atoms in a planar nine-membered cycle (Figure 7), expresses a high affinity toward various anions (Cl^-, Br^-, I^-, SCN^-, BH_4^-, $[B_{10}H_{10}]^{2-}$, etc.).[36-39] This molecule also effectively transport anions across membranes, a property which may be harnessed to construct anion-selective electrodes.[40-41] Based on these principles, Rothmaier and Simon also described a tetranuclear organomercury macrocycle (**10**), which can be used as the anion carrier in chloride-sensitive electrodes (Figure 7).[42]

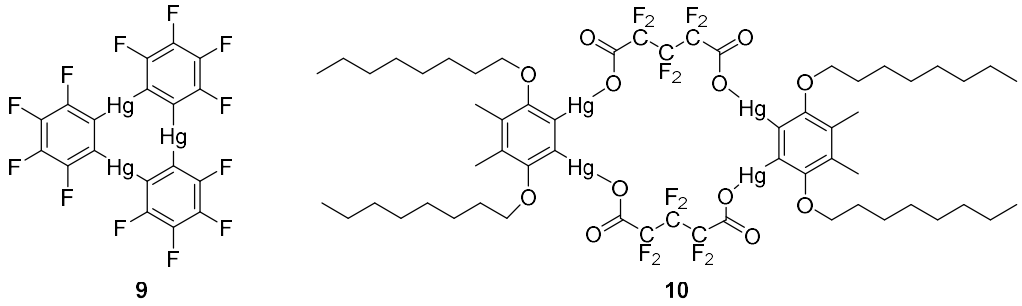

Figure 7. Structure of compounds **9** and **10**, which are effective anion carriers in anion-selective electrodes.

Organotin compounds have also been studied as polyfunctional Lewis acids. In the given studies, methylene-, dimethylene- and *ortho*-phenylene-bridged ditin derivatives preferably chelate fluoride over chloride anions.[43-44] By introducing lipophilic substituents, the stability of these compounds is largely increased while simultaneously retaining their

Lewis acidity. The ability of compound **11** and **12** to bind fluoride ions selectively and reversibly enables the development of robust fluoride-selective electrodes (Figure 8).[45]

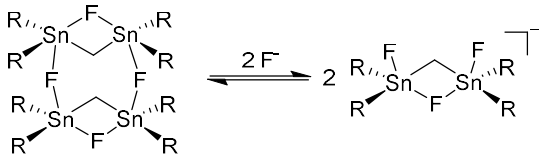

11 (R = n-octyl)
12 (R = n-dodecyl)

Figure 8. Structure of compounds **11** and **12** and the formation of the organostannate complexes with fluoride anion.

Recently, the scope of anion transport by main-group based compounds has been extended to halogen-bond[46-47] and chalcogen-bond[48] donors as described by the Matile group. Halogen[49-51] and chalcogen[52-54] bonds form between anionic or neutral nucleophiles, and the areas of highly localized positive-charged density on the halogen or chalcogen atoms appearing opposite to their covalent bonds. The Lewis acidity of such group 16 and 17 compounds may be enhanced by introducing adjacent Lewis acidic sites on rigid backbones. Recent examples include compound **13**, an iodine-based halogen-bond donor, and compound **14**, which features sulfur atoms as chalcogen-bond donors (Figure 9). Both **13** and **14** transport chloride anions across bilayer membranes in a highly selective manner. While structural evidence has not been observed, theoretical calculations suggest that the two chalcogen-bond donors of compound **14** engage the chloride anion via formation of the S-Cl-S bridge.

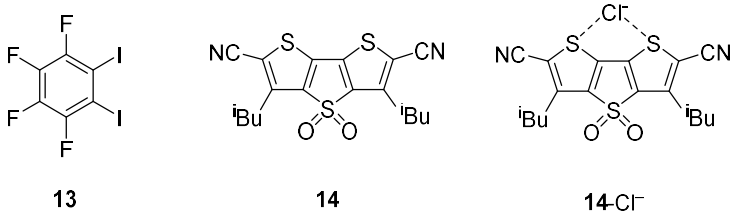

13 14 14-Cl⁻

Figure 9. Chloride transporter compounds **13** and **14** and the computed chloride anion complex of **14**.

1.3 Organocatalysis by main-group polyfunctional Lewis acids

Recently, a great deal of effort has been devoted to the chemistry of Lewis acid catalyzed organic reactions. Examples of such reactions include the hydrogenation of imines, hydrosilylation of carbonyl compounds and reactions featuring anion pairing. The catalysis of these organic transformations relies on the acid-base interaction of the Lewis acidic catalysts and the basic functionalities of the organic substrates. Following initial adduct formation, the activated substrates can further react with their counterparts in the reaction and complete the catalytic cycle by releasing the Lewis acid catalyst.

Some early monofunctional examples of such Lewis acidic catalysts include main-group halides, for example BF_3[55] and SbF_5.[56] Despite their high Lewis acidity and catalytic reactivities, these main-group halides are extremely prone to hydrolysis, a property which significantly limits their applicability in organic synthesis. In the context of developing more robust substitutes for these sensitive main-group halides, alkyl- and aryl-substituted main-group compounds have received considerable attention due to their stability. For example, tris(pentafluorophenyl)borane (BCF), which bears electron-withdrawing pentafluorophenyl groups, features greater stability compared to the boron trihalides while retaining comparable Lewis acidity. Due to its enhanced stability, BCF can catalyze a broader range of organic reactions, such as hydrosilylation and olefin polymerization.[57]

Because bifunctional 1,8-diboryl-naphthalene derivatives display higher anion affinities in sensing chemistry due to the chelation effect, efforts to apply such systems to catalysis have also been considered. For example, a naphthalene-based diborane featuring pentafluorophenyl substituents (**15**) was reported by Berke to catalyze the hydrogenation

reaction of imines.[58] Compound **15** reacts with H_2 in the presence of 2,2,6,6-tetramethylpiperidine to afford the corresponding hydride complex, which has been characterized by X-ray diffraction (XRD). In the solid-state structure of the hydride complex, the hydride anion is chelated by the two boron atoms resulting in a B-H-B bridge. Given the fact that monofunctional BCF does not react with H_2 under the same conditions, the observation of the formation of a B-H-B bridge indicates that the bifunctionality of the molecule enhances its reactivity. Based on this observed reactivity, compound **15** was then tested as a catalyst for hydrogenation reaction of imines (Figure 10). The formation of the corresponding amines was observed under elevated H_2 pressure with excellent yields, pointing to the catalytic competency of diborane **15**.

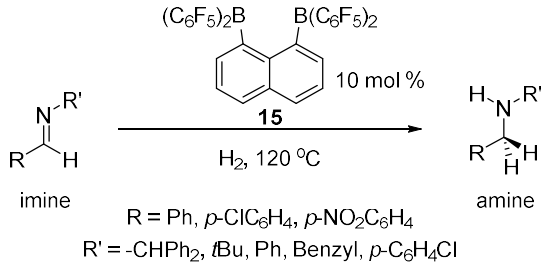

Figure 10. Diborane **15** catalyzes hydrogenation of imines.

In addition to the imine hydrogenation reactions, a Diels-Alder/cyclopropanation reaction catalyzed by a diborane was reported by the Wegner group in 2012.[59] Diborane (**16**) catalyzes the Diels-Alder reaction of oxyfurans and phthalazine, which is followed by a rearrangement to afford the cyclopropanated naphthalene derivatives with a variety of substrates (Figure 11). The domino reaction starts with the formation of a Lewis acid-base adduct between phthalazine and **16**, which was unambiguously confirmed by XRD.[60-61] The observation of the adduct exemplifies the necessity of the suitable size match

between the preorganized polyfunctional Lewis acid and dienes in catalyzing Diels-Alder reactions.

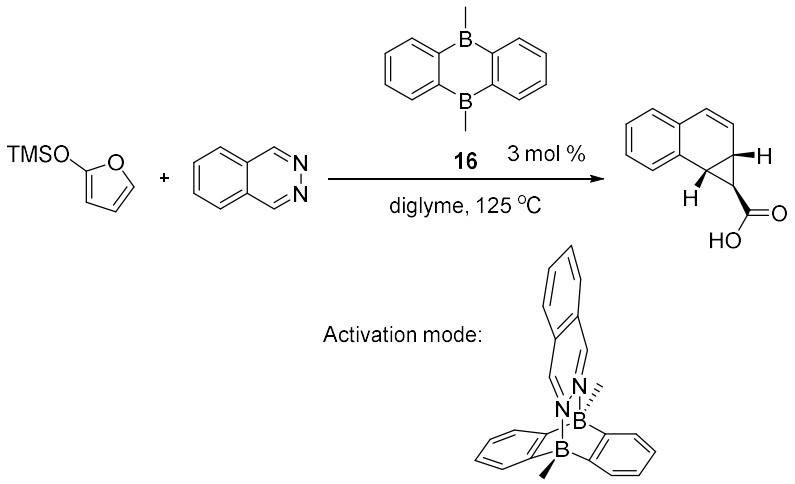

Figure 11. Compound **16** as an effective catalyst for Diels-Alder reaction and the schematic representation of the phthalazine complex formation.

Bidentate Lewis acid catalyst based on group 15 elements have also been investigated. A distibonium cation (**17**) based on an *ortho*-phenylene backbone has been reported as an efficient catalyst for the hydrosilylation of benzaldehyde (Figure 12). Notably, compound **17** catalyzes this reaction at ambient temperature, whereas the monofunctional stibonium cation $[Ph_3SbMe]^+$ exhibited no reactivity under the same conditions. The unique reactivity of **17** supports the double electrophilic activation of the carbonyl functionality of benzaldehyde. This view is further supported by the fact that **17** forms a 1:1 complex with dimethylformamide (DMF), with the carbonyl oxygen atom chelated by two antimony (V) atoms.[62] The stretching frequency observed for the C=O double bond in DMF was lowered from 1675 cm^{-1} in free DMF to 1634 cm^{-1}. These observations strongly suggest that the double activation of benzaldehyde *via* the two stibonium cations of **17** plays a significant role in its activity as a hydrosilylation catalyst.

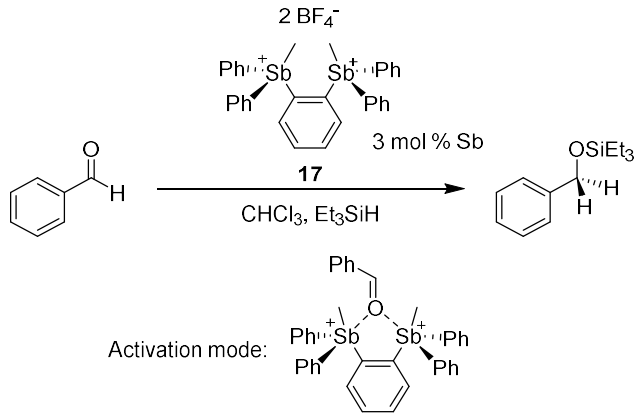

Figure 12. Hydrosilylation of benzaldehyde by **17** and the double electrophilic activation of benzaldehyde.

The double activation of carbonyl substrates by polyfunctional Lewis acidic molecules has also been investigated by the Huber group who has investigated bifunctional halogen-bond donors as catalysts for Diels-Alder reactions[63] and Michael additions[64] (Figure 13A and B). In both reactions, preorganized bidentate halogen-bond donors displayed higher catalytic reactivities than their monofunctional analogues, pointing to the effective double activation of carbonyl groups. By applying the same strategy, the cationic bidentate halogen-bond donor **18** was found to be active in catalyzing reactions necessitating chloride abstraction (Figure 13C), which can also be catalyzed by hydrogen-bond donors.[65-66] The reaction is facilitated *via* formation of the adduct of Lewis acid **18** and the chloride anion from 1-chloroisochroman, followed by the nucleophilic addition of a silyl enol ether. The catalytic activities of different halogen-bond donor derivatives for this particular reaction have been also investigated. The best catalyst among all the derivatives studied was found to be compound **18**, which features a cationic backbone and the *cis* orientation of two halogen-bond donors. This observation

points to the effective chloride anion chelation by the two halogen-bond donating units. The enhancement of the catalytic reactivity was also observed in similar chemistry with chalcogen-bond donors as the Lewis acids. A preorganized bidentate chalcogen-bond donor (**19**) featuring the same cationic backbone is reported by the Huber group.[67] Compound **19** catalyzes the reaction involving chloride abstraction (Figure 13C), albeit with a lower catalytic reactivity compared to **18**.[67]

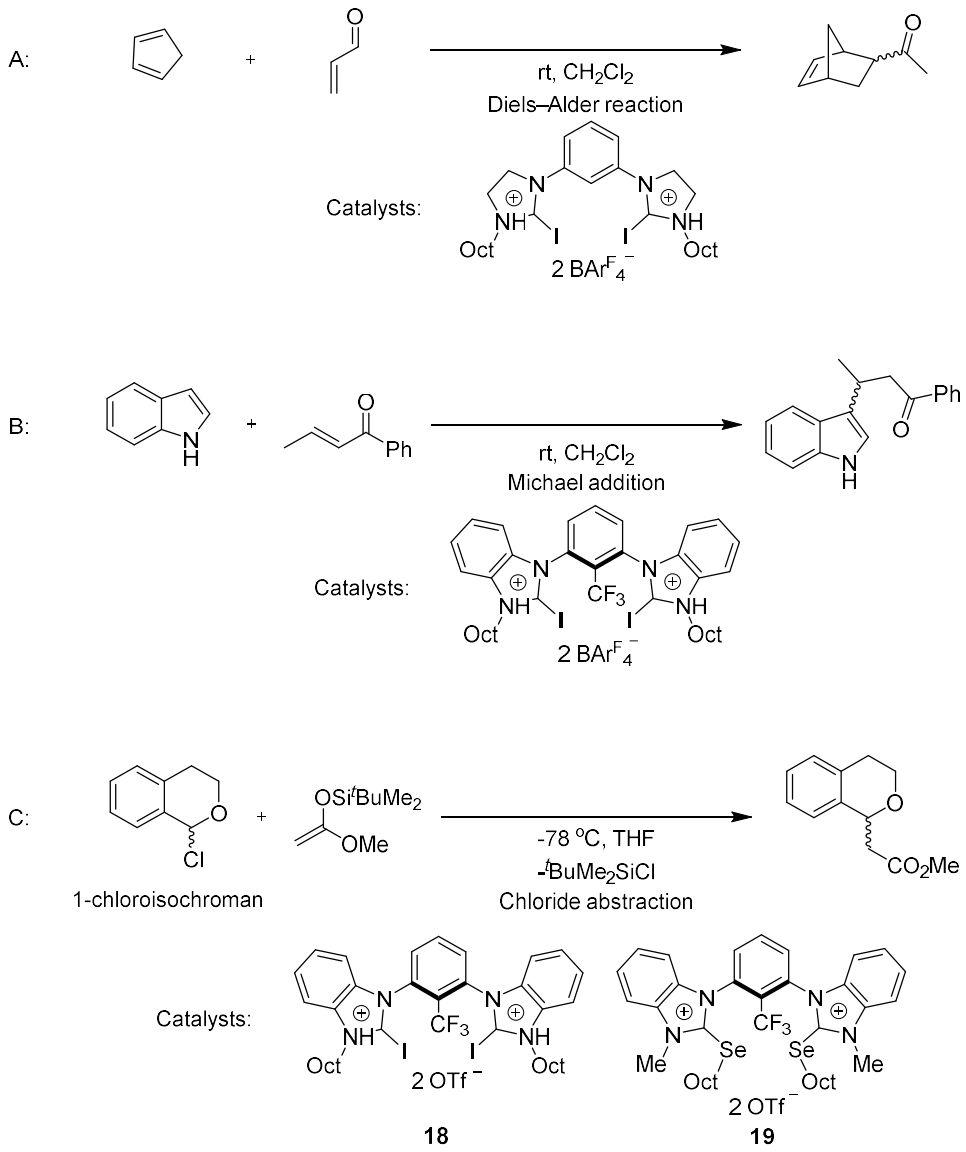

Figure 13. Diels-Alder reaction (A), Michael addition (B) and chloride abstraction reaction (C) catalyzed by polyfunctional halogen-bond donors.

Given the fact that Lewis acidic molecules are known to catalyze transfer hydrogenation reactions, polyfunctional chalcogen-bond donors have also been used in catalyzing such reactions with quinolines as substrates. Bifunctional chalcogen-bond donors (**20** and **21**) presented by the Matile group were found reactive in catalyzing

transfer hydrogenation of quinolines with a rate enhancement factor (k_{cat}/k_{uncat}) of 10^3 for **20** and 10^5 for **21** (Figure 14). The difference in the activities of **20** and **21** was investigated by computational methods, which indicated that **21** features a higher affinity toward the substrates. The results from these computational studies also indicate that these chalcogen-bond donors are directional. They also indicate that the preorganization of the chalcogen-bond donors is required for the double activation of quinolines.

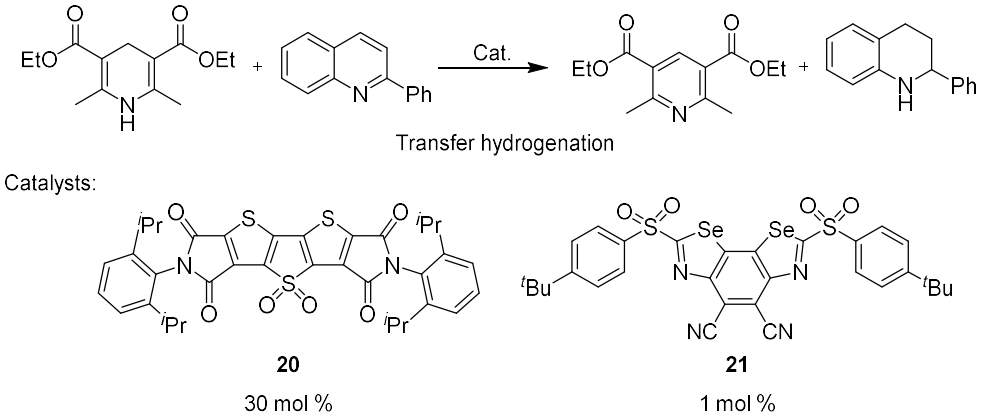

Figure 14. Transfer hydrogenation reaction of quinoline by bidentate chalcogen-bond donors **20** and **21**.

1.4 Small molecule activation by main-group polyfunctional Lewis acids

Owing to their ability to strongly activate organic substrates *via* formation of Lewis acid-base adducts, polyfunctional Lewis acidic molecules have also been investigated for the activation of strong bonds. For example, diborane (**22**) featuring an *ortho*-tetrafluorophenylene linker can be used to initiate the polymerization of isobutene by activating a C-Cl bond homolysis (Figure 15).[12-13] Reaction of diborane **22** with Ph_3C-Cl results in the formation of a stable anionic chloroborate complex and a trityl cation. The solid-state structure of the chloroborate complex was characterized by XRD, which confirmed the formation of the B-Cl-B bridge (Figure 15). The ability of the diborane to chelate a chloride anion is crucial to the activation of the C-Cl bonds, as evidenced by the inability of monofunctional BCF to form a chloroborate complex under the same conditions. Correspondingly, BCF also fails to initiate the polymerization reaction shown in Figure 15.

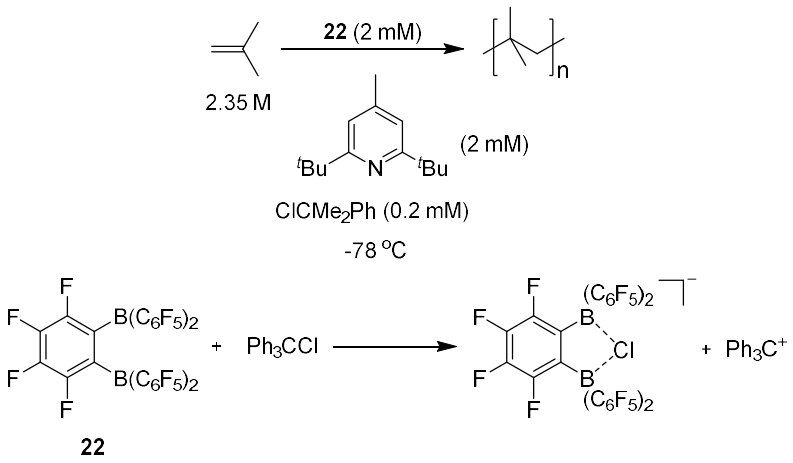

Figure 15. Isobutene polymerization reaction initiated by **22** and the ion pair formation of **22** and Ph_3CCl.

As monofunctional boranes have been demonstrated to be redox active, diboranes have also been investigated for use in electrochemical reactions.[68-70] For example, 9,10-dihydro-9,10-diboraanthracene (**23**) can reversibly accept two electrons to form the corresponding dianion ([**23**]$^{2-}$). Interestingly, [**23**]$^{2-}$ irreversibly cleaves H_2 to afford the symmetrical hydridoborate complex, Li_2[**23**-H_2], under mild reaction conditions (Figure 16). The mechanism of this reaction has been investigated by computational studies, which suggest a concerted, homolytic addition of H_2 across both boron atoms. Similar to other reducing hydridoborate derivatives, Li_2[**23**-H_2] can be used as a reductant for converting element-halide bonds into element-H bonds. For example, reaction of Li_2[**23**-H_2] with Me_3SiCl afforded Me_3SiH quantitatively (Figure 16). These results suggest that the [**23**]$^{2-}$/[**23**-H_2]$^{2-}$ system may be well suited for the reduction of element-halide bonds.

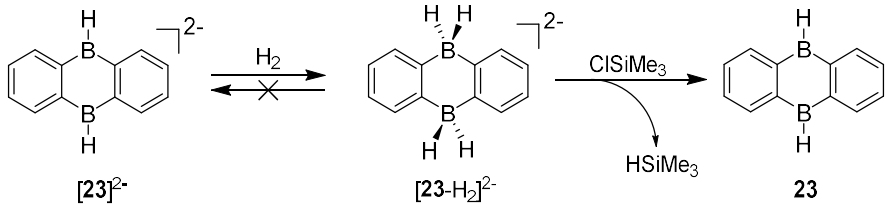

Figure 16. Dihydrogen activation by [**23**]$^{2-}$ and the reaction of [**23**-H_2]$^{2-}$ with Me_3SiCl.

Diboranes can also be used for other small molecule activation reactions, such as the reduction of CO_2 and O_2. An NHC-stabilized boraanthrene (**24**) reported by the Harman group, shows reactivities toward O_2, C_2H_4 and CO_2. The reaction of **24** with O_2, C_2H_4 and CO_2 proceeds *via* formal [4+2] cycloaddition to the central diborabutadiene core to afford the corresponding addition products (Figure 17).[72]

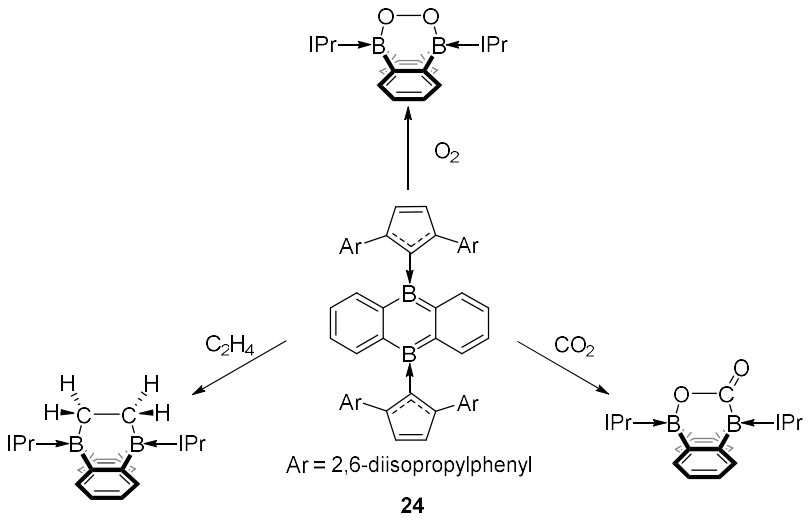

Figure 17. Reaction of **24** with O_2, C_2H_4 and CO_2 and formation of the corresponding cycloaddition products.

In addition to boranes, it has been well documented that phosphorous compounds are strongly Lewis acidic at high oxidation states. The use of Lewis acidic phosphorus (V) compounds in small molecule activation has been investigated by the Stephan group.[73-76] Bifunctional examples of this chemistry includes a naphthalene-based diphosphonium dication (**25**) which activates robust chemical bonds.[77] The reaction of diphosphonium **25** with compounds containing stable element-H bonds, such as B-H, Si-H, C-H and H-H bonds, in the presence of Lewis basic phosphines affords the corresponding hydride complexes (Figure 18). This unusual reactivity of **25** can be rationalized by the accumulated positive charges on the molecule which results in high Lewis acidity.

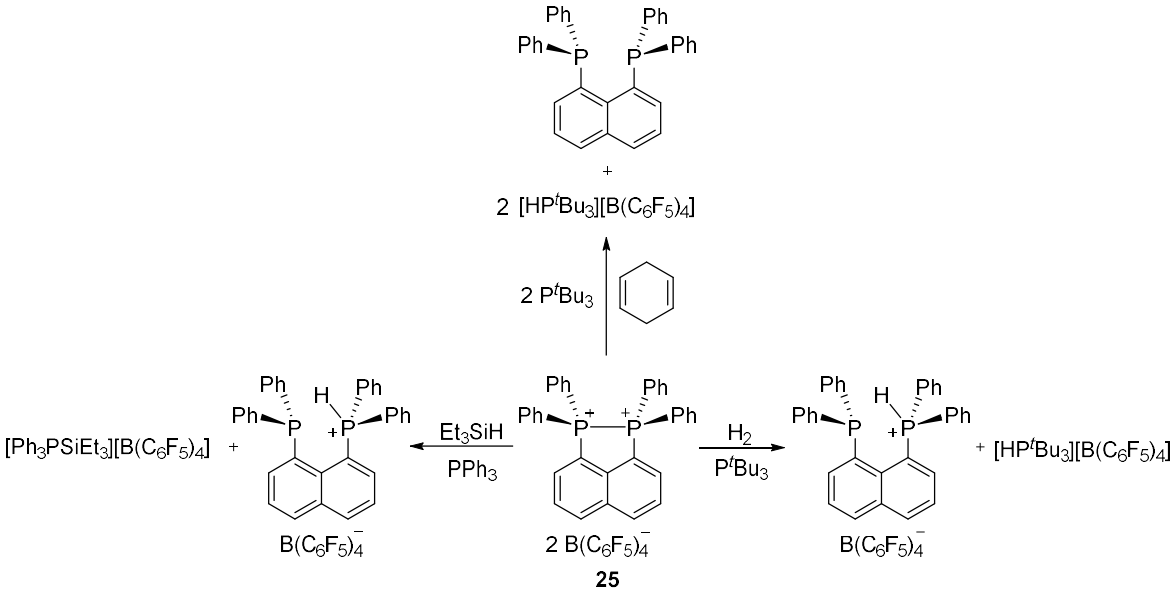

Figure 18. Reaction of **25** with H_2, Et_3SiH and 1,4-cyclohexadiene.

Polyfunctional chalcogen-[78] (**26**) and halogen-bond donors[79] (**27**) have also been reported as effective activators of molecules featuring strong bonds. For example, the benchmark reaction of benzhydryl bromide with **26** or **27** in acetonitrile to afford *N*-benzhydryl acetamide suggests that **26** and **27** effect bromide abstraction *via* the formation of the bromide complex (Figure 19). In these studies, the reactivities of **26** and **27** were compared with that of other halogen- and chalcogen-bond donors derivatives, such as monofunctional analogues and isomers adopting *anti*-orientation with of the two acidic functionalities. The results from the benchmark reaction clearly show that the bidentate chalcogen- and halogen-bond donors featuring *cis*-orientation of the acidic units are the most efficient activators to induce bromide abstraction. Compound **27** also converts the more stable α-methylbenzyl bromide to the corresponding acetamide product, pointing to the broader applicability of this compound.

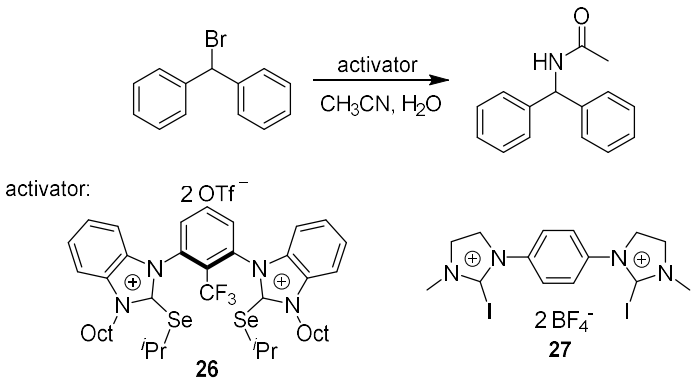

Figure 19. Benchmark reaction of benzhydryl bromide with **26** or **27**.

1.5 Objectives

In the chemistry of bidentate Lewis acids, the backbones used to support the Lewis acidic units play an import role in determining the properties of the polyfunctional assembly. Common backbones, such as naphthalene and *ortho*-phenylene, have been widely used. However, the short spacing offered by these backbones largely restricts the type of guest molecules or anions that these compounds can accommodate. To diversify the set of available bidentate Lewis acids, we have become interested in backbones which afford an extended separation between their individual substituents. In the search of such scaffolds, triptycene and biphenylene came to our attention due to the large separation between the substituents on their C1 and C8 carbons. It occurred to us that the large separation between the Lewis acidic units may facilitate the complexation of larger electron rich species. The objective of this thesis has been to test this possibility by investigating the synthesis and properties of triptycene- and biphenylene-based bifunctional Lewis acids (Figure 20). As secondary objectives, we have also chosen to understand how the nature of the backbone and the identity of the Lewis acids inform the properties of these new derivatives.

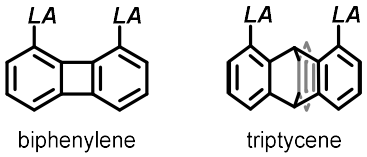

Figure 20. Schematic representation of the bidentate Lewis acids based on biphenylene and triptycene backbones.

CHAPTER II

FLUORIDE ANION COMPLEXATION BY A TRIPTYCENE-BASED DISTIBORANE: TAKING ADVANTAGE OF WEAK BUT OBSERVABLE C-H···F INTERACTION*

2.1 Introduction

The cooperative binding of anions by polytopic hosts is an area of increasing interests with applications in anion sensing,[1-4, 44, 68, 80-87] anion transfer catalysis[65, 88-90] as well as energy research.[91] While organic anion receptors that interact with the anionic guests continue to be at the forefront,[85-87] polyfunctional Lewis acids based on main group elements have emerged as valuable alternative anion receptors,[1-4, 44, 68, 80-84] especially for applications that necessitate the tight coordination of the anions. Examples of such systems include diboranes in which the two boron atoms are connected by an *ortho*-phenylene (**A**)[11-13, 92] or a 1,8-naphthalenediyl (**B**)[7, 9-10, 58] backbone. Given the increasing interest that the chemistry of group 15 Lewis acids is drawing,[18, 20-21, 24, 26-27, 73-74, 93-103] a few groups including ours,[28, 62] have started to investigate bidentate Lewis acids bearing two pnictogen atoms in the +V state[77, 104] as in the case of compound **28**,[76] a bis(phosphonium) derivative which has been used to catalyze hydrodefluorination reactions. Realizing that the separation between the Lewis acidic sites impacts the

---

* Reprinted in part with permission from: "Fluoride anion complexation by a triptycene-based distiborane: Taking advantage of weak but observable C-H···F interaction"; Chen, C.-H.; Gabbaï F. P. *Angew. Chem. Int. Ed.* **2017**, *56*, 1799-1804. Copyright 2017 by John Wiley & Sons, Inc.

chelating properties of these systems, it occurred to us that the use of inherently bulkier pentavalent group 15 centers may benefit from scaffolds that offer a larger separation. With this in mind, we recently targeted compound **4**, a distiborane based on the 4,5-dimethylxanthenediyl backbone.[28] While this neutral Lewis acid proved to be sufficiently potent to chelate fluoride anions in water, we observed that the chelated anion is forced into proximity of the Lewis basic, electron rich oxygen site. Because this situation may reduce the overall anion affinity of the receptor through repulsive forces, we have now decided to focus on a backbone that does not present such a central Lewis basic site. These considerations have led us to consider use of the 1,8-triptycenediyl backbone which has received a great deal of attention in the context of bis(phosphine) chemistry[105-111] but has, to our knowledge, never been used for the construction of bidentate Lewis acids. This backbone was chosen for two reasons. First, its roof-shaped barrelene core projects the Lewis acidic site away from the bridgehead atom lessening the occurrence of possible repulsions. Second, bearing in mind that C-H···F bonds have been previously observed (**C**),[112-115] it occurred to us that the triptycene bridgehead C-H group oriented toward the binding pocket could augment anion binding. In this chapter, we report the first triptycene-based bidentate Lewis acid. We also demonstrate that the bridgehead C-H unit directed toward the anion binding pocket acts as a hydrogen bond donor and thus play a favorable role in the binding of the anionic guest.

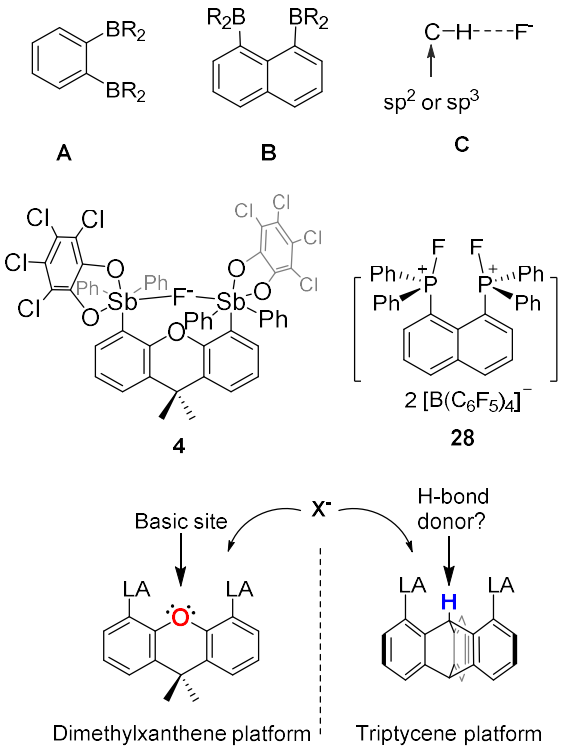

Figure 21. Depiction of the structures of **A**-**C**, and the comparison of dimethylxanthene and triptycene backbones.

2.2 Synthesis and characterization of the distibine and distiborane

To obtain the target bifunctional Lewis acid, we first synthesized 1,8-bis(diphenylstibino)triptycene (**29**) starting from 1,8-dibromotriptycene. While the dilithiation of triptycene has been previously described,[105] we found that **29** could be more reliably obtained by the sequential lithiation of each position followed by metathesis with Ph_2SbCl as described in Figure 22. Compound **29** was obtained as a colorless air-stable solid in an overall 52% yield. This compound has been fully characterized. Its ^1H NMR spectrum shows two distinct methine hydrogen signals at 5.40 and 5.92 ppm. We first attempted to convert this new distibine into a bidentate Lewis acid by methylation of the two antimony centers. Unfortunately, these efforts proved unsuccessful with the only compound identified from this mixture being the monomethylated derivative. By contrast, we found that distibine **29** reacts with *o*-chloranil cleanly in dichloromethane at room temperature to afford the corresponding distiborane **30** (Figure 22). This compound was isolated as an air-stable yellow powder in 83% yield. Its ^1H NMR spectrum resembles that of **29** but shows a measurable displacement of the two distinct methine hydrogen signals that now appear at 5.55 and 5.84 ppm. The three signals arising from the hydrogen atoms attached to the C2 (C9)-, C3 (C10)- and C4 (C11)-positions of the triptycene indicate that the molecule adopts an apparent *C*s symmetry in solution.

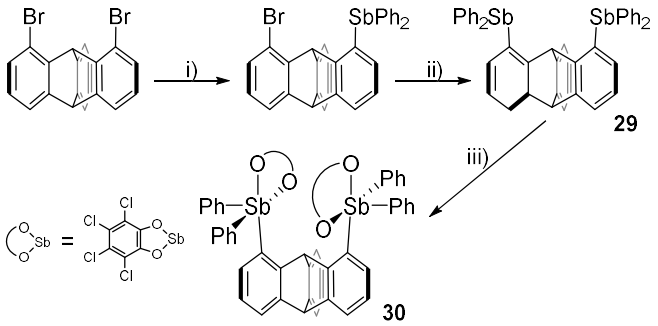

Figure 22. Synthesis of distiborane **30**. i) 1 equiv *n*BuLi, 1 equiv Ph_2SbCl, THF, -78 ºC; b) 2 equiv *t*BuLi, 1 equiv Ph_2SbCl, THF/Et_2O (v/v = 1/1), -78 ºC; iii) *o*-chloranil, CH_2Cl_2, RT.

A further elucidation of the structure of **30** was derived from single crystal X-ray diffraction. Interestingly, we observed that two crystalline forms could be obtained. The first form (form a) was obtained by crystallization from CH_2Cl_2 (Figure 23). The second form (form b) was obtained by layering a solution of **30** in $CHCl_3$ with pentane (Figure 24). Analysis of these two sets of crystals indicates that they differ by the respective orientations of the tetrachlorocatecholates. In form a, the two tetrachlorocathecholate ligands adopt a face-to-face orientation while in form b, these two ligands point in opposite directions. The sharpness and number of signals observed in the ^1H NMR spectrum of **30** indicates that these two forms are in rapid exchange. Despite the difference seen in these two structures, they possess several common features. In both forms, the two antimony atoms adopt a distorted square-pyramidal geometry (average τ-value: 0.32).[116] In both cases, the bases of each square pyramid are facing each other, leading to a Sb-Sb separation of 5.190(1) Å for form a and 5.216(1) Å for form b. These separations are notably larger than that in the dimethylxanthene analogue **4** (4.780(1) Å).[28]

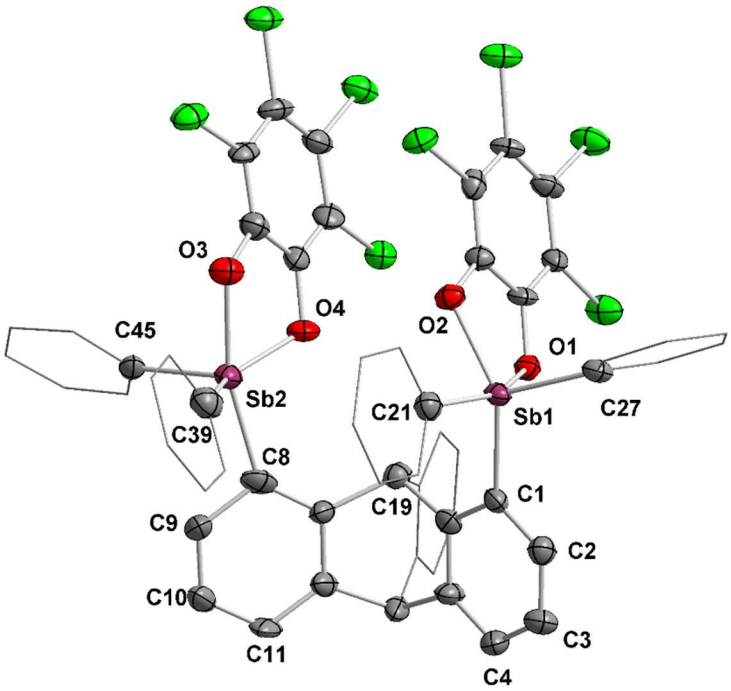

Figure 23. Solid-state structure of the crystallized **30** (form a). Thermal ellipsoids are drawn at the 50% probability level. The hydrogen atoms and the CH_2Cl_2 molecules are omitted for clarity. Selected bond lengths [Å] and angles [deg]: Sb1-O1 2.063(6), Sb1-O2 2.038(6), Sb1-C1 2.144(8), Sb1-C21 2.102(8), Sb1-C27 2.142(9), Sb2-O3 2.028(5), Sb2-O4 2.070(5), Sb2-C8 2.113(7), Sb2-C33 2.085(8), Sb2-C39 2.120(8); O1-Sb1-O2 78.5(2), C1-Sb1-C27 97.4(3), C21-Sb1-C27 110.6(3), C1-Sb1-C21 98.4(3), O3-Sb2-O4 78.1(2), C8-Sb2-C33 110.5(3), C33-Sb2-C39 104.5(3), C8-Sb2-C39 99.7(3).

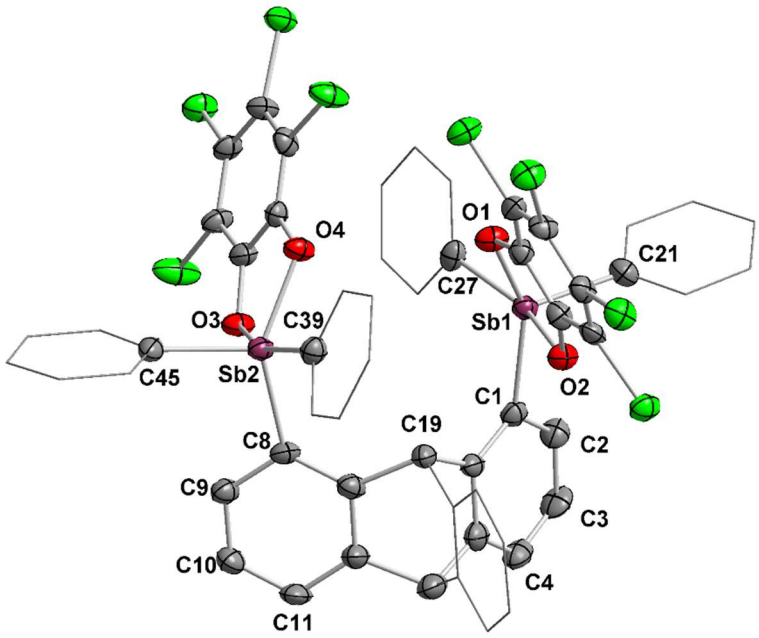

Figure 24. Solid-state structure of the crystallized **30** (form b). Thermal ellipsoids are drawn at the 50% probability level. The hydrogen atoms and the $CHCl_3$ molecules are omitted for clarity. Selected bond lengths [Å] and angles [deg]: Sb1-O1 2.107(5), Sb1-O2 2.008(4), Sb1-C1 2.130(6), Sb1-C21 2.116(7), Sb1-C27 2.129(6), Sb2-O3 2.043(4), Sb2-O4 2.049(4), Sb2-C8 2.132(6), Sb2-C33 2.091(7), Sb2-C39 2.113(6); O1-Sb1-O2 77.9(2), C1-Sb1-C27 99.8(2), C21-Sb1-C27 104.4(3), C1-Sb1-C21 106.1(3), O3-Sb2-O4 78.8(2), C8-Sb2-C33 105.9(3), C33-Sb2-C39 102.2(3), C8-Sb2-C39 100.2(2).

Distiborane **30** was also investigated computationally by density functional theory (DFT) methods (B3LYP functional with the mixed basis set: 6-31g for C,H and O; 6-311g(d) for Cl; 6-31g+(d') for F; cc-pVTZ-pp for Sb) starting from the crystal structure geometry. In both isomers, the lowest unoccupied molecular orbitals (LUMO) bear strong contributions from the Sb-CPh σ* orbitals localized at antimony atoms (Figure 25).

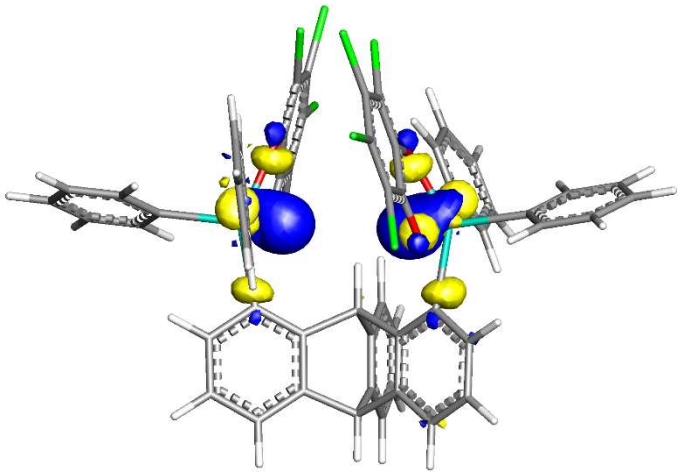

Figure 25. Contour plot of the LUMO of **30** (form b, isovalue = 0.05).

2.3 Synthesis and characterization of the fluoride complex of 30

With this newly designed distiborane in hand, we decided to study its fluoride ion affinity (FIA) both computationally and experimentally. The reaction of compound **30** with [N*n*Bu$_4$][Ph$_3$SiF$_2$] (TBAT, 1 equiv) in CH_2Cl_2 at room temperature, afforded [N*n*Bu$_4$][**30**-μ_2-F] as an air- and moisture-stable white powder (Figure 26).

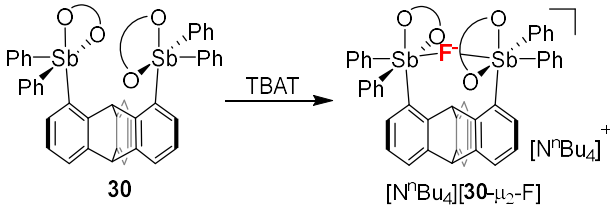

Figure 26. The reaction of distiborane **30** with TBAT in CH_2Cl_2 at room temperature.

The ^{19}F NMR spectrum shows a singlet at -26.4 ppm in CD_2Cl_2. The formation of [N*n*Bu$_4$][**30**-μ_2-F] is always accompanied by the formation of a side product characterized by a ^{19}F NMR resonance at -34.5 ppm. This product is also observed in the ^{1}H NMR spectrum. It is assigned to the isomer of [N*n*Bu$_4$][**30**-μ_2-F] in which the two catecholate ligands are oriented face to face. The formation of [N*n*Bu$_4$][**30**-μ_2-F] obviously affects the ^{1}H NMR resonance of the adjacent methine proton. The resonance of this proton is shifted downfield from 5.84 to 7.36 ppm in CD_2Cl_2. Furthermore, the methine proton resonance shows coupling to the fluorine nucleus ($^1J_{HF}$ = 4.9 Hz) and appears as a doublet partially embedded in the aromatic signals. A similar observation is made in the $^{13}C\{^1H\}$ NMR spectrum which shows that the bridgehead carbon atom is also coupled to the fluorine atom (J_{CF} = 7.4 Hz). These assignments were confirmed by recording the fluorine

decoupled ^{1}H and $^{13}C\{^{1}H\}$ NMR spectra as shown in Figure 27. These spectroscopic features are consistent with the existence of a C-H···F hydrogen bond which, we hypothesize, contributes to the stability of the anionic complex.[112]

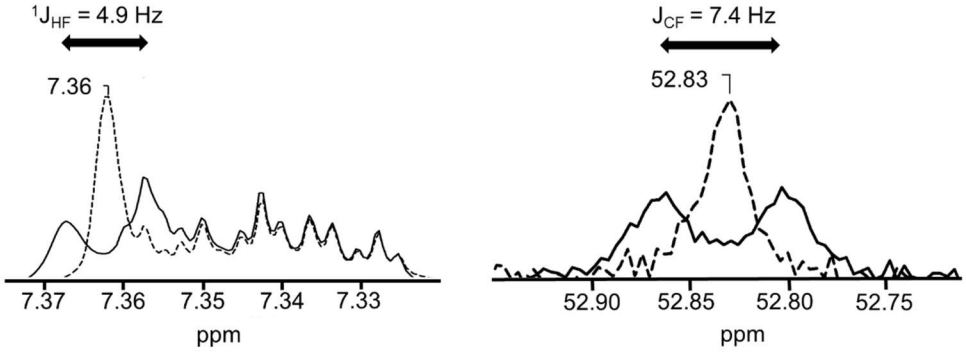

Figure 27. Left: ^{1}H (solid line) and $^{1}H\{^{19}F\}$ (dash line) NMR spectra showing how the resonance of the hydrogen atom attached to the bridgehead carbon atom collapses to a singlet upon ^{19}F decoupling. Right: ^{13}C (solid line) and $^{13}C\{^{19}F/^{1}H\}$ (dash line) spectra revealing the resonance of the bridgehead carbon atom collapses to a singlet upon ^{19}F decoupling.

Crystals of [N*n*Bu$_4$][**30**-μ_2-F] suitable for XRD analysis were obtained by layering a solution of [N*n*Bu$_4$][**30**-μ_2-F] in CH_2Cl_2 with Et_2O. Examination of the structure shows that the tetrachlorocathecolates are directed away from each other (Figure 28). A salient feature of this structure is the formation of a Sb-F-Sb bridge pointing to the tight chelation of the fluoride anion. The metrical parameter of this bridge including the Sb-F bond lengths of 2.251(2) and 2.158(2) Å and the Sb-F-Sb angle of 174.4(1)° are similar to those of other antimony fluoride bridged species such as [**4**-μ_2-F]$^{-}$.[28] It is also interesting to note that the Sb1-Sb2 separation is significantly decreased from an average value of 5.203(2) Å in **30** to 4.404(1) Å in [**30**-μ_2-F]$^{-}$. This notable decrease shows that the molecule is flexible and can very effectively clamp down on the fluoride anion. In agreement with this

view, we note that the dihedral angle α formed by the two antimony-substituted phenylene rings of the triptycene backbone is more acute in [**30**-μ_2-F]$^-$ (α = 108.7°) than in **30** (α = 119.8° for form a and α = 121.4° for form b). Interestingly, the C19-F1 distance (2.915(4) Å) is short; it is in fact comparable to the distance of 2.963 Å computed for the CH_4-F^- adduct,[117] thereby suggesting the existence of a hydrogen bond between the fluorine and the methine hydrogen atom.[112] This distance is comparable to that observed in other systems also proposed to be stabilized by C-H···F contacts.[112-115] The presence of this stabilizing interaction stands in stark contrast to the repulsive O···F interaction of 2.66 Å present in the structure ([N*n*Bu$_4$][**4**-μ_2-F]).[28] Hence, in addition to being sufficiently flexible to support anion chelation, the triptycene backbone is also unique in its ability to provide a C-H group available for hydrogen bonding with the fluoride anion.

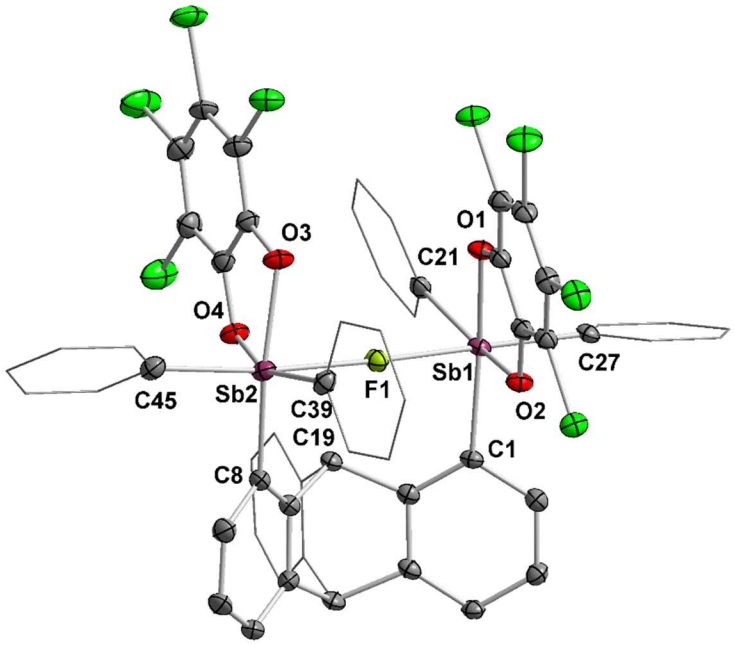

Figure 28. The solid-state structure of the crystallized [**30**-μ_2-F]$^-$. Thermal ellipsoids are drawn at the 50% probability level. The hydrogen atoms, ([N*n*Bu4]$^+$ and CH_2Cl_2 molecules are omitted for clarity. Selected bond lengths [Å] and angles [deg]: Sb1-F1 2.251(2), Sb1-O1 2.060(2), Sb1-O2 2.074(2), Sb1-C1 2.144(3), Sb1-C21 2.141(4), Sb1-C27 2.135(3), Sb2-F1 2.158(2), Sb2-O3 2.069(2), Sb2-O4 2.082(2), Sb2-C33 2.154(3), Sb2-C39 2.141(3), Sb2-C8 2.134(3); Sb1-F1-Sb2 174.4(1), O1-Sb1-C1 164.0(1), C21-Sb1-F1 172.3(1), O2-Sb1-C27 159.6(1), O3-Sb2-C8 164.2(1), C33-Sb2-F1 172.1(1), O4-Sb2-C39 162.2(1).

This view is supported by NBO calculations which identify a weak donor-acceptor lp(F)→σ*(bridgehead C-H) interaction of $E^{(2)}$ = 5.9 kJ/mol, a value that fall in the expected range for a weak hydrogen bond (Figure 29).[118] NBO calculations carried out on [**4**-μ_2-F]$^-$ do not show any donor-acceptor between the fluorine atom and the xanthene-oxygen atom. Instead, these calculations show an oxygen and a fluorine lone pair directed toward one another suggesting an O-F Pauli repulsion (Figure 30).

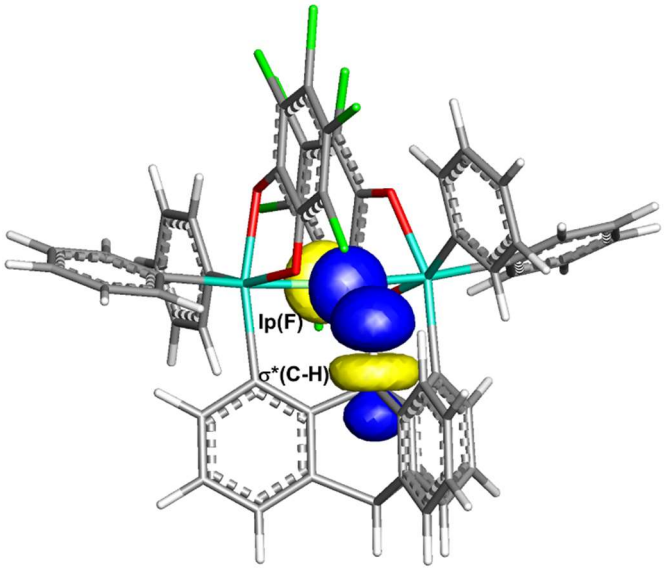

Figure 29. The NBO lp(F)→σ*(bridgehead C-H) donor-acceptor interaction of 5.9 kJ/mol.

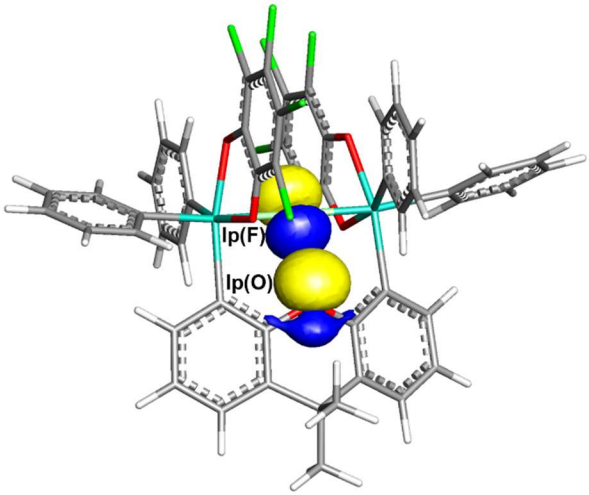

Figure 30. NBO view of lp(F) and lp(O) orbitals in [**4**-μ_2-F]$^-$.

Computational means have also been used to calculate the fluoride ion affinity (FIA)[119-121] of **30**. Following geometry optimization, the enthalpy of **30** and [**30**-μ_2-F]$^-$ was calculated using B3LYP functional with mixed basis set (6-311+g(2d,p) for C, H, O, F and Cl; cc-pVTZ-pp for Sb).[10] Interestingly, the computed FIA of forms a and b of

compound **30** (395 and 387 kJ/mol, respectively) are slightly different, with that of form a being the highest. This difference indicates that form a is somewhat destabilized by the co-facial orientation of the two catecholate units, leading to a larger exotherm. A more important outcome of these calculations is the fact that the FIA of both forms of **30** exceed the value of 365 kJ/mol calculated for **4** at the same level of theory.[28]

2.4 Competition experiment of 30 with main-group based Lewis acids

To corroborate these computational findings with experimental ones, we decided to carry out a competition reaction with **30** and **4**. This experiment was performed with the fluoride adduct of the dimethylxanthene analogue ([N*n*Bu$_4$][**4**-μ_2-F]) and the distiborane **30** in $CHCl_3$ at room temperature (Figure 31). The reaction was monitored by ^{19}F NMR. Incremental addition of distiborane **30** results in fluoride ions transfer from [**4**-μ_2-F]$^-$ to distiborane **30** and the formation of [**30**-μ_2-F]$^-$ quantitatively in 5 minutes (Figure 32). This result unambiguously shows that **30** has a higher fluoride ion affinity than **4**, a factor that we assign to the above noted differences between the triptycene and dimethylxanthene backbone. Compound **30** also abstracts a fluoride anion from the mononuclear fluoroantimonate anion [$Ph_3(O_2C6Cl)SbF$]$^-$[28] but leaves BF_4^-, PF_6^- and $(C_6F_5)_3BF^-$ untouched. In fact, $B(C_6F_5)_3$ cleanly abstracts the fluoride anion from [**30**-μ_2-F]$^-$ showing that fluoride anion binding by **30** is reversible. Finally, we have confirmed that distiborane **30** is capable of capturing fluoride from dilute solutions ([F^-] = 10 ppm) under biphasic solution, with the distiborane dissolved in a CH_2Cl_2 solution. Formation of [**30**-μ_2-F]$^-$, which was observed within 10 minutes of mixing, was confirmed by the disappearance of the methine proton NMR resonance at 5.84 ppm in ^{1}H NMR as well as the appearance of a ^{19}F NMR signal at -26.4 ppm.

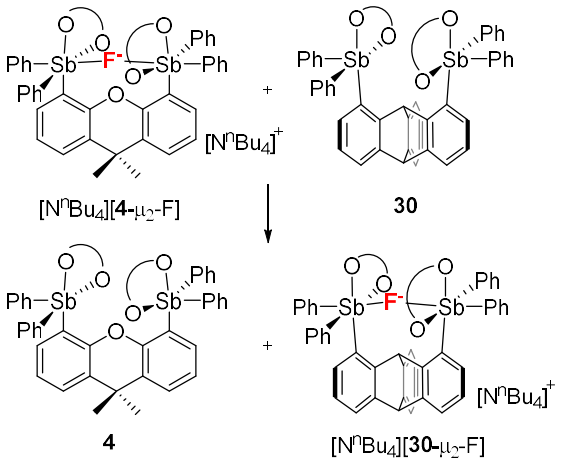

Figure 31. The reaction of distiborane **30** with [N*n*Bu$_4$][**4**-μ$_2$-F] in $CHCl_3$ at rt.

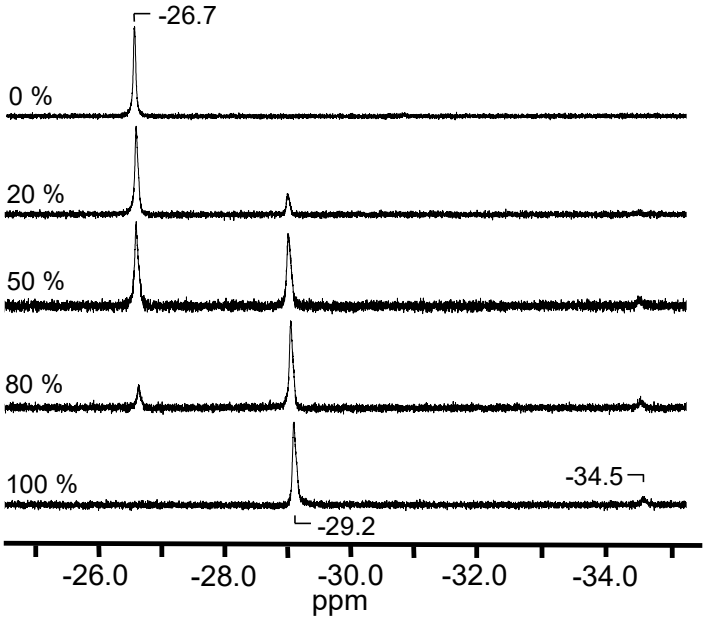

Figure 32. Reaction of [N*n*Bu$_4$][**4**-μ$_2$-F] with **30** in $CDCl_3$ monitoring by ^{19}F NMR at room temperature. The consumption of [**4**-μ$_2$-F]$^-$ and the formation of [**30**-μ$_2$-F]$^-$ were quantified by the peaks at –26.7 and –29.2 ppm respectively (The minor isomer of [**30**-μ$_2$-F]$^-$ is observed at –34.5 ppm).

2.5 Synthesis and characterization of the anthracene-based distiborane

In an exploratory part of this work, we synthesized 1,8-distiboranylanthracene (**31**) in order to investigate its affinity for anions. We first prepared the anthracene-based distibine (**32**) by following the strategy used for compound **29**. Compound **32** can be reliably obtained by the sequential lithiation of each position followed by metathesis with Ph_2SbCl as described in Figure 33.

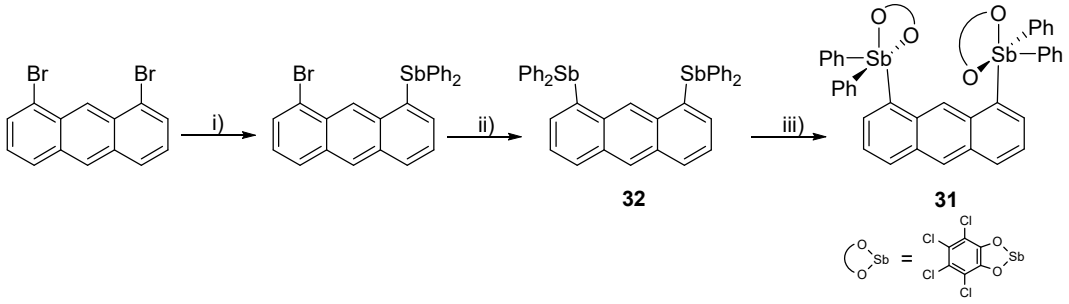

Figure 33. Synthesis of distibine **32** and distiborane **31**. i) 1 equiv *n*BuLi, 1 equiv Ph_2SbCl, THF, -78 °C; b) 2 equiv *t*BuLi, 1 equiv Ph_2SbCl, THF/Et_2O (v/v = 1/1), -78 °C; iii) *o*-chloranil, CH_2Cl_2, RT.

Compound **32** was obtained as a pale-yellow air-stable solid in an overall 62% yield. This compound has been characterized by ^1H NMR spectroscopy. Its ^1H NMR spectrum shows two distinct central anthracene proton signals at 9.03 and 8.47 ppm. By analogy with the oxidation of **29**, we found that distibine **32** reacts with *o*-chloranil cleanly in dichloromethane at room temperature to afford the corresponding distiborane **31** (Figure 33). This compound was isolated as an air-stable yellow powder in 84% yield. Its ^1H NMR spectrum resembles that of **32** but shows a measurable displacement of the two distinct central anthracene proton signals that now appear at 8.77 and 8.75 ppm.

A further elucidation of the structure of **31** was derived from single crystal X-ray diffraction. In the solid-state structure of **31**, the two tetrachlorocathecholate ligands adopt an *anti*-orientation, which is reminiscent of the arrangement found in the structure of **30** (form b). Distiborane **31** features an Sb1-Sb2 separation of 5.3725(7) Å and both antimony atoms adopt a distorted square-pyramidal geometry.

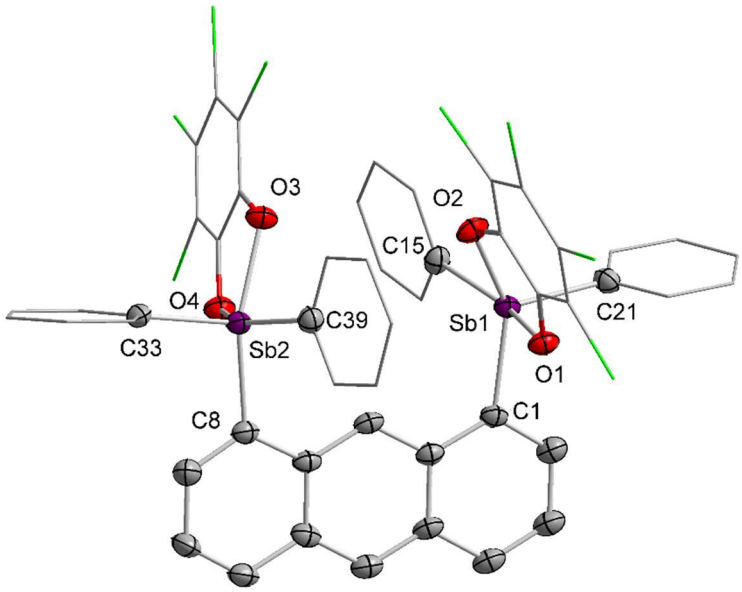

Figure 34. Solid-state structure of the crystallized **31**. Thermal ellipsoids are drawn at the 50% probability level. The hydrogen atoms and the $CHCl_3$ molecules are omitted for clarity. Selected bond lengths [Å] and angles [deg]: Sb1-O1 2.084(3), Sb1-O2 2.029(4), Sb1-C1 2.126(5), Sb1-C15 2.125(5), Sb1-C21 2.094(5), Sb2-O3 2.049(3), Sb2-O4 2.052(4), Sb2-C8 2.145(5), Sb2-C33 2.089(5), Sb2-C39 2.127(5); O1-Sb1-O2 78.2(1), C1-Sb1-C15 101.3(2), C1-Sb1-C21 105.1(32, C15-Sb1-C21 102.8(2), O3-Sb2-O4 78.4(1), C8-Sb2-C33 102.9(2), C33-Sb2-C39 105.0(2), C8-Sb2-C39 100.6(2).

With distiborane **31** at our disposal, we decided to test its ability to bind fluoride anions. We attempted to obtain the fluoride adduct by reacting **31** with TBAT and TASF in CH_2Cl_2. Unfortunately, **31** does not react with these fluoride sources in CH_2Cl_2. We

believe that this lack of reactivity results from the steric crowding of the anion binding pocket by the C-H unit at the 9-position of the anthracene backbone.

2.6 Conclusion

In summary, we describe the first triptycene-based bidentate Lewis acid and show that this compound is ideally suited for the complexation of the small fluoride anion. Our results show that the fluoride anion affinity of such bidentate Lewis acids is readily influenced by the nature of the backbone, which in the case of triptycene projects a C-H bond toward the fluoride anion binding pocket. The latter helps stabilize the fluoride complex by a weak but readily observable C-H···F hydrogen bonding interaction. Meanwhile, we synthesized 1,8-distiboranylanthracene to investigate its fluoride affinity. In the reactions of this anthracene-based distiborane with fluoride sources, no fluoride complexation was observed, pointing to the steric crowding of the anion binding pocket.

2.7 Experimental section

General considerations. Antimony compounds are potentially toxic and should be handled with caution. N,N,N'N'-tetramethylethylenediamine (tmeda) was purchased from Alfa Aesar and distilled with NaOH (10 wt. %) under N_2. Antimony trichloride ($SbCl_3$), triphenyl stibine (Ph_3Sb), *n*-butyllithium (2.2 M in hexane) were purchased from Alfa Aesar and used without further purification. Ph_2SbCl was obtained by directly reacting $SbCl_3$ (1 equiv) with Ph_3Sb (2 equiv) at room temperature under N_2 for 3 days. The resulting solid was used without further purification. Tetrachloro-*o*-benzoquinone (*o*-chloranil) was purchased from Acros Organics and used without further purification. Tetra-*n*-butylammonium difluorotriphenylsilicate (TBAT) was purchased from TCI and used as received. 1,8-Dibromotriptycene was synthesized by the reported procedure.[105] All preparations were carried out under a dry N_2 atmosphere employing either a glovebox or standard Schlenk techniques. Solvents were dried by passing through an alumina column (pentane and CH_2Cl_2) or by refluxing under N_2 over Na/K (Et_2O and THF). All other solvents were ACS reagent grade and used as received. NMR spectra were recorded on an Inova 500 FT NMR (499.41 MHz for ^1H, 469.99 MHz for ^{19}F, 125.63 MHz for ^{13}C) spectrometer or a Varian NMRS 500RM NMR spectrometer (499.69 MHz for ^1H, 469.97 MHz for ^{19}F, 125.66 MHz for ^{13}C) at room temperature. Chemical shifts are given in ppm and are referenced to residual ^1H, ^{13}C solvent signals and external $BF_3 \cdot Et_2O$ (-153.0 ppm) for ^{19}F NMR. Elemental analyses were performed by Atlantic Microlab (Norcross, GA).

Computational details. Density functional theory (DFT) structural optimizations were done with the Gaussian 09 program. In all cases, the structures were optimized using

the B3LYP functional and the following mixed basis set: Sb, cc-pVTZ-PP; F, 6-31g(d'); C/O/H, 6-31g; Cl, 6-311g(d). For all optimized structures, frequency calculations were carried out to confirm the absence of imaginary frequencies. The molecular orbitals were visualized and plotted using the Jimp2 program.[122] The enthalpy of each compound was derived from a single point energy calculation using the B3LYP functional with mixed basis set (6-311+g(2d,p) for C, H, O, F and Cl; cc-pVTZ-pp for Sb[123-124]) and the application of the relevant thermal correction terms. The fluoride ion affinity was calculated by following a procedure published earlier.[121] The NBO analysis was performed using the NBO 5.9 program. The energy of the C-H···F interaction was derived from the second order perturbation energy associated to the donor-acceptor interaction shown in Figure 29.

Crystallographic details. The crystallographic measurements were performed at 110(2) K using a Bruker APEX-II CCD area detector diffractometer, with a graphite-monochromated Mo-Kα radiation (λ = 0.71073 Å). A specimen of suitable size and quality was selected and mounted onto a nylon loop. The semi-empirical method SADABS was applied for absorption correction. The structure was solved by direct methods, which successfully located most of the non-hydrogen atoms. Subsequent refinement on F^2 using the SHELXTL/PC package (version 6.1) and Olex^2 allowed location of the remaining non-hydrogen atoms. All H-atoms were geometrically placed and refined using a standard riding model.

Table 1. Crystal data, data collection, and structure refinement for **30**.

Crystal data	Form a	Form b
Empirical formula	$C_{57.5}H_{34.42}Cl_{11}O_4Sb_2$	$C_{114}H_{65.05}Cl_{22}O_8Sb_4$
Formula weight	1422.71	2829.61
Temperature	110 K	110 K
Wavelength	0.71073 Å	0.71073 Å
Crystal system	Monoclinic	Triclinic
Space group	P 1 21/c 1	P-1
Unit cell dimensions	a = 13.2942(8) Å b = 25.9095(14) Å c = 17.0197(9) Å α= 90° β= 112.731(3)° γ = 90°	a = 12.1841(17) Å, b = 12.8836(18) Å c = 18.583(3) Å α= 84.0664(18)° β= 71.2403(16)° γ = 75.8626(18)°
Volume	5407.0(5) $Å^3$	2677.4(6) $Å^3$
Z	4	1
Density (calculated)	1.748 Mg/m^3	1.755 Mg/m^3
Absorption coefficient	1.591 mm^{-1}	1.606 mm^{-1}
F(000)	2802	1391
Crystal size	0.23 x 0.15 x 0.09 mm^3	0.17 x 0.09 x 0.04 mm^3
Theta range for data collection	1.517 to 26.362°.	1.825 to 26.566°.
Index ranges	-16<=h<=16, -32<=k<=32, -21<=l<=21	-15<=h<=15, -16<=k<=16, -23<=l<=23
Reflections collected	96960	100967
Independent reflections	10983 [R(int) = 0.1488]	11093 [R(int) = 0.1290]
Completeness to theta = 25.242°	100.00%	99.90%
Absorption correction	Semi-empirical from equivalents	Semi-empirical from equivalents
Max. and min. transmission	0.7454 and 0.6451	0.7454 and 0.6783
Refinement method	Full-matrix least-squares on F^2	Full-matrix least-squares on F^2
Data / restraints / parameters	10983 / 0 / 704	11093 / 1 / 671
Goodness-of-fit on F^2	1.046	1.09
Final R indices [I>2sigma(I)]	R1 = 0.0579, wR2 = 0.1382	R1 = 0.0567, wR2 = 0.1318
R indices (all data)	R1 = 0.1215, wR2 = 0.1843	R1 = 0.0940, wR2 = 0.1516
Largest diff. peak and hole	1.753 and -1.366 $e.Å^{-3}$	3.149 and -2.333 $e.Å^{-3}$

Table 2. Crystal data, data collection, and structure refinement for [N*n*Bu$_4$][**30**-μ_2-F].

Empirical formula	$C_{148}H_{144}Cl_{24}F_2N_2O_8Sb_4$
Formula weight	3454.44
Temperature	110 K
Wavelength	0.71073 Å
Crystal system	Triclinic
Space group	P-1
Unit cell dimensions	a = 12.5549(10) Å b = 15.9435(13) Å c = 19.8417(16) Å α = 83.210(5)°. β = 75.582(4)°. γ = 88.400(5)°.
Volume	3819.6(5) Å^3
Z	1
Density (calculated)	1.502 Mg/m^3
Absorption coefficient	1.177 mm^{-1}
F(000)	1740
Crystal size	0.5 x 0.45 x 0.35 mm^3
Theta range for data collection	1.067 to 27.406°.
Index ranges	-16<=h<=16, -20<=k<=20, -25<=l<=25
Reflections collected	266130
Independent reflections	17281 [R(int) = 0.0507]
Completeness to theta = 25.242°	100.00%
Absorption correction	Semi-empirical from equivalents
Max. and min. transmission	0.7455 and 0.6608
Refinement method	Full-matrix least-squares on F^2
Data / restraints / parameters	17281 / 3 / 851
Goodness-of-fit on F^2	1.111
Final R indices [I>2sigma(I)]	R1 = 0.0384, wR2 = 0.1069
R indices (all data)	R1 = 0.0494, wR2 = 0.1259
Largest diff. peak and hole	2.781 and -1.713 e.Å^{-3}

Synthesis of 29. *n*BuLi (2.2M in hexane, 0.88ml, 1 equiv) was slowly added to a cold solution (-78 ºC) of 1,8-dibromotriptycene (800 mg, 1.94 mmol) and tetramethylethylenediamine (TMEDA, 0.75 ml, 2.5 equiv) in dry THF (10 mL). After 60 min of stirring at -78 ºC, a solution of Ph_2SbCl (610mg, 1 equiv) in THF (5 mL) was slowly (10 min) transferred into the reaction flask using a cannula. The resulting pale-yellow solution was kept at low temperature for 2 h and then stirred for an additional 12 h at room temperature. The solution was then treated with a drop (50 μL) of saturated NH_4Cl(aq) and the solvent was removed under vacuum. The resulting white solid was then dissolved in CH_2Cl_2 (15 mL). The resulting solution was filtered and brought to dryness under vacuum. The resulting solid, identified as 1-bromo-8-diphenylantimony-triptycene (81 %), was washed with MeOH (20 mL) and used in the next step without further purification. Crude 1-bromo-8-diphenylantimony-triptycene (300 mg, 0.49 mmol) was dissolved in a dry THF/Et_2O (15 mL/15 mL) at low temperature (-78 ºC) and treated with *t*BuLi (1.5M in pentane, 0.66 ml, 2 equiv) using a syringe. The solution was stirred for 1.5 h at low temperature and an additional 12 h at room temperature. The solution was then treated with a drop (50 μL) of saturated NH_4Cl(aq) and the solvent was removed under vacuum. The resulting solid was purified by chromatography (hexanes/CH_2Cl_2 = 2/1) under ambient conditions to afford **29** in 64% yield. ^{1}H NMR (499.41 MHz, $CDCl_3$): δ 7.38-7.35 (m, 12 H, Sb*Ph*), 7.34- 7.31 (m, 3 H, triptycene-C*H*), 7.30-7.28 (m, 4 H, Sb*Ph*), 7.21 (t, 4 H, $^3J_{H-H}$ = 7.3 Hz, Sb*Ph*), 6.91 (pseudo t, 1 H, $^3J_{H-H}$ = 7.3 Hz, triptycene-C*H*), 6.87 (pseudo t, 2 H, $^3J_{H-H}$ = 7.3 Hz, triptycene-C*H*), 6.77 (dd, 2 H, $^3J_{H-H}$ = 7.8 Hz, $^4J_{H-H}$ = 1.0 Hz, triptycene-C*H*), 6.68 (pseudo t, 1 H, $^3J_{H-H}$ = 7.3 Hz, triptycene-C*H*) 6.10 (d, 1 H,

$^{3}J_{H\text{-}H}$ = 7.3 Hz, triptycene-C*H*), 5.92 (s, 1 H, triptycene-C*H*), 5.40 (s, 1 H, triptycene-C*H*). $^{13}C\{^{1}H\}$ NMR (125.63 MHz, $CDCl_3$): δ 151.03, 145.13, 144.77, 143.78, 137.69, 137.67, 136.69, 136.59, 133.83, 132.20, 128.88, 128.85, 128.57,128.48, 125.76, 124.90, 124.60, 124.41,124.20, 122.98, 57.47, 54.83. m.p. 150 °C. Elemental analysis calculated (%) for $C_{44}H_{32}Sb_2$: C, 65.71; H, 4.01; found C, 65.32; H, 4.32.

Synthesis of 30. A solution of *o*-chloranil (92 mg, 0.38 mmol, 2 equiv) in CH_2Cl_2 (3 mL) was slowly transferred via cannula into a flask containing a solution of **30** (150 mg, 0.19 mmol, 1 equiv) in CH_2Cl_2 (5 mL) under N_2 at room temperature. The oxidation of the distibine was observed by the disappearing of the bright red color of *o*-chloranil. After stirring for 2 h at room temperature, the solvent was removed under vacuum. The resulting yellow solid was washed by pentane (20 mL) twice to afford **30** as a yellow solid in 83 % yield. ^{1}H NMR (499.41 MHz, $CDCl_3$): δ 7.60 (d, 2 H, $^{3}J_{H\text{-}H}$ = 7.3 Hz, triptycene-C*H*), 7.46-7.42 (m, 10 H, Sb*Ph*), 7.36 (d, 1 H, $^{3}J_{H\text{-}H}$ = 7.3 Hz, triptycene-C*H*), 7.25-7.19 (m, 10 H, Sb*Ph*), 7.07 (pseudo t, 2 H, $^{3}J_{H\text{-}H}$ = 7.3 Hz, triptycene-C*H*), 7.02 (pseudo t, 1 H, $^{3}J_{H\text{-}H}$ = 7.3 Hz, triptycene-C*H*), 6.89 (m, 3 H, triptycene-C*H*), 6.17 (d, 1 H, $^{3}J_{H\text{-}H}$ = 7.3 Hz, triptycene-C*H*), 5.84 (s, 1 H, triptycene-C*H*), 5.55 (s, 1 H, triptycene-C*H*). $^{13}C\{^{1}H\}$ NMR (125.63 MHz, $CDCl_3$): δ 148.44, 147.60, 144.35, 143.09, 142.14, 134.78, 134.64, 133.82, 131.83, 131.80, 131.16, 130.02, 129.97, 129.39, 127.22, 126.73, 126.29, 125.46, 125.42, 122.78, 120.82, 116.93, 57.75,55.09. m.p. 252 °C (dec). Elemental analysis calculated (%) for $C_{56}H_{32}Cl_8O_4Sb_2 \cdot 1.5\ CH_2Cl_2$: C, 48.74; H, 2.47; found: C, 48.71; H, 2.34.

Synthesis of [N*n*Bu$_4$][30-μ$_2$-F]. A solution of **30** (120 mg, 0.09 mmol) in CH_2Cl_2 (10 mL) was slowly added a solution of TBAT (48 mg, 1 equiv) in CH_2Cl_2 (5 mL). After

stirring for 2 h at room temperature, the solvent was removed under vacuum. The resulting solid was washed by Et_2O (10 mL) twice to afford [N*n*Bu$_4$][**30**-μ_2-F] as a white powder in 90 % yield. Single crystal of [N*n*Bu$_4$][**30**-μ_2-F] was obtained by slow diffusion of Et_2O into a CH_2Cl_2 solution of [N*n*Bu$_4$][**30**-μ_2-F] at room temperature. ^{1}H NMR (499.41 MHz, CD_2Cl_2): δ 7.79 (d, 2 H, ^{3}J = 7.1 Hz), 7.58 (dd, 1 H, ^{3}J = 6.9 Hz, 4J = 1.5 Hz), 7.51-7.48 (m, 3 H), 7.45-7.42 (m, 1 H), 7.40 (dd, 1 H, ^{3}J = 7.3 Hz, ^{4}J = 0.7 Hz), 7.37-7.33 (m, 3 H, triptycene-C*H*), 7.23-7.20 (m, 2 H), 7.16-6.93 (m, 16 H), 6.75 (t, 1 H, ^{3}J = 7.3, triptycene-C*H*), 6.44 (dd, 1 H, ^{3}J = 7.6 Hz, ^{4}J = 1.0 Hz, triptycene-C*H*), 5.56 (s, 1 H, riptycene-C*H*), 2.87 (m, 8 H, N-C*H*$_2$-), 1.47 (m, 8 H, -C*H*$_2$-), 1.31 (m, 8 H, -C*H*$_2$-), 0.97 (t, 12 H, ^{3}J = 7.3 Hz, -C*H*$_3$). ^{13}C{^{1}H} NMR (125.63 MHz, CD_2Cl_2): δ 148.45, 147.36, 145.79, 144.73, 134.94, 134.80, 134.67, 134.09, 133.89, 133.66, 133.42, 131.81, 131.68, 129.38, 129.34, 129.26, 129.24, 128.96, 128.81, 128.78, 128.46, 128.36, 128.20, 128.08, 128.01, 125.87, 125.72, 125.46, 125.41, 125.34, 125.11, 125.09, 118.53, 118.40, 118.20, 118.01, 116.49, 116.09, 59.54 (N-*C*H$_2$), 55.29 (s, triptycene-*C*H), 52.85 (d, J_{CF} = 7.4 Hz, triptycene-*C*H) 24.34 (TBA-*C*H$_2$), 20.21 (TBA-*C*H$_2$), 13.88 (TBA-*C*H$_3$). ^{19}F NMR (469.99 MHz, CD_2Cl_2): δ -26.4 (major product, 85 % by integration), -34.5 (minor product, 15 %) ppm. m.p. 240 °C.

Reactivity of 30 toward BF_4^- and PF_6^-: [N*n*Et$_4$][BF_4] (2.3 mg, 10.5 μmol) was dissolved in CH_2Cl_2 (0.4 ml) and combined with distiborane **30** (13.6 mg, 10.5 μmol) in an NMR tube. After 30 min of sonication at room temperature, the ^{19}F NMR spectrum of the mixture showed that no reaction had occurred. To the same tube, one equivalent of

[N*n*Bu$_4$][PF$_6$] (4.1 mg, 10.5 μmol) was added. Again, no reaction was observed after 30 min of sonication.

Reactivity of 30 with [N*n*Bu$_4$][Ph$_3$(O$_2$C$_6$Cl$_4$)SbF]: [N*n*Bu$_4$][Ph$_3$(O$_2$C$_6$Cl$_4$)SbF] (6.6 mg, 7.7 μmol) was dissolved in CDCl$_3$ (0.2 ml) and combined in two equal increments with a solution of distiborane **30** (10 mg, 7.7 μmol) in CDCl$_3$ (0.2 ml). ^{19}F NMR monitoring of the reaction confirmed the formation of [**30**-μ$_2$-F]$^-$ (^{19}F NMR δ = -29 ppm) as well as the consumption of the [Ph$_3$(O$_2$C$_6$Cl$_4$)SbF]$^-$ (^{19}F NMR δ = -84 ppm) ().

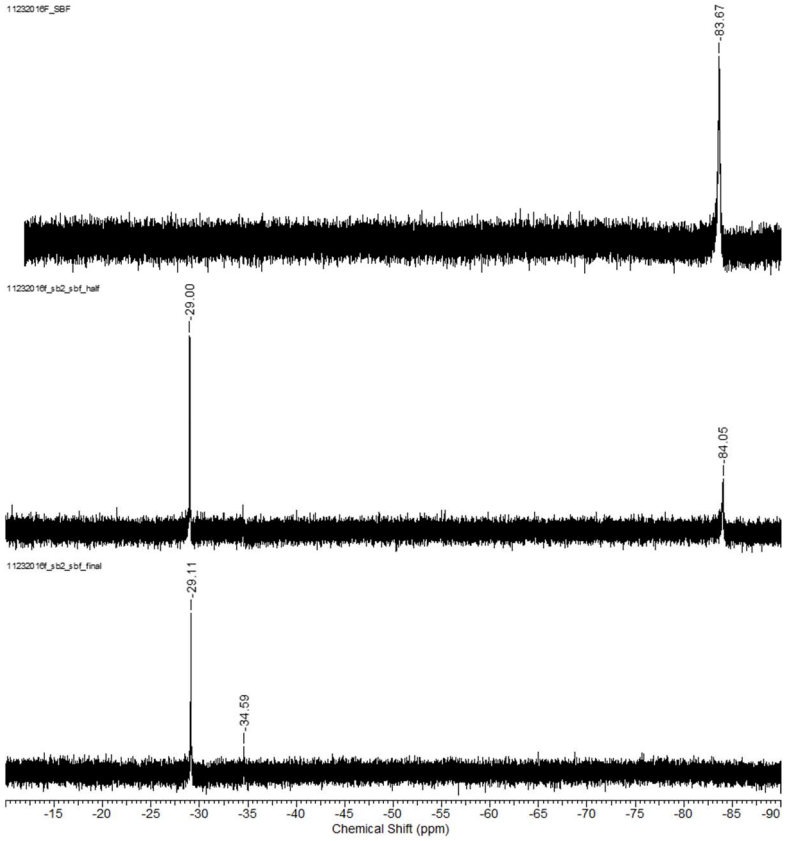

Figure 35. ^{19}F NMR monitoring of the reaction of **30** with [N*n*Bu$_4$][Ph$_3$(O$_2$C$_6$Cl$_4$)SbF]. The first spectrum corresponds to [N*n*Bu$_4$][Ph$_3$(O$_2$C$_6$Cl$_4$)SbF]. The second and third spectra were obtained after addition of one equivalent of 30 in two increments, respectively.

Reaction of $B(C_6F_5)_3$ with 30: [N*n*Bu$_4$][**30**-μ_2-F] (10 mg, 6.4 μmol) and $B(C_6F_5)_3$ (3.3 mg, 6.4 μmol) were combined in $CDCl_3$ (2 ml). The mixture was stirred for 30 min at room temperature under N_2. During this time, [N*n*Bu$_4$][**30**-μ_2-F] which formed a suspension in this solvent was slowly consumed. At the same time, the color of the solution turned yellow indicating the formation of free distiborane **30**. Formation of $[(C_6F_5)_3BF]^-$ and free **30** was confirmed by NMR spectroscopy (Figure 36).

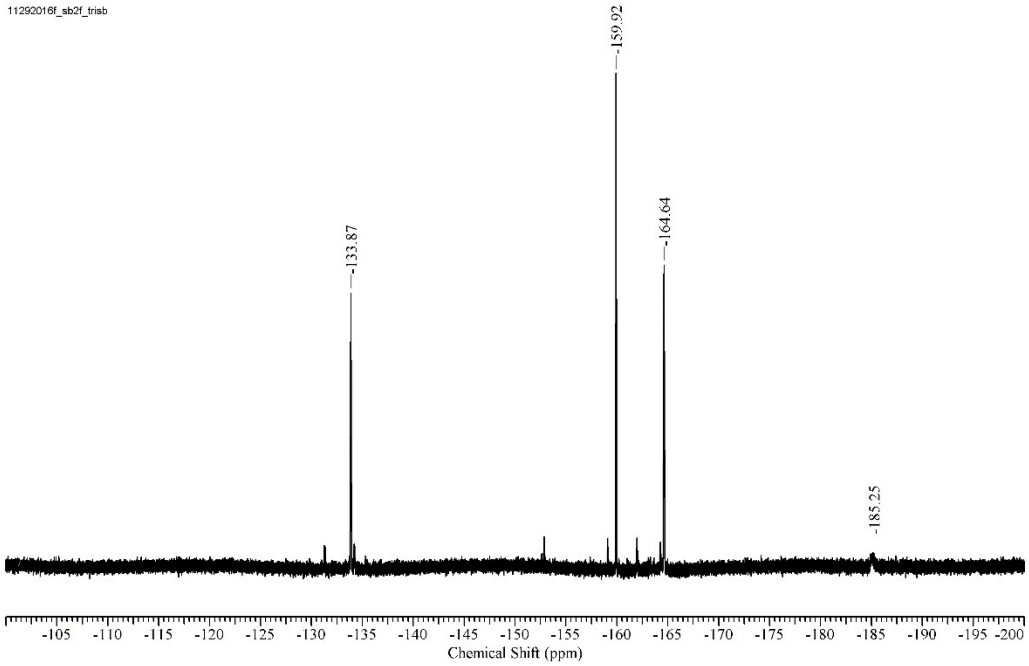

Figure 36. ^{19}F NMR monitoring of the reaction of $B(C_6F_5)_3$ with [N*n*Bu$_4$][**30**-μ_2-F]. The peaks observed at -133.9, -159.9, -164.6 and -185.2 correspond to $[(C_6F_5)_3BF]^-$.

Reaction of 30 with [N*n*Bu$_4$][4-μ_2-F]: [N*n*Bu$_4$][**4**-μ_2-F] (6 mg, 3.9 μmol) was dissolved in $CDCl_3$ (0.45 mL) and combined in four equal increments with a solution of distiborane **30** (5 mg, 3.9 μmol) in $CDCl_3$ (0.4 mL). ^{19}F NMR monitoring of the reaction confirmed the formation of [**30**-μ_2-F]$^-$ and the consumption of the [**4**-μ_2-F]$^-$.

Biphasic fluoride anion capture experiments: Tetrabutylammonium fluoride trihydrate (TBAF·3H_2O, 11 mg, 34.8 μmol) was dissolved in water (HPLC grade, 66 mL) to afford a 10 ppm fluoride ion solution. This solution was mixed with a CD_2Cl_2 (1 mL) solution of distiborane **30** (9 mg, 7 μmol). The biphasic solution was stirred for 30 min at room temperature before the organic layer was separated. The organic solution was subjected to ^1H and ^{19}F NMR measurements without purification.

Synthesis of 32. *n*BuLi (2.6 M in hexane, 0.68ml, 1 equiv) was slowly added to a cold solution (-78 ºC) of 1,8-dibromoanthracene (600 mg, 1.78 mmol) in dry THF (10 mL). After 60 min of stirring at -78 ºC, a solution of Ph_2SbCl (560 mg, 1 equiv) in THF (5 mL) was slowly (10 min) transferred into the reaction flask using a cannula. The resulting pale-yellow solution was kept at low temperature for 2 h and then stirred for an additional 12 h at room temperature. The solution was then treated with a drop (50 μL) of saturated NH_4Cl(aq) and the solvent was removed under vacuum. The resulting white solid was then dissolved in CH_2Cl_2 (15 mL). The resulting solution was filtered and brought to dryness under vacuum. The resulting solid, identified as 1-bromo-8-diphenylantimony-anthracene (84 %), was washed with MeOH (20 mL) and used in the next step without further purification. Crude 1-bromo-8-diphenylantimony-anthracene (600 mg, 1.13 mmol) was dissolved in a dry THF/Et_2O (10 mL/10 mL) at low temperature (-78 ºC) and treated with *t*BuLi (1.67 M in pentane, 1.35 ml, 2 equiv) using a syringe. A solution of Ph_2SbCl (352 mg, 1 equiv) in THF (5 mL) was slowly (10 min) transferred into the reaction flask using a cannula. The solution was stirred for 1.5 h at low temperature and an additional 12 h at room temperature. The solution was then treated

with a drop (50 μL) of saturated NH_4Cl(aq) and the solvent was removed under vacuum. The resulting solid was then washed with MeOH (10 ml) twice to afford **32** in 76 % yield. ^{1}H NMR (399.48 MHz, $CDCl_3$, Figure 37): δ 9.03 (s, 1 H), 8.47 (s, 1 H), 8.00 (d, 2 H, $^3J_{HH}$ = 7.32 Hz), 7.43 (m, 8 H), 7.35-7.24 (m, 16 H) ppm.

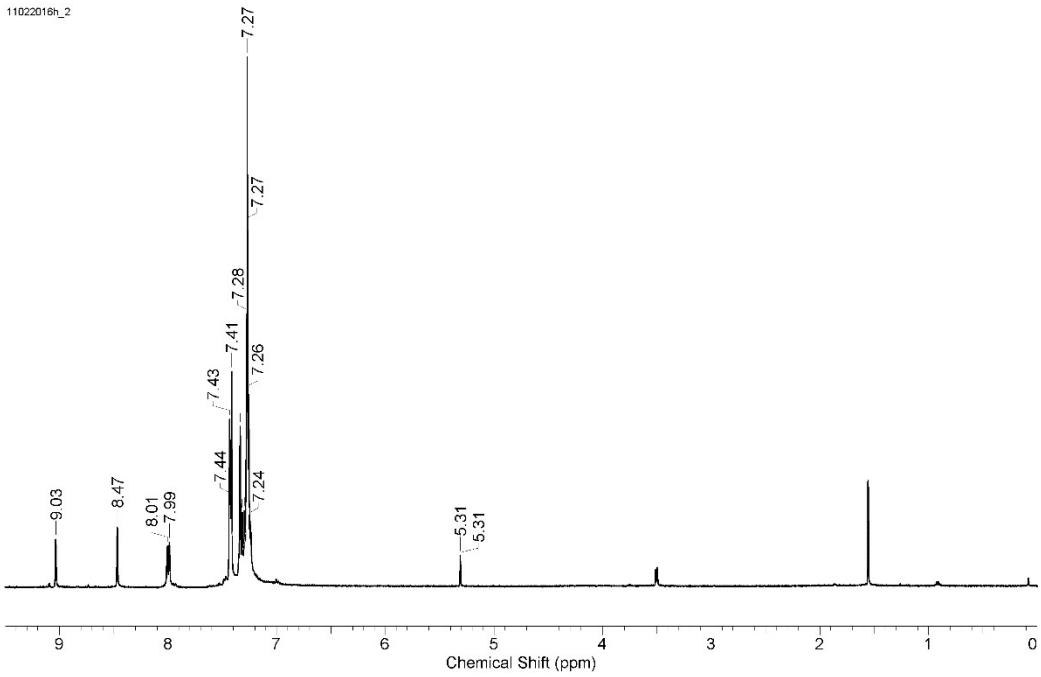

Figure 37. ^{1}H NMR spectrum of **32** in $CDCl_3$.

Synthesis of 31. A solution of *o*-chloranil (270 mg, 2 equiv) in CH_2Cl_2 (5 mL) was slowly transferred via cannula into a flask containing a solution of **32** (400 mg, 0.55 mmol, 1 equiv) in CH_2Cl_2 (8 mL) under N_2 at room temperature. The oxidation of the distibine was observed by the disappearing of the bright red color of *o*-chloranil. After stirring for 2 h at room temperature, the solvent was removed under vacuum. The resulting yellow solid was washed by pentane (20 mL) twice to afford **31** as a yellow solid in 84 % yield. ^{1}H NMR (399.48 MHz, $CDCl_3$, Figure 38): δ 8.77 (s, 1 H), 8.75 (s, 1 H), 8.24 (d, 2 H,

$^3J_{HH}$ = 8.29 Hz), 7.44 (d, 8 H, $^3J_{HH}$ = 7.80 Hz), 7.39-7.32 (m, 6 H), 7.27-7.24 (m, 10 H) ppm.

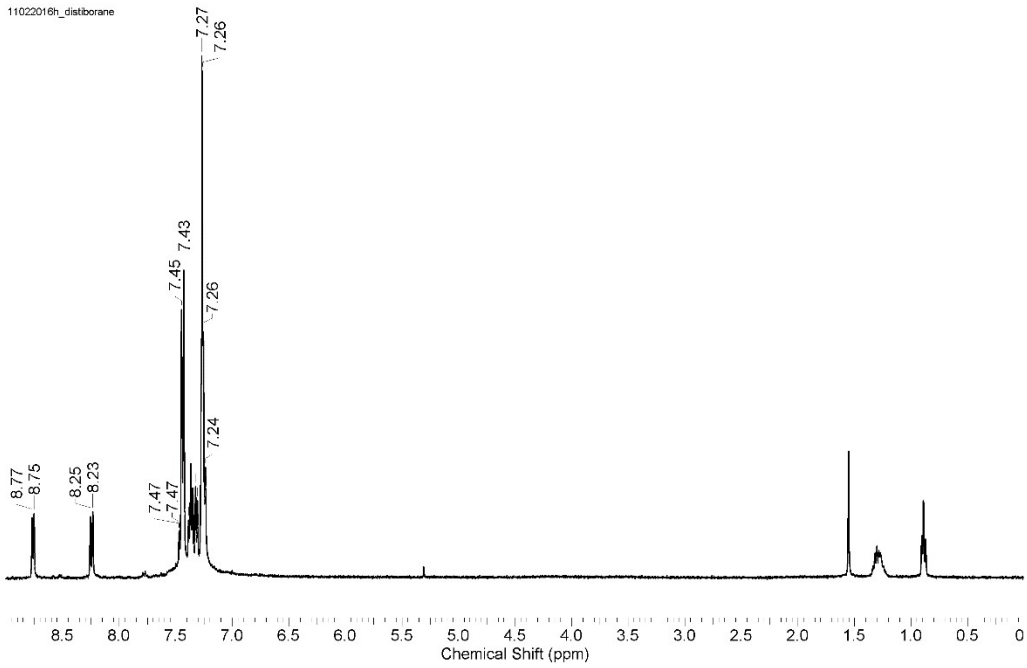

Figure 38. ^{1}H NMR spectrum of **31** in $CDCl_3$.

CHAPTER III

EXPLOITING THE STRONG HYDROGEN BOND DONOR PROPERTIES OF THE BORINIC ACID FUNCTIONALITY FOR FLUORIDE ANION RECOGNITION*

3.1 Introduction

Hydrogen bond donor derivatives that bind small halide anions are of increasing importance in the area of anion sensing[32, 85-87, 125-128] and anion transfer catalysis.[129-132] Such systems are now also emerging as useful tools to adjust the redox chemistry of energy relevant anions.[91, 133] In most cases, the hydrogen bond donor is a nitrogen-based functionality as in the case of protonated amines, ureas, and pyrroles.[32, 126-128] The strong hydrogen bond donor properties of these compounds derived from inductive effects imparted by the electron attractor properties of the nitrogen containing functionality. The same effect can be invoked to rationalize the formation of complexes between halide anions and alcohols.[134-139] A less conventional approach to anion complexation chemistry deals with the use of silanols.[88, 140-141] The strong hydrogen bond donor properties of these main group compounds result from the ability of the silicon atom to dissipate negative charges in α-position by negative mesomeric effects.[142-146] In principle, the same effects could be invoked in the case of borinic acids which should be significantly acidified by the π-accepting properties of the trivalent boron atom (Figure 39).[147-156] In turn, borinic

---

* Reprinted in part with permission from: "Exploiting the Strong Hydrogen Bond Donor Properties of a Borinic Acid Functionality for Fluoride Anion Recognition"; Chen, C.-H.; Gabbaï F. P. *Angew. Chem. Int. Ed.* **2018**, *57*, 521-525. Copyright 2018 by John Wiley & Sons, Inc.

acids are expected to be potent hydrogen bond donor groups, a conclusion supported by the isolation of complexes featuring intramolecular $R_2BOH\cdots LB$ interactions (LB = Lewis base).[80, 157-162] However, borinic acids are typically unstable toward condensations into the corresponding anhydride, thereby preventing an investigation of their hydrogen bond donor properties. In the context of our efforts toward the design of fluoride receptors for drinking water analysis and $[^{18}F]^-$ positron emission tomography,[17, 28, 163-164] we now present the synthesis and structure of a bulky borane/borinic acid bifunctional derivative which resists condensation. We also demonstrate that the borinic acid functionality of this bifunctional Lewis acid/hydrogen bond donor system augments the fluoride anion binding properties, making it compatible with aqueous environments.

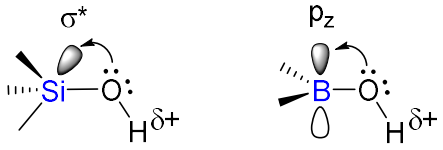

Figure 39. Influence of negative mesomeric effect on the acidity of silanols and borinic acids.

3.2 Synthesis and characterization of the diborane and the bifunctional borane/borinic acid

1,8-Bis(dimesitylboryl)biphenylene (**33**) was obtained from dilithiation of 1,8-dibromobiphenylene[165] followed by metathesis with Mes_2BF as described in Figure 40. Compound **33**, which was isolated as an air-stable yellow solid in 81% yield, has been fully characterized. The three signals arising from the hydrogen atoms attached to the C2(C9)-, C3(C10)-, C4(C11)-positions of the biphenylene backbone confirm the formation of a symmetrical derivative. The ^{11}B NMR spectrum shows a broad peak at 76.7 ppm which falls within the typical range expected for triarylboranes. Single crystals suitable for X-ray diffraction analysis of **33** were obtained by layering MeOH onto a solution of **33** in CH_2Cl_2.

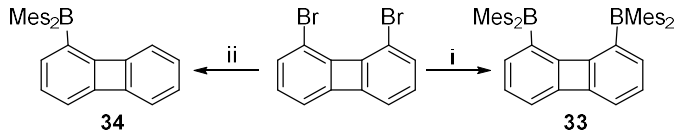

Figure 40. Synthesis of **33** and **34**. i) 2.3 equiv *n*BuLi, 2 equiv Mes_2BF, Et_2O, -78 ºC; ii) (1) 1 equiv *n*BuLi, Et_2O, -78 ºC (2) water (3) 1.1 equiv *n*BuLi, 1 equiv Mes_2BF, Et_2O, -78 ºC

Analysis of the solid-state structure of **33** (Figure 41) indicates that the boron atoms adopt a trigonal planar geometry as indicated by the sum of the C_{aryl}-B-C_{aryl} angles ($\sum\angle_{C\text{-}B1\text{-}C} = 359.1^o$, $\sum\angle_{C\text{-}B2\text{-}C} = 358.6^o$). The B1-B2 separation of 4.566(5) Å in **33** is larger than that in its 1,8-naphthalenediyl analogues.[6, 9] The B1-B2 separation also deviates from the C1-C8 distance (3.899(4) Å) indicating the steric repulsion between the two boryl moieties.

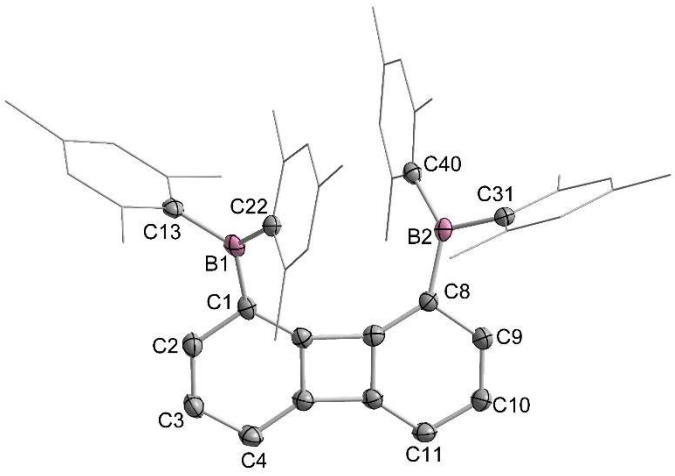

Figure 41. Solid-state structure of **33**. Thermal ellipsoids are drawn at the 50% probability level. The hydrogen atoms are omitted for clarity. Selected bond lengths [Å] and angles [°]: B1-C1 1.570(4), B1-C13 1.586(4), B1-C22 1.568(4), B2-C8 1.580(4), B2-C31 1.581(4), B2-C40 1.569(4); C1-B1-C13 116.1(2), C13-B1-C22 119.1(2), C1-B1-C22 123.9(2), C8-B2-C31 114.7(2), C31-B2-C40 118.3(2), C8-B2-C40 125.6(2).

The CV of compound **33** (Figure 42) shows two quasi-reversible reduction waves at -2.23 and –2.74 V vs Fc/Fc^+ suggesting that the molecule can be reduced by two electrons. It is interesting to note that the potential of the first reduction is shifted to anodic potentials by 490 mV when compared to the reduction potential of Mes_3B (-2.72 V). This data suggests that the biphenylene substituent is electron withdrawing,[166] a conclusion consistent with a recent paper by Wagner on 2,3-borylated biphenylene derivatives.[167] A similar conclusion can be derived from the CV of the model compound 1-dimesitylborylbiphenylene (**34**) that we synthesized for the sake of comparison (Figure 40). This compound shows a quasi-reversible reduction wave at -2.37 V which is anodically shifted by 350 mV from that of Mes_3B (Figure 43).

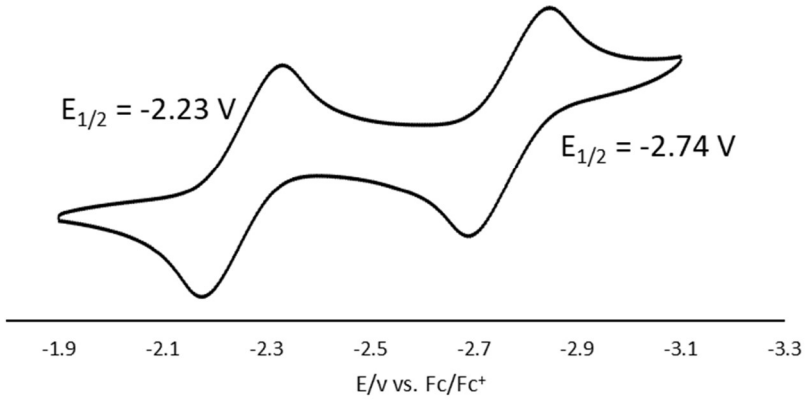

Figure 42. Cyclic voltammogram of **33** in THF recorded with a glassy carbon working electrode (0.1 M $TBAPF_6$). Scan rate: v = 100 mV/s.

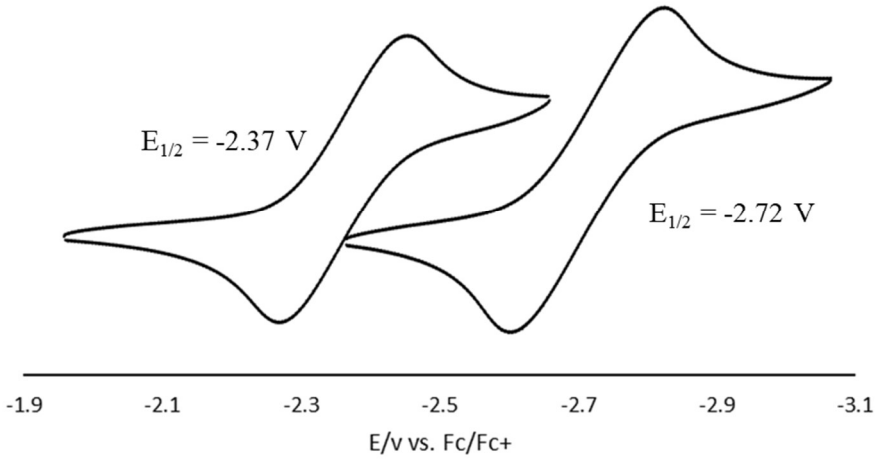

Figure 43. Cyclic voltammogram of **34** (left) and Mes_3B (right) in THF recorded with a glassy carbon working electrode (0.1 M $TBAPF_6$). Scan rate: v = 100 mV/s.

Reaction of compound **33** with tris(dimethylamino)sulfonium difluorotrimethylsilicate (TASF) in THF in an open flask followed by addition of an aqueous solution of $Al(NO_3)_3$ afforded the triarylborane-borinic acid (**35**) as an air- and

moisture-stable yellow solid (Figure 44). This compound, whose formation is assigned to the fluoride-promoted hydrolysis of a B-C_{Mes} bond,[168] has been characterized by conventional means.

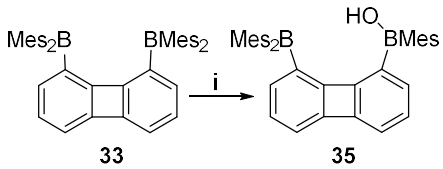

Figure 44. Synthesis of **35**. i) (1) 1 equiv TASF, THF in open flask, rt. (2) 2 equiv $Al(NO_3)_{3(aq)}$, rt.

By contrast with **33**, the CV of **35** shows two irreversible reduction waves (Figure 45). The ^{11}B NMR spectrum of **35** shows two distinct broad signals at 47.5 and 73.3 ppm, which arise from the boron atom of the borinic acid and the triarylborane, respectively. The ^{1}H NMR spectrum of **35** shows four different resonances for the methyl groups of the mesityl substituents in a 3:6:12:6 ratio indicating differentiation of the triarylborane and borinic acid functionalities. This ratio also reflects the hydrolysis of a single mesityl group. More importantly, the proton signal of the hydroxy group of the borinic acid is observed at 5.25 ppm as a sharp singlet in $CDCl_3$ (Figure 46).

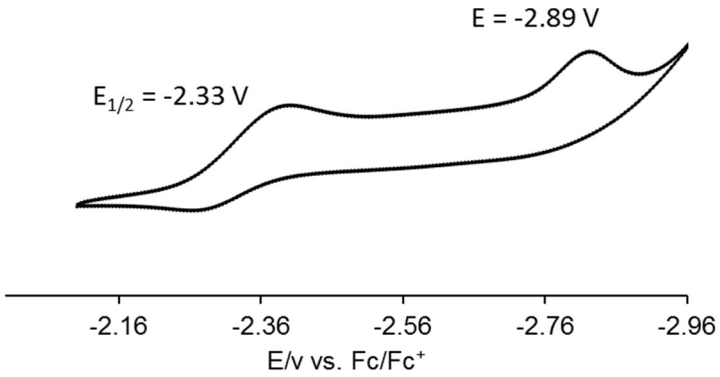

Figure 45. Cyclic voltammogram of **35** in THF with a glassy carbon working electrode (0.1 M $TBAPF_6$). Scan rate: v = 100 mV/s.

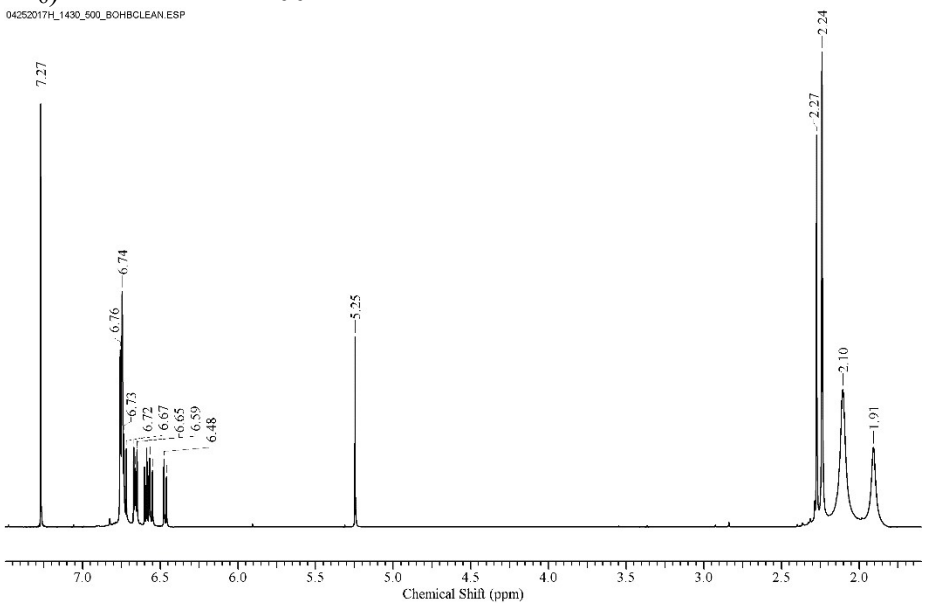

Figure 46. ^1H NMR spectrum of **35** in $CDCl_3$.

Further elucidation of the structure of **35** was derived from X-ray diffraction analysis. As indicated by the solid-state structure (Figure 47), both boron atoms adopt a trigonal planar geometry as indicated by the sum of the C_{aryl}-B-C_{aryl} and O-B-C_{aryl} angles ($\sum\angle_{C\text{-}B1\text{-}C} = 360.2^{o}$, $\sum\angle_{C\text{-}B2\text{-}C + \angle O\text{-}B2\text{-}C + \angle C\text{-}B2\text{-}O} = 360.0^{o}$). The B1-B2 separation of 4.359(3) Å is greater than the C1-C8 distance indicating significant steric encumbrance. DFT calculations indicate that the LUMO of **35** bears a large contribution from the empty p orbital at the borane center (Figure 48).

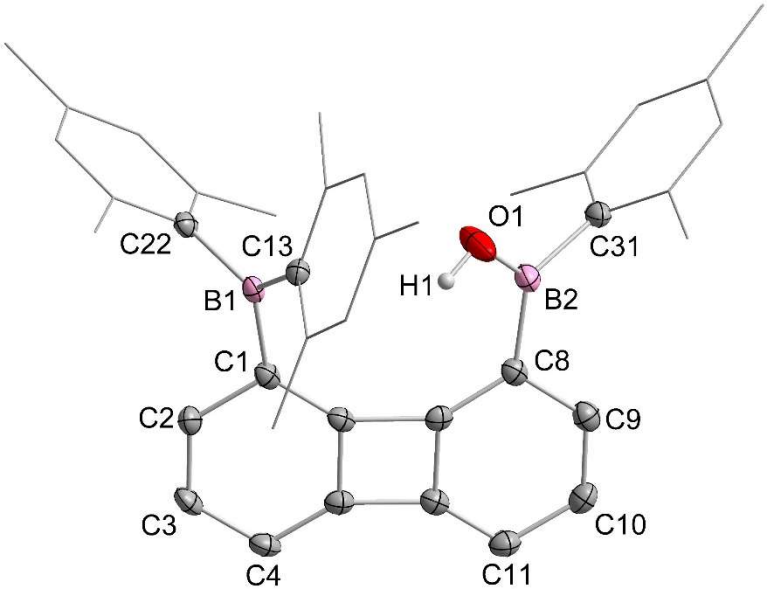

Figure 47. Solid-state structure of **35**. Thermal ellipsoids are drawn at the 50% probability level. The hydrogen atoms, except that bound to the oxygen, are omitted for clarity. Selected bond lengths [Å] and angles [°]: B1-C1 1.581(2), B1-C13 1.573(2), B1-C22 1.584(2), B2-C8 1.574(3), B2-C31 1.584(3), B2-O1 1.353(3); C1-B1-C13 122.0(2), C13-B1-C22 121.8(2), C1-B1-C22 116.0(1), C8-B2-C31 123.8(2), C31-B2-O1 114.0(2), C8-B2-O1 122.1(2).

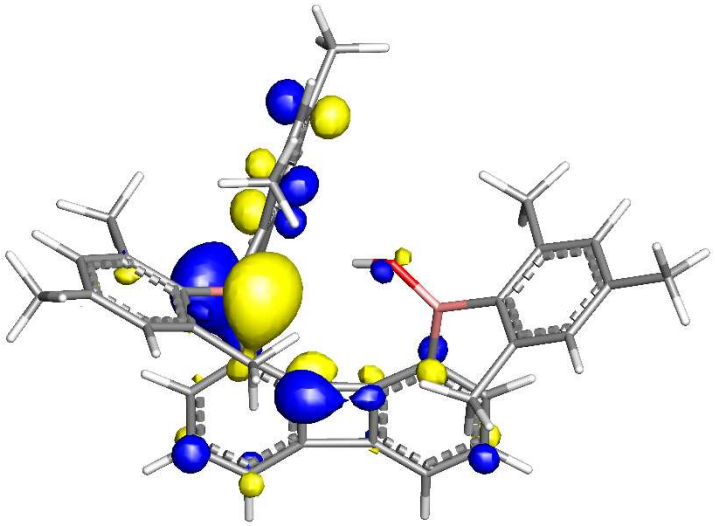

Figure 48. Contour plot of the LUMO of **35** (isovalue = 0.05).

3.3 Reaction of the bifunctional borane/borinic acid with fluoride anion in organic solvents and aqueous media

Given that triarylboranes are well known for their complexing ability toward anions,[1-3, 68, 169-177] we became eager to investigate the occurrence of possible cooperative effects between the borane and borinic acid functionality in **35**. To this end, **35** was subjected to a fluoride titration experiment monitored by UV-Vis spectroscopy. The incremental addition of TBAF (2.17×10^{-3} M) to a solution of **35** (6.10×10^{-5} M) in THF induced a notable change of the UV-Vis spectrum , suggesting the quantitative formation of a 1:1 fluoride complex as indicated by the fact that the isotherm plateaus at exactly one equivalent ($K > 10^8$ M^{-1}) (Figure 49).

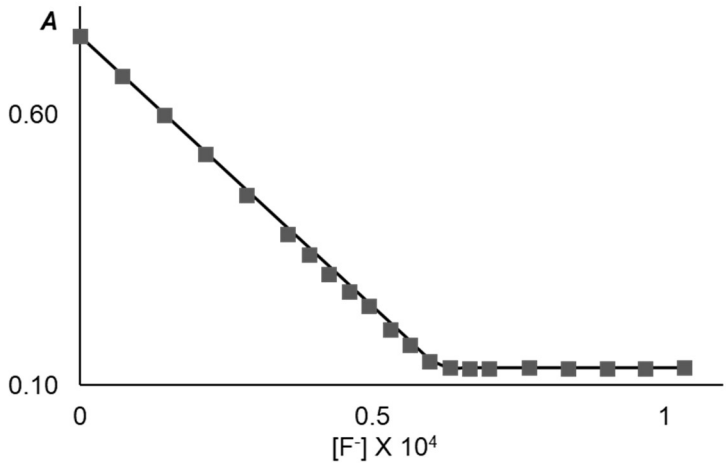

Figure 49. The experimental and the calculated 1:1 binding isotherms for **35** in THF at 320 nm. The data were fitted with $K = 10^{10}$ M^{-1}. (ε(**35**) = 12130 $M^{-1}cm^{-1}$ and (ε([**35**-F]$^-$) = 2163 $M^{-1}cm^{-1}$).

To our surprise, we also observed significant fluoride anion binding in $CHCl_3$ (K = 1.4 (± 0.1) × 10^6 M^{-1}) (Figure 50), a competing solvent in which most neutral boranes[3] including the model monofunctional borane **34** shows no affinity for the fluoride anion.

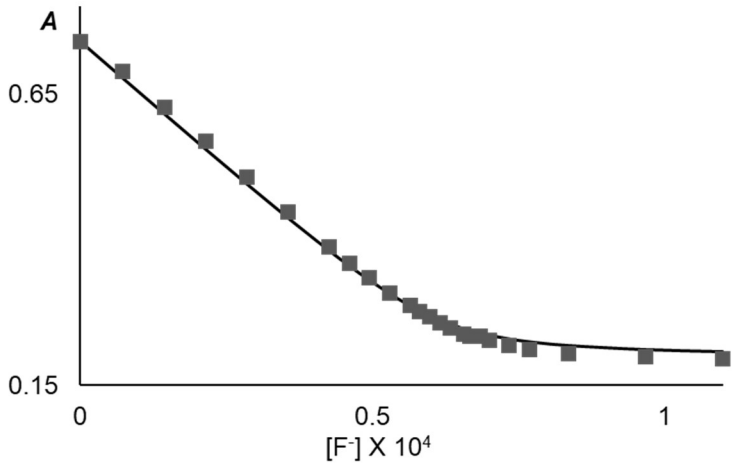

Figure 50. The experimental and the calculated 1:1 binding isotherms for **35** in $CHCl_3$ at 320 nm. The data were fitted with K = 1.4 (± 0.1) ×10^6 M^{-1}. (ε(**35**) = 12048 $M^{-1}cm^{-1}$ and (ε([**35**-F]$^-$) = 3203 $M^{-1}cm^{-1}$).

Encouraged by these results, we also tested binding in more competing environments. Gratifyingly, we observed significant fluoride binding in THF/H_2O mixture (v/v = 4/1). Fitting of the UV-Vis absorption data based on a 1:1 binding model afforded K = 1.4 (± 0.1) × 10^4 M^{-1} (Figure 51). The tolerance of this neutral boron-based fluoride anion receptor to water bears no precedent. We also observed that the monofunctional analogue **34** does not complex fluoride under these conditions pointing to the crucial role played by the borinic acid functionality.

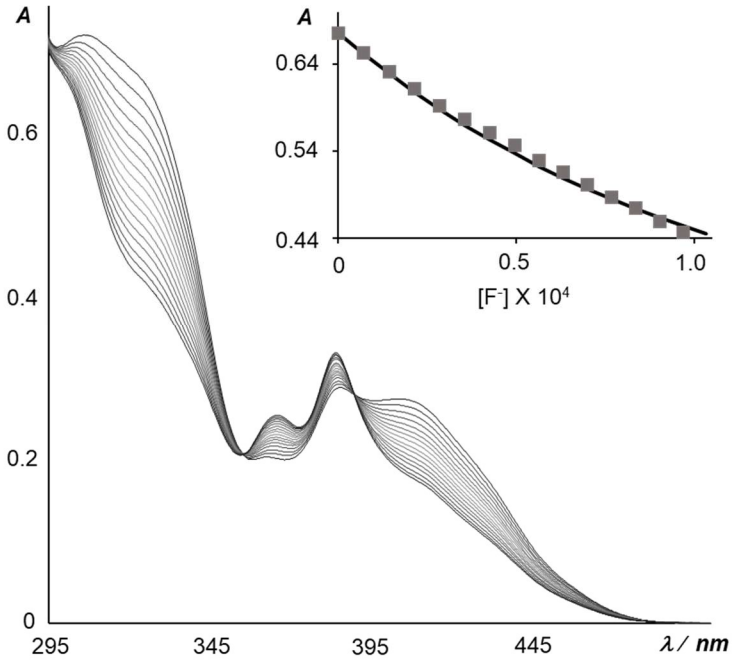

Figure 51. Spectral changes in the UV-Vis absorption spectra of **35** (6.10 × 10^{-5} M) in THF/H_2O (v/v = 4/1) solution upon addition of fluoride (2.17 × 10^{-3} M). The inset shows the experimental and the calculated 1:1 binding isotherms for 35 in THF/H_2O (v/v = 4/1) at 320 nm. The data were fitted with K = 1.4 (± 0.1) × 10^4 M^{-1}, ε(**35**) = 11082 $M^{-1}cm^{-1}$ and ε([**35**-F]$^-$) = 3597 $M^{-1}cm^{-1}$.

3.4 Synthesis and characterization of the fluoride complex of bifunctional borane/borinic acid

To identify the origin of the high fluoride ion affinity of **35**, efforts to characterize the fluoride complex were undertaken. The salt [TAS][**35**-F] was obtained by combining **35** with TASF (1 equiv) in THF/CH_2Cl_2 co-solvent. It was isolated as an air- and moisture-stable pale-yellow solid in 85% yield (Figure 52).

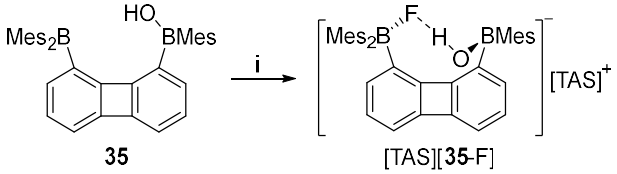

Figure 52. Synthesis of [TAS][**35**-F]. i) TASF, 1 equiv, THF/CH_2Cl_2, rt.

The ^{11}B NMR spectrum of [TAS][**35**-F] features two distinct resonances at 7.1 ppm and 44.8 ppm, consistent with the presence of a fluoroborate and a borinic acid functionality, respectively. Complexation of the fluoride anion to the triarylborane moiety of **35** is further confirmed by a ^{19}F NMR signal observed at -163 ppm, a value similar to that typically measured for triarylfluoroborate salts.[3, 121, 178] The most conspicuous spectroscopic features are those related to the borinic acid hydroxy group. Indeed, its ^{1}H NMR resonance is shifted from δ = 5.25 in **35** to 11.12 ppm in [**35**-F]$^-$ (Figure 53). This large downfield shift of almost 6 ppm is taken as a clear indication of hydrogen bond formation with the fluoride anion. This view is further supported by the fact that the hydroxy ^{1}H NMR signal in [**35**-F]$^-$ is coupled to the ^{19}F nucleus by a value of $^{1}J_{HF}$ = 57.2 Hz as confirmed by the $^{1}H\{^{19}F\}$ NMR experiment (Figure 53).

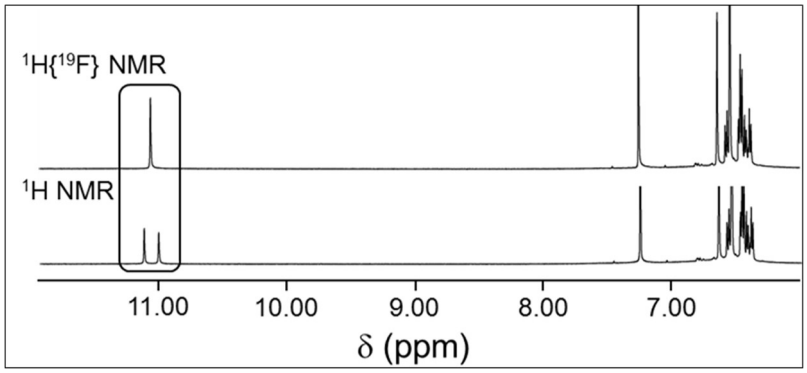

Figure 53. The $^{1}H\{^{19}F\}$ (top) and ^{1}H (bottom) NMR spectra showing the resonance of the hydrogen atom of the hydroxy group of borinic acid collapses to a singlet upon ^{19}F decoupling.

Infrared spectroscopy shows a weakening of the O-H stretching frequency from $\nu_{O\text{-}H}$ = 3503 cm^{-1} in **35** (Figure 54) to $\nu_{O\text{-}H}$ = 3193 cm^{-1} in [TAS][**35**-F] (Figure 55). The large decrease observed in this stretching frequency is reminiscent in magnitude to that observed for CH_3CO_2H upon dimerization,[179] thus offering corroborating evidence for the formation of a strong B-F···H-O-B hydrogen bond.

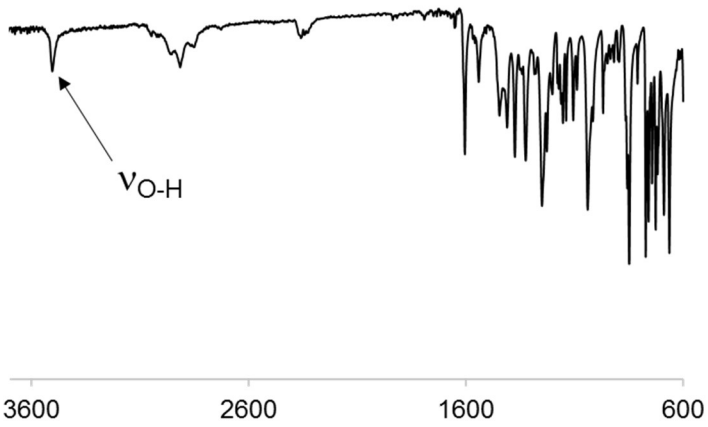

Figure 54. IR spectrum of **35** in the solid state.

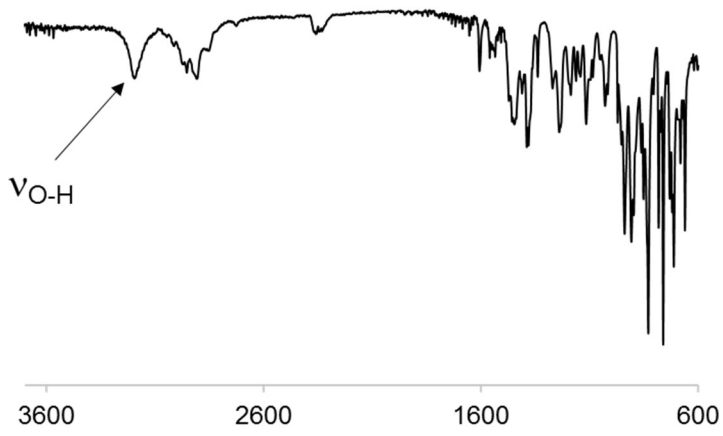

Figure 55. IR spectrum of [TAS][**35**-F] in the solid state.

The presence of this hydrogen bond is also readily observed in the crystal structure of [TAS][**35**-F] which confirms that the fluorine atom is trapped between the boron atom and the hydroxy proton (Figure 56). The latter, which was located on the difference map and refined anistropically, forms a H···F contact of 1.79(3) Å confirming the presence of a hydrogen bond. The fluorine atom is also coordinated to the boron atom B1 via a B-F bond length of 1.492(2) Å which is comparable to those found in triarylborate anions (1.47 Å).[3] It is interesting to note that the B-O bond length of 1.330(2) Å in [**35**-F]$^-$ is slightly shorter than in **35** (1.353(3) Å). This observation points to an increased double bond character of the B-O bond in [**35**-F]$^-$, an effect that we correlate to the partial proton abstraction induced by the H···F hydrogen bond. While the involvement of a borinic acid as a hydrogen bond donor toward a fluoroborate is to our knowledge unprecedented, we note that fluoride complexes with intramolecular N-H···F-B[180-183] and C-H···F-B[80, 112, 184] bonds have been previously observed.

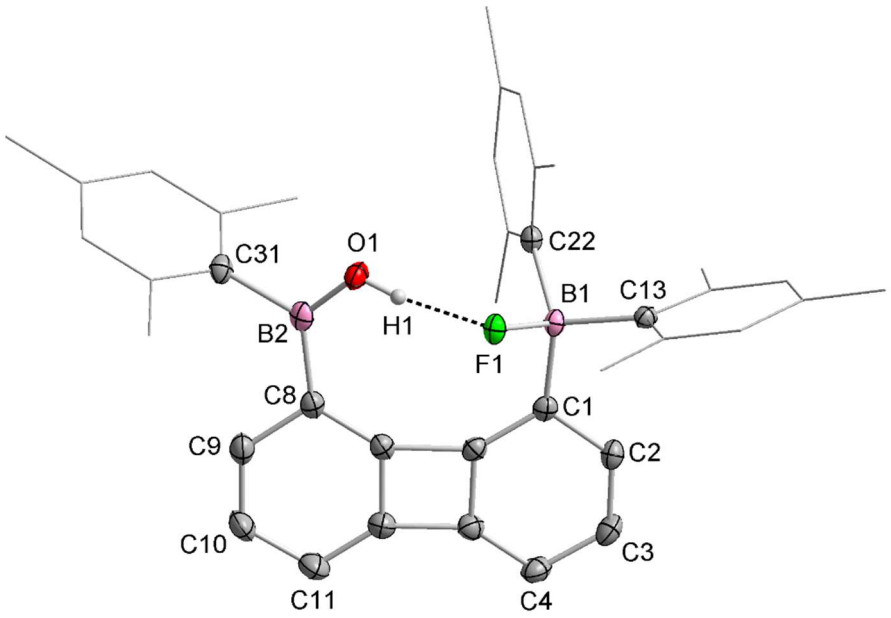

Figure 56. Solid-state structure of [**35**-F]$^{-}$. Thermal ellipsoids are drawn at the 50% probability level. The [TAS]$^{+}$ and hydrogen atoms, except that bound to the oxygen, are omitted for clarity. O1-F1 2.576(2) Å, B1-F1 1.492(2), B1-C1 1.638(3), B1-C13 1.658(3), B1-C22 1.650(3), B2-C8 1.581(3), B2-C31 1.595(3), B2-O1 1.330(2); C1-B1-F1 102.4(1), F1-B1-C13 109.7(1), C1-B1-C13 108.8(1), C13-B1-C22 110.5(1), C1-B1-C22 120.6(2), C8-B2-C31 120.0(2), C31-B2-O1 115.6(2), C8-B2-O1 124.4(2).

This B-F···H-O-B hydrogen bond in [**35**-F]- is readily visualized using both the Atom In Molecule (AIM)[185] and Natural Bond Orbital (NBO) methods,[186] which we implemented using the DFT optimized geometry of the anionic complex. The AIM analysis reveals a bond path connecting H1 and F1 (Figure 57). This path is characterized by a bond critical point (bcp) with an electron density $\rho(r)$ of 5.82 x 10^{-2} e/bohr^3 and a positive Laplacian $\nabla^2\rho(r)$ of +2.13 x 10^{-1} e/bohr^5. The electron density at this bcp falls in the range expected for strong hydrogen bonds,[118, 187] a finding that corroborates the high $^1J_{HF}$ measured by NMR and the short H···F observed in the crystal structure. NBO analysis provides a complementary picture with a strong donor-acceptor lp(F)→σ*(O-H)

interaction ($E^{(2)}$ = 118.3 kJ/mol) connecting the fluorine and hydrogen atom (Figure 58). Last but not least, our computations also show that the fluoride ion affinity of **35** (317 kJ/mol) exceeds that of **34** (267 kJ/mol) by 50 kJ/mol.[121] This large difference illustrates the crucial stabilizing influence of the borinic acid.

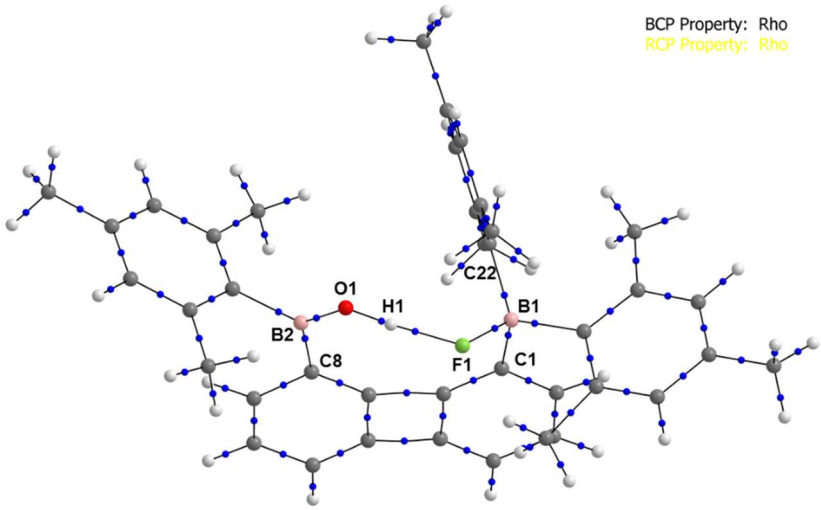

Figure 57. QTAIM bond path and BCP analysis for [**35**-F]$^-$.

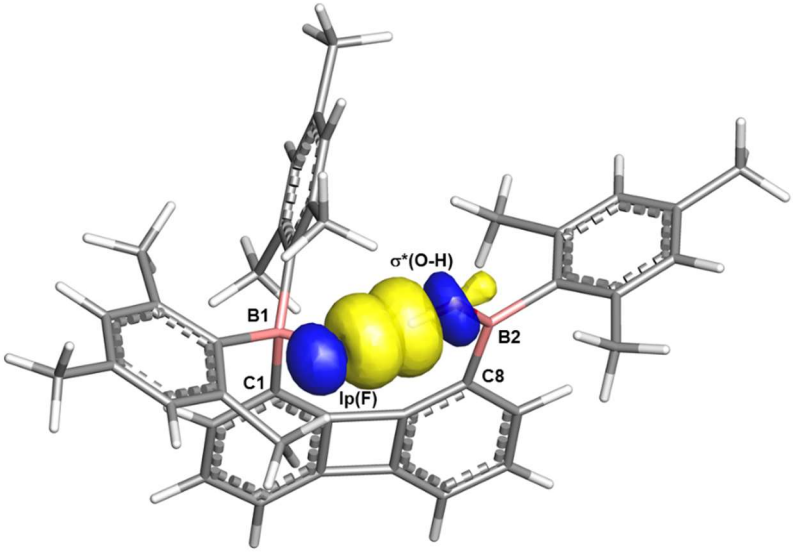

Figure 58. NBO view of the lp(F)→σ*(O-H) donor-acceptor interaction in [**35**-F]$^-$.

3.5 Conclusion

In summary, we describe a boron-based, bifunctional Lewis acid/hydrogen bond donor platform in which the two boron functionalities are connected by the 1,8-biphenylenediyl backbone. Anion complexation experiments show that the respective positioning of these two functionalities promotes strong fluoride anion binding. The crux of this study lies in the fact that the hydrogen bond donor functionality is a borinic acid unit which engages the fluoride guest in a strong B-F···H-O-B interaction. These results suggest that borinic acid functionalities could become useful for the design of not only anion receptors but also possibly organocatalysts.

3.6 Experimental section

General considerations. Dimesitylboron fluoride (Mes_2BF) was purchased from TCI and used as received. Tris(dimethylamino)sulfonium difluorotrimethylsilicate (TASF) was purchased from Sigma-Aldrich and used as received. 1,8-Dibromobiphenylene was synthesized by the reported procedure.[165] All preparations were carried out under a dry N_2 atmosphere employing either a glovebox or standard Schlenk techniques. Solvents were dried by passing through an alumina column (*n*-pentane and CH_2Cl_2) or by refluxing under nitrogen over Na/K (hexanes, Et_2O and THF). All other solvents were ACS reagent grade and used as received. NMR spectra were recorded on an Inova 500 FT NMR (499.41 MHz for ^1H, 469.99 MHz for ^{19}F, 125.63 MHz for ^{13}C) spectrometer or a Varian NMRS 500RM NMR spectrometer (499.69 MHz for ^1H, 469.97 MHz for ^{19}F, 125.66 MHz for ^{13}C) at room temperature. Chemical shifts are given in ppm and are referenced to residual ^1H, ^{13}C solvent signals or external $BF_3 \cdot Et_2O$ (-153.0 ppm for ^{19}F and 0 ppm for ^{11}B) for ^{19}F and ^{11}B NMR. Elemental analyses were performed by Atlantic Microlab (Norcross, GA). Electronic absorption spectra were recorded at ambient temperature using an UV-2501PC spectrometer from Shimadzu Corporation.

Computational details. Density functional theory (DFT) structural optimizations were done with the Gaussian 09 program. In all cases, the structures were optimized using the B3LYP functional and the following mixed basis set: F/B, 6-31+g(d'); C/O/H, 6-31g. For all optimized structures, frequency calculations were carried out to confirm the absence of imaginary frequencies. The molecular orbitals were visualized and plotted using the Jimp2 program.[122] The enthalpy of each compound was derived from a single

point energy calculation at the B3LYP/6-311+g(2d,p) level of theory and the application of the relevant thermal correction terms. The fluoride ion affinity was calculated by following a procedure published earlier.[121] The NBO analysis was performed using the NBO 5.9 program.[186] The energy of the O-H···F interaction was derived from the second order perturbation energy associated to the donor-acceptor interaction shown in Figure 58. QTAIM calculations were carried out on the wave functions derived from the optimized structure using the AIMAll program.[188]

Crystallographic details. The crystallographic measurements were performed at 110(2) K using a Bruker APEX-II CCD area detector diffractometer, with a graphite-monochromated Mo-Kα radiation (λ = 0.71073 Å). A specimen of suitable size and quality was selected and mounted onto a nylon loop. The semi-empirical method SADABS was applied for absorption correction. The structure was solved by direct methods, which successfully located most of the non-hydrogen atoms. Subsequent refinement on F^2 using the SHELXTL/PC package (version 6.1) allowed location of the remaining non-hydrogen atoms.

Table 3. Crystal data, data collection, and structure refinement for **33**.

Empirical formula	$C_{48}H_{50}B_2$
Formula weight	648.5
Temperature	110 K
Wavelength	0.71073 Å
Crystal system	Monoclinic
Space group	P 1 21/c 1
Unit cell dimensions	a = 10.801(7) Å b = 20.599(12) Å c = 17.848(11) Å α = 90°. β = 106.428(8)°. γ = 90°.
Volume	3809(4) $Å^3$
Z	4
Density (calculated)	1.131 Mg/m^3
Absorption coefficient	0.063 mm^{-1}
F(000)	1392
Crystal size	0.5 x 0.3 x 0.1 mm^3
Theta range for data collection	1.547 to 27.533°.
Index ranges	-14<=h<=13, -26<=k<=26, -23<=l<=23
Reflections collected	43763
Independent reflections	8723 [R(int) = 0.1111]
Completeness to theta = 25.242°	100.00%
Absorption correction	Semi-empirical from equivalents
Max. and min. transmission	0.7456 and 0.6718
Refinement method	Full-matrix least-squares on F^2
Data / restraints / parameters	8723 / 0 / 463
Goodness-of-fit on F^2	1.017
Final R indices [I>2sigma(I)]	R1 = 0.0709, wR2 = 0.1521
R indices (all data)	R1 = 0.1536, wR2 = 0.1961
Largest diff. peak and hole	0.274 and -0.296 $e.Å^{-3}$

Table 4. Crystal data, data collection, and structure refinement for **35**.

Empirical formula	$C_{39}H_{40}B_2O$
Formula weight	546.33
Temperature	110 K
Wavelength	0.71073 Å
Crystal system	Triclinic
Space group	P-1
Unit cell dimensions	a = 8.6324(13) Å b = 12.4436(19) Å c = 15.370(2) Å α = 106.172(7)°. β = 101.752(7)°. γ = 93.431(8)°.
Volume	1540.5(4) $Å^3$
Z	2
Density (calculated)	1.178 Mg/m^3
Absorption coefficient	0.067 mm^{-1}
F(000)	584
Crystal size	0.73 x 0.6 x 0.27 mm^3
Theta range for data collection	1.417 to 27.387°.
Index ranges	-11<=h<=11, -16<=k<=15, -19<=l<=19
Reflections collected	57413
Independent reflections	6934 [R(int) = 0.0560]
Completeness to theta = 25.242°	100.00%
Absorption correction	Semi-empirical from equivalents
Max. and min. transmission	0.7455 and 0.5803
Refinement method	Full-matrix least-squares on F^2
Data / restraints / parameters	6934 / 0 / 389
Goodness-of-fit on F^2	1.103
Final R indices [I>2sigma(I)]	R1 = 0.0591, wR2 = 0.1665
R indices (all data)	R1 = 0.0752, wR2 = 0.1822
Largest diff. peak and hole	0.427 and -0.288 $e.Å^{-3}$

Table 5. Crystal data, data collection, and structure refinement for [TAS][**35**-F].

Empirical formula	$C_{45}H_{58}B_2FN_3OS$
Formula weight	729.62
Temperature	110 K
Wavelength	0.71073 Å
Crystal system	Monoclinic
Space group	P 1 21/n 1
Unit cell dimensions	a = 17.180(3) Å b = 14.284(3) Å c = 17.949(4) Å α = 90°. β = 111.819(2)°. γ = 90°.
Volume	4089.2(14) $Å^3$
Z	4
Density (calculated)	1.185 Mg/m^3
Absorption coefficient	0.121 mm^{-1}
F(000)	1568
Crystal size	0.89 x 0.79 x 0.23 mm^3
Theta range for data collection	1.878 to 27.528°.
Index ranges	-22<=h<=22, -18<=k<=18, -23<=l<=23
Reflections collected	46745
Independent reflections	9347 [R(int) = 0.0520]
Completeness to theta = 25.242°	99.90%
Absorption correction	Semi-empirical from equivalents
Max. and min. transmission	0.7456 and 0.6672
Refinement method	Full-matrix least-squares on F^2
Data / restraints / parameters	9347 / 0 / 497
Goodness-of-fit on F^2	1.037
Final R indices [I>2sigma(I)]	R1 = 0.0514, wR2 = 0.1131
R indices (all data)	R1 = 0.0818, wR2 = 0.1279
Largest diff. peak and hole	0.366 and -0.376 $e.Å^{-3}$

Electrochemistry. Electrochemical experiments were performed with an electrochemical analyzer from CH Instruments (model 610A) with a glassy-carbon working electrode and a platinum auxiliary electrode. The reference electrode was built from a silver wire inserted into a small glass tube fitted with a porous Vycor frit at the tip and filled with a THF solution containing tetrabutylammonium hexafluorophosphate (TBAPF6, 0.1 M) and $AgNO_3$ (0.005 M). All three electrodes were immersed in a deoxygenated THF solution (5 mL) containing $TBAPF_6$ (0.1 M) as a support electrolyte and the boranes (**33**, **34** and **35**) (0.003 M). Ferrocene was used as an internal standard, and all potentials are reported with respect to $E_{1/2}$ of the Fc/Fc^+ redox couple.

Synthesis of 33. *n*BuLi (2.65 M, 0.63 ml, 1.67 mmol, 2.1 equiv) was slowly added to a solution of 1,8-dibromobiphenylene (244 mg, 0.79 mmol, 1 equiv) in dry Et_2O (5 ml) at room temperature. After 30 min of stirring at room temperature, a solution of Mes_2BF (490 mg, 1.83 mmol, 2.3 equiv) in Et_2O (5 ml) was slowly transferred into the reaction flask using a cannula. The resulting pale-yellow solution was stirred for an additional 12 h at room temperature. The solution was then treated with saturated NH_4Cl(aq) (1 ml) and the solvent was removed under vacuum. The resulting yellow solid was then dissolved in CH_2Cl_2 (5 ml). The resulting solution was filtered and brought to dryness under vacuum. The resulting solid was washed with MeOH (15 ml) twice and dried under vacuum to afford diborane **33** as a yellow powder in 86% yield. ^{1}H NMR (499.53 MHz, $CDCl_3$): δ 6.67 (d, 2 H, J = 1.5 Hz, biphenylene-C*H*), 6.66 (s, 2 H, biphenylene-C*H*), 6.65 (br, 8 H, mes-C*H*), 6.40 (m, 2 H, biphenylene-C*H*), 2.24 (s, 12 H, -C*H*$_3$), 1.61 (br, 24 H, -C*H*$_3$). ^{13}C{^{1}H} NMR (125.62 MHz, $CDCl_3$): δ 160.65, 151.44, 141.53, 139.12 (br), 133.62,

128.62 (br), 128.38, 117.15, 23.60 (br, mes-*C*CH_3), 21.24 (mes-*C*H_3). $^{11}B\{^1H\}$ (128.16 MHz, $CDCl_3$): δ 76.7 (br, Ar_3B). m.p. 268 °C. Elemental analysis calculated (%) for C48H50B2: C, 88.90; H, 7.77; found C, 88.60; H, 7.78.

Synthesis of **34**. *n*BuLi (2.65 M, 0.50 ml, 0.99 equiv) was slowly added to a solution of 1,8-dibromobiphenylene (415 mg, 1.34 mmol, 1 equiv) in dry THF (8 ml) at room temperature. After 30 min of stirring at room temperature, water (1 ml) was added into the reaction flask. The solvent was removed under vacuum and the resulting solid was dissolved into Et_2O (20 ml). The resulting solution was washed with brine and the organic layer was dried over anhydrous $MgSO_4$ (1 g). The solvent was removed under vacuum to afford the pale-yellow solid which was identified as 1-bromobiphenylene (85 %) and used without further purification in the following reaction. Crude 1-bromobiphenylene (290 mg) was dissolved in Et_2O (8 ml) at room temperature and treated with *n*BuLi (2.65M, 0.47 ml, 1 equiv) using a syringe. After 30 min, a solution of Mes_2BF (370 mg, 1.38 mmol, 1.1 equiv) in Et_2O (5 ml) was slowly transferred into the reaction flask using a cannula. The resulting yellow suspension was stirred for an additional 12 h at room temperature. The solution was then treated with saturated NH_4Cl (aq) (1 ml) and the solvent was removed under vacuum. The crude solid was then dissolved in CH_2Cl_2 (5 ml). The resulting solution was filtered and brought to dryness under vacuum. The resulting solid was washed by MeOH (15 ml) twice and dried under vacuum to afford diborane **34** as a yellow powder in 80 % yield. ^1H NMR (499.56 MHz, $CDCl_3$): δ 6.82 (s, 4 H, mes-C*H*), 6.76 (d, 1 H, J = 7.4 Hz, biphenylene-C*H*), 6.71-6.63 (m, 3 H, biphenylene-C*H*), 6.58 (d, 1 H, J = 6.6 Hz, biphenylene-C*H*), 6.45 (t, 1 H, J = 7.6 Hz, biphenylene-C*H*), 4.77 (d, 1 H, J = 7.4 Hz,

biphenylene-C*H*), 2.31 (s, 6 H, mes-C*H*$_3$), 2.13 (s, 12 H, mes-C*H*$_3$). ^{13}C NMR (125.62 MHz, $CDCl_3$): δ 159.88, 152.85, 152.09, 151.15, 141.34 (br), 140.46 (br), 138.80, 136.09 (br), 134.14, 128.47, 128.46, 128.31, 127.65, 119.16, 118.89, 116.82, 23.17 (br, mes-*C*H$_3$), 21.22 (mes-*C*H$_3$). ^{11}B (128.16 MHz, $CDCl_3$): δ 72.5 (br, Ar_3B). m.p. 164 ºC. Elemental analysis calculated (%) for C30H29B: C, 90.00; H, 7.30; found C, 89.72; H, 7.44.

Synthesis of 35. A solution of **33** (77 mg, 0.12 mmol, 1 equiv) in THF (10 ml) was slowly added a solution of TASF (32 mg, 0.12 mmol, 1 equiv) in CH_2Cl_2 (2 ml) under N_2 at room temperature. The solution was then stirred for 6 h under ambient condition in an open flask and a solution of $Al(NO_3)_3 \cdot 9H_2O$ (90 mg, 0.24 mmol, 2 equiv) in H_2O (10 ml) was added to the flask. The mixture was stirred for an additional 2 h and the solution was washed with CH_2Cl_2 (20 ml) twice. After separation, the combined organic layer was dried over anhydrous MgSO4 (1 g) and the solvent was then removed under vacuum. The resulting yellow solid was washed with hexanes (2 ml) and dried under vacuum to afford compound **35** as a yellow solid in 70% yield. 1H NMR (499.69 MHz, CDCl3): δ 6.76 (s , 2 H, mes-C*H*), 6.74 (s, 4 H, mes-C*H*), 6.73 (dd, 1 H, J = 8.07 Hz, J = 6.85 Hz, biphenylene-C*H*), 6.66 (m, 2 H, biphenylene-C*H*), 6.60-6.55 (m, 2 H, biphenylene-C*H*), 6.47 (dd, 1 H, J = 8.31 Hz, J = 0.98 Hz), 5.25 (s, 1 H, B-O*H*), 2.27 (s, 3 H, -C*H*$_3$), 2.24 (s, 6 H, -C*H*$_3$), 2.10 (br, 12 H, -C*H*$_3$), 1.91 (br, 6 H, -C*H*$_3$). ^{13}C{^{1}H} NMR (125.66 MHz, $CDCl_3$): δ 159.81, 157.20, 151.78, 151.61, 141.57 (br), 139.44, 137.94, 135.86, 132.67, 128.70 (br), 128.55, 127.53, 127.04, 118.16, 117.27, 23.74 (br, mes-*C*H3), 21.70 (mes-*C*H$_3$), 21.21 (mes-*C*H$_3$), 21.15 (mes-*C*H$_3$). ^{11}B{^{1}H} (128.16 MHz, $CDCl_3$): δ 73.3 (br, Ar_3B), 47.5 (br, Ar_2BOH).

m.p. 215 ºC. Elemental analysis calculated (%) for C39H40B2O: C, 85.74; H, 7.38; found C, 85.10; H, 7.42.

Synthesis of [TAS][35-F]. A solution of TASF (tris(dimethylamino)sulfonium difluorotrimethylsilicate, 70 mg, 0.25 mmol, 1 equiv) in CH_2Cl_2 was added into a solution of **33** (163 mg, 0.25 mmol, 1 equiv) in THF (8 ml) under N_2 at room temperature. The bright yellow color of the solution turned into pale yellow immediately after addition of 1 equiv of TASF. After stirring for an additional 1 h, the solvent was removed under vacuum. The resulting solid was washed with n-pentane (5 ml) twice and dried under vacuum to afford [TAS][**35**-F] as a pale-yellow solid in 85% yield. ^{1}H NMR (499.69 MHz, $CDCl_3$): δ 11.12 (d, 1 H, $^1J_{HF}$ = 57.2 Hz, B-OH), 6.65 (s, 2 H, mes-C*H*), 6.58 (d, 1 H, J = 8.1 Hz, biphenylene-C*H*), 6.55 (s, 4 H, mes-C*H*), 6.48-6.38 (m, 5 H, biphenylene-C*H*), 2.73 (s, 18 H, N-CH_3), 2.22 (s, 3 H, mes-CH_3), 2.17 (s, 6 H, mes-CH_3), 2.09 (s, 12 H, mes-CH_3), 1.94 (s, 6 H, mes-CH_3). ^{13}C{^{1}H} NMR (125.61 MHz, CD_3CN): δ 163.10, 163.09, 158.36, 158.34, 153.25, 151.45, 151.44, 142.52 (br), 139.28, 137.06, 137.02 ,136.99, 136.96, 133.01, 129.29, 127.37, 127.34, 126.86, 117.11, 113.73, 38.85 (N-*C*H_3), 25.38 (mes-*C*H_3), 21.88 (mes-*C*H_3), 21.30 (mes-*C*H_3), 21.02 (mes-*C*H_3). ^{11}B{^{1}H} (128.16 MHz, $CDCl_3$): δ 44.8 (br), 7.1 (s). ^{19}F (469.94 MHz, CD_3CN): δ -162.3 (br). m.p. 189 ºC. Elemental analysis calculated (%) for C45H58B2OFN3S·Et_2O: C, 73.22; H, 8.53; found C, 73.00; H, 8.08.

Alternative synthesis for [TAS][35-F]. A solution of TASF (tris(dimethylamino)sulfonium difluorotrimethylsilicate, 44 mg, 0.16 mmol, 1 equiv) in dry CH_2Cl_2 (2 ml) was slowly added into a flask containing a solution of **33** (104 mg, 0.16

mmol) in dry THF (5 ml) under N2 at room temperature. The flask was then opened to ambient atmosphere and the solution was stirred for an additional 6 h under air at room temperature. The solvent was then removed under vacuum and the resulting solid was washed by n-pentane (5 ml) twice to afford [TAS][**35**-F] as a pale-yellow solid in 91% yield.

CHAPTER IV

LARGE-BITE DIBORANES FOR THE μ(1,2) COMPLEXATION OF HYDRAZINE AND CYANIDE*

4.1 Introduction

The chemistry of main group-based polydentate Lewis acids[1-4, 85, 125, 189] has drawn considerable attention over the past decades, leading to application in anion sensing,[14-15, 28-30] anion transport,[33, 40, 42, 45-46, 48, 190] small molecule activation and catalysis.[62, 65, 77, 191-194] Diboranes featuring the rigid 1,8-naphthalenediyl[6-7, 9-10, 58, 195-196] or *ortho*-phenylene[11-13, 59, 71-72, 92, 197-198] backbones are the most studied examples of such systems. Owing to the short spacing of the two boron centers, these diboranes are well-suited for the chelation of monoatomic anions such as hydride,[6-7, 11] fluoride[7, 9-11] and chloride[12, 195] or polyatomic anions amenable to μ(1,1) ligation such as azide.[9, 13] The strength of the diborane host-anionic guest interaction in these system has led to the development of application in selective anion sensing[6-7, 9-11, 195] as well as catalysis.[10, 12-13, 194] Although no structural evidence has been obtained for the ditopic complexation of neutral molecules by diboranes of type **A** and **B** (Figure 59), it has been demonstrated recently that 9,10-dihydroanthracenes of type **C** are able to engage 1,2-diazines in complex formation and

---

* Reprinted in part with permission from: "Large-bite diboranes for the μ(1,2) complexation of hydrazine and cyanide"; Chen, C. -H.; Gabbaï, F. P. *Chem. Sci.* **2018**, *9*, 6210-6218. Copyright 2018 by The Royal Society of Chemistry.

catalyze their Diels Alder chemistry (Figure 59).[59-60, 199] The ability of **C** to complex 1,2-diazines is reminiscent of the adduct formed by 2,2′-diborabiphenyl and pyridazine.[200]

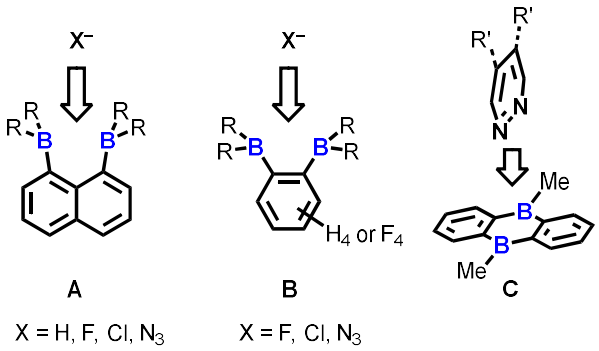

Figure 59. Diboranes of type **A**, **B** and **C**.

Bearing in mind that the selectivity of these diboranes for their respective guests is dictated by the size match that exists between the host and the guest, we have recently become interested in diboranes with an increased separation between the Lewis acidic centers. It occurred to us that such systems may display a different selectivity and may become well adapted to the μ(1,2) chelation of diatomic molecules.[91, 133, 201-202] We also speculated that the rigidity of the targeted diboranes may inform the molecular recognition properties of these bidentate Lewis acidic hosts.

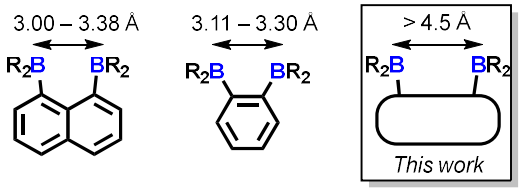

In this chapter, we report a series of results concerning the synthesis and properties of bidentate diboranes in which the two boron atoms are separated by more than 4.5 Å.

We also show that this increased separation allows for the selective μ(1,2) complexation of hydrazine and cyanide, two diatomic molecules that are known for their high toxicity.

4.2 Synthesis, characterization and properties of the diboranes

We have described the synthesis of 1,8-bis(dimesitylboryl)biphenylene (**30**) in Chapter III, a diborane in which the two boron atoms are separated by 4.566(5) Å. To assess the influence of the backbone over the properties of such large-bite diboranes, we have now decided to prepare its 1,8- triptycenediyl analogue (**36**). By analogy with the approach we employed to access **33**, diborane **36** was obtained via the dilithiation of 1,8-dibromotriptycene, followed by metathesis with Mes_2BF (Figure 60).

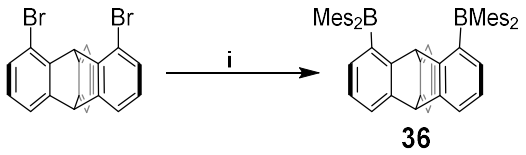

Figure 60. Synthesis of diborane **36**. i) 2.3 equiv *n*BuLi, 2.2 equiv Mes_2BF, THF, -78 ºC.

Compound **36** is a colorless air-stable solid which was isolated in moderate yield. The ^{1}H NMR signals of the triptycene backbone are consistent with a symmetrical structure. The detection of six sharp signals arising from the methyl groups and the four *meta*-H signals of the mesityl groups suggest that the molecule retains mirror symmetry in solution. The ^{11}B NMR spectrum shows a broad peak at 73.0 ppm which falls within the typical range expected for triarylboranes. The cyclic voltammogram (CV) of compound **36** shows two quasi-reversible reduction waves at -2.62 and -3.00 V vs Fc/Fc^{+}, suggesting that the molecule can be reduced by two electrons (Figure 61).

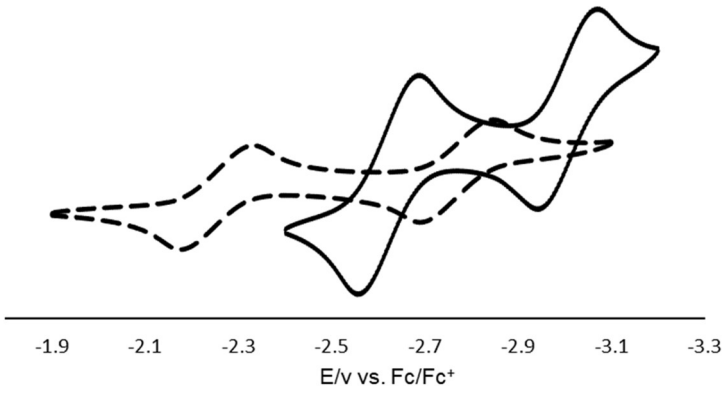

Figure 61. Cyclic voltammograms of **33** (dash line, $E_{1/2}$ = -2.23 and -2.74 V) and 36 (solid line, $E_{1/2}$ = -2.62 and -3.00 V) in THF. Scan rate = 100 mVs^{-1}.

Compared to the biphenylene derivative **33** for which the two reduction waves are observed at $E_{1/2}$ = -2.23 and -2.74 V (Figure 61), the first reduction of **36** is shifted toward cathodic potentials by 390 mV. This observation indicates that the biphenylene backbone is substantially more electron withdrawing. This conclusion is in agreement with two previous studies dealing with related biphenylene boron derivatives.[167, 203] Also, the shorter separation observed between the first and second reduction wave in **36** ($\Delta E_{1/2}$ = 0.51 V for **33** vs $\Delta E_{1/2}$ = 0.38 V for **36**) signals a decreased electronic communication between the boron atoms, an effect that we assign to the absence of extended conjugation in the triptycene backbone. The importance of electronic communication in **33** is further supported by the fact that the $\Delta E_{1/2}$ measured for **33** (0.51 V) is comparable to the largest value measured for naphthalene-based diboranes ($\Delta E_{1/2}$ range = 0.3 V - 0.52 V), a class of compounds in which the two boron atoms are separated by only 3.002-3.385 Å.[10, 204-205]

Computational studies show that the LUMO of **33** (Figure 62) is dominated by the two boron p_π orbitals which are in conjugation with the biphenylene π system. The makeup of this LUMO underscores the effective electronic communication that exists between the two boron centers.

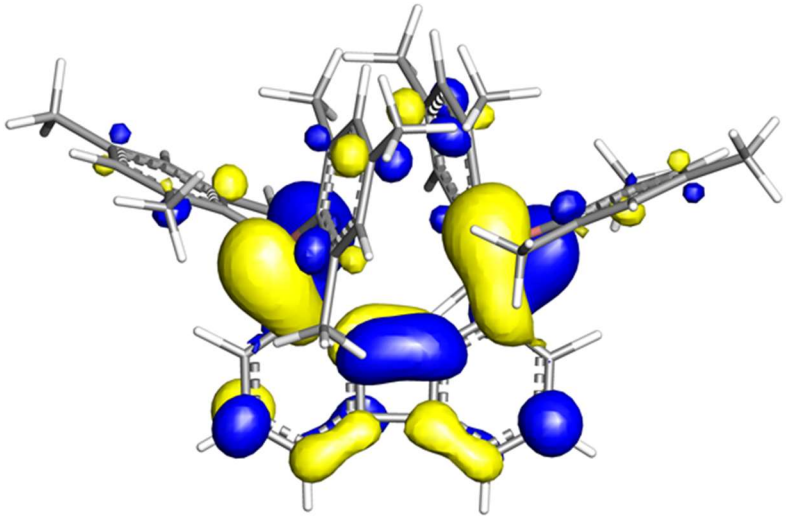

Figure 62. LUMO of **33** (isovalue = 0.03).

In the case of **36**, which lacks mirror symmetry because of steric repulsions between the mesityl substituents, the LUMO bears a larger contribution from the p_π orbital of one boron atom (Figure 63). The LUMO+1, which lies only 0.14 ev above the LUMO, shows a large contribution from the opposite boron atom (Figure 64). More importantly, π-conjugation between the two boron atoms in **36** is interrupted by the sp^3 triptycene bridgehead carbon atoms. These features corroborate the conclusion that the two boron atoms of **33** are in closer electronic communication than in **36**, as confirmed from the CV measurements.

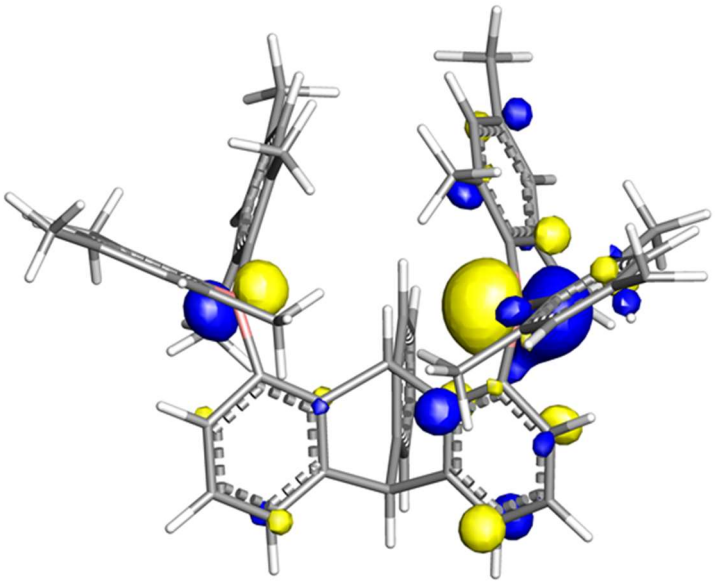

Figure 63. LUMO of **36** (isovalue = 0.05).

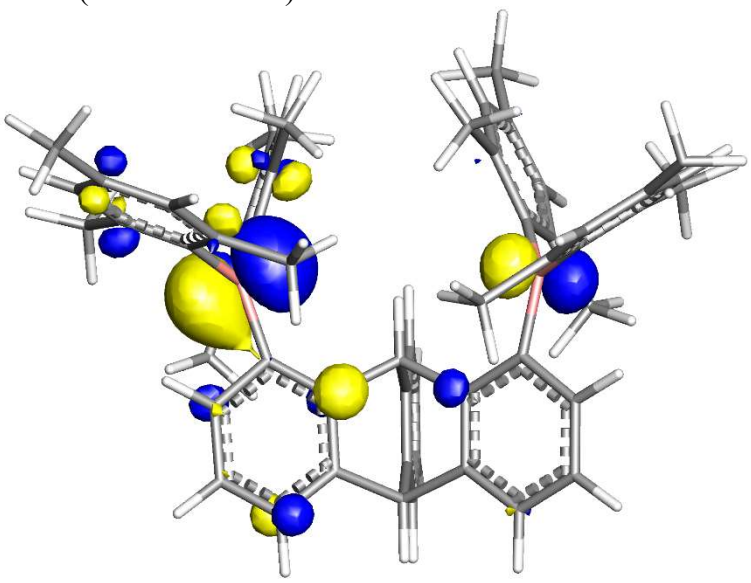

Figure 64. LUMO+1 of **36** (isovalue = 0.05).

Single crystals of compound **36** could be obtained by layering a solution of **36** in CH_2Cl_2 with MeOH. The solid-state structure of **36** shows that the boron atoms adopt a trigonal planar geometry as indicated by the sum of the C_{aryl}-B-C_{aryl} angles ($\sum_{\angle C\text{-}B1\text{-}C}$ = 359.7°, $\sum_{\angle C\text{-}B2\text{-}C}$ = 359.4°) (Figure 65).The B1-B2 separation of 5.559(4) Å in **36** is notably larger than that in **33** (4.566(5) Å) and the 1,8-bis(diphenylboryl)naphthalene (3.002(2) Å).[204]

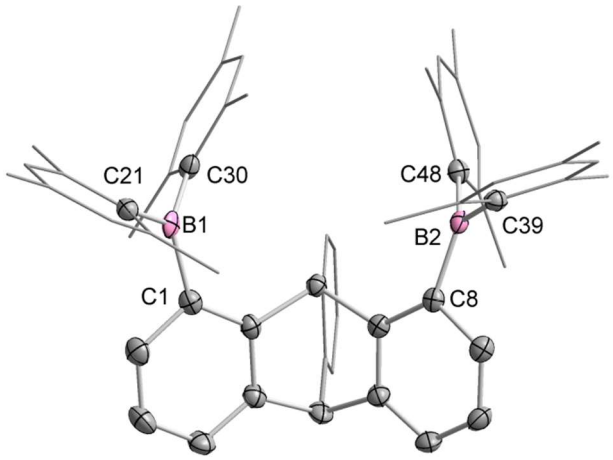

Figure 65. Solid-state structure of **36**. Thermal ellipsoids are drawn at the 50% probability level. The hydrogen atoms are omitted for clarity. Selected bond lengths [Å] and angles [°]: B1-C1 1.564(4), B1-C21 1.518(3), B1-C30, 1.571(4), B2-C8 1.572(4), B2-C39 1.577(4), B2-C48 1.570(4); C1-B1-C21 117.5(2), C1-B1-C30 119.1(2), C21-B1-C30 123.1(2), C8-B2-C39 117.6(2), C8-B2-C48 121.1(2), C39-B2-C48 120.7(2).

In $CHCl_3$/MeOH (1/1 vol.), the UV-Vis spectra of **33** and **36** feature a low-energy absorption band at 424 nm for **33** (Figure 66) and 316 nm for **36** (Figure 66). Time-dependent density functional theory (TD-DFT) calculations and Natural Transition Orbitals (NTO) analysis show the dominant HOMO-LUMO character of these transitions as observed for most triaryl boranes.[17, 175, 206-208] Both **33** and **36** are weakly fluorescent (QY = 0.05 for **33** and 0.04 for **36**) at a wavelength of 528 nm and 383 nm, respectively.

Given that the boron orbitals are involved in the LUMO of both derivatives, it can be anticipated that the coordination of Lewis bases to the tricoordinate boron centers will dramatically affect these spectral features.[5, 208-210]

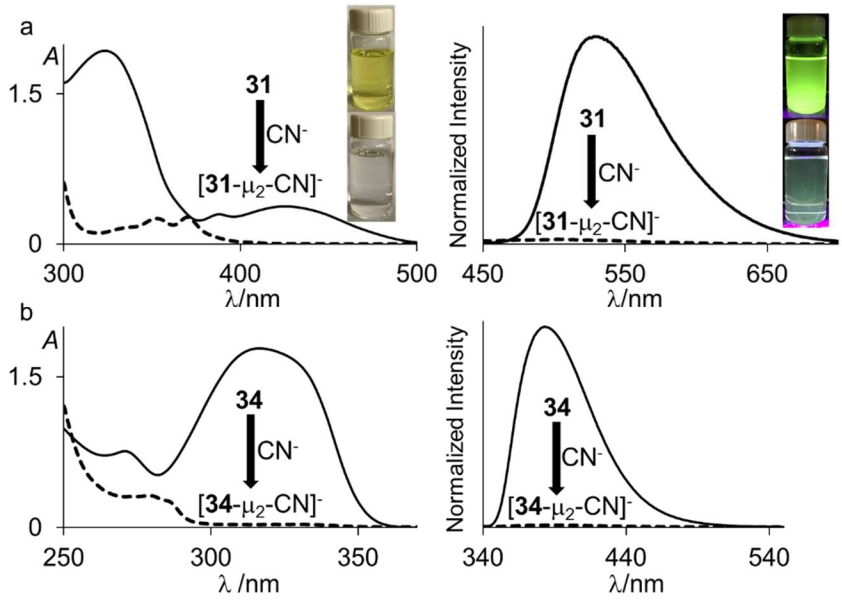

Figure 66. UV-Vis absorption (left) and emission (right) spectra of (a) **33** (solid line) and [**33**-μ_2-CN]$^-$ (dash line) (6.91×10^{-5} M, λ_{ex} = 370 nm) and (b) **36** (solid line) and [**36**-μ_2-CN]$^-$ (dash line) (6.22×10^{-5} M, λ_{ex} = 280 nm) in $CHCl_3$/MeOH (1/1 vol.). The pictures of the solutions were taken at the same concentration and the fluorescent images were illuminated with a hand-held UV lamp.

4.3 Reaction of diboranes with cyanide anion

With **33** and **36** at our disposal, we decided to focus on the case of anions and especially the cyanide anion which is known for its acute toxicity and which has often been considered as a target in molecular recognition assays,[81, 211-213] including using boron-based hosts.[22, 80, 209, 214-218]

Both diboranes quickly react with KCN in a CH_2Cl_2/MeOH (1/1 vol.) mixture containing dibenzo-18-crown-6. As expected, this reaction is accompanied by a quenching of both the absorption and emission band (Figure 66). In the case of **33**, these changes results in a distinct loss of both the yellow color and the green fluorescence of the starting diborane (Figure 66). Workup of these reactions afforded the corresponding cyanide complexes [**33**-μ_2-CN]$^-$ and [**36**-μ_2-CN]$^-$ as air-stable [K(dibenzo-18-crown-6)]$^+$ salts (Figure 67).

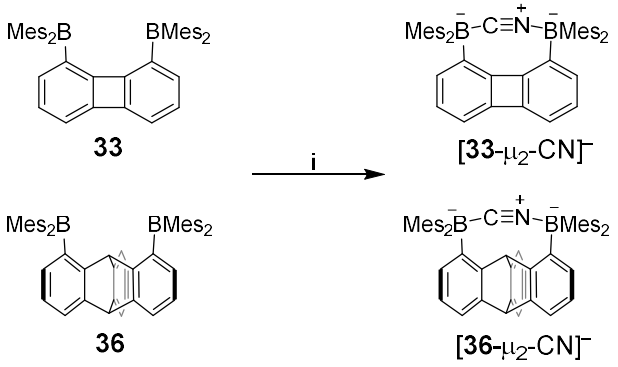

Figure 67. Synthesis of [**33**-μ_2-CN]$^-$ and [**36**-μ_2-CN]$^-$ as [K(dibenzo-18-crown-6)]$^+$ salts. i) 1 equiv KCN, 1 equiv dibenzo-18-crown-6, CH_2Cl_2/MeOH (1/1 vol.), rt.

The ^{11}B NMR signals detected for these anionic complexes (-15.8 ppm for [**33**-μ_2-CN]$^-$ and -11.7 ppm for [**36**-μ_2-CN]$^-$) are consistent with the existence of four-coordinate boron atoms. These signals are somewhat broad, possibly indicating the presence of two

closely spaced and overlapping resonances corresponding to the N_{CN}-bound and C_{CN}-bound boron atoms, respectively. The presence of the cyanide anion in these complexes is confirmed by IR spectroscopy which shows that, in both cases, the cyanide stretching frequency (ν_{CN} = 2229 cm^{-1} for **33** and 2184 cm^{-1} for **36**) is higher than that of free cyanide (ν_{CN} = 2158 cm^{-1}). The higher energy of these vibrations is typical of cyanoborates. This effect can be rationalized by invoking a stabilization of the π and π* molecular orbitals of the cyanide anion.[219] The absence of π-backbonding can also be invoked as a cause for this effect. The greater ν_{CN} observed for [**33**-μ_2-CN]$^-$ can be corroborated to the CV results and again suggest that the biphenylene backbone is more electron withdrawing than the triptycene backbone. The methyl region of the ^{1}H NMR spectrum recorded for both [**33**-μ_2-CN]$^-$ and [**36**-μ_2-CN]$^-$ as [K(dibenzo-18-crown-6)]$^+$ salts in $CDCl_3$ shows a level of complexity that is not consistent with equivalence of the two boryl moieties. We interpret these features as an evidence that the two boryl moieties are differentiated by their ligation to the C or N terminus of the cyanide anion.

Interestingly, diborane **33** and **36** appear to be highly selective for cyanide since no interaction with HCO_3^-, HSO_4^-, $H_2PO_4^-$, CH_3COO^-, Cl^-, Br^-, I^-, and N_3^- is observed in $CHCl_3$/MeOH (1/1 vol.) by UV-Vis spectrometry. Boranes are known to also display a large affinity for the fluoride anion. However, under these conditions, neither **33** nor **36** show any evidence of binding with fluoride. We propose that this selectivity is assisted by the specific architecture of the compounds that are well adapted to cyanide complexation (*vide infra*). However, considering that this selectivity could be biased by the protic nature of the medium which solvates the fluoride anion more effectively than the cyanide anion,

we also tested the reaction with fluoride in dry $CDCl_3$. When **33** and **36** were combined with TBAT, no changes were observed in the ^1H NMR spectra of the diboranes indicating the absence of any interaction. When $TBAF{\cdot}3H_2O$ was used in dry $CDCl_3$, **33** underwent hydrolysis as previously described in Chapter III while **36** remained unperturbed. Under the same conditions, both **33** and **36** quickly react with TBACN to give the corresponding cyanide complexes. These results show that these diboranes are also selective for cyanide in organic solvents. Such selectivity is not unprecedented in the chemistry of boron-based Lewis acids.[22, 80, 209, 214-218] Lastly, these diboranes do not react with $LiHBEt_3$ in dry $CDCl_3$.

The structures of the cyanide complexes as $[K(\text{dibenzo-18-crown-6})]^+$ salts have been investigated by single crystal X-ray diffraction which confirms the μ(1,2) chelation of the cyanide anions (Figure 68 and Figure 69). Both structures were solved on the basis of a model in which the cyanide anion is disordered over two overlapping head-to-tail positions, which as indicated by the refinements, contribute almost equally to the observed structures. In both structures, the boron atoms are distinctly pyramidal as indicated by the sum of the C_{aryl}-B-C_{aryl} angles which fall in the 341.7(4)°-343.2(4)° range for [**33**-μ_2-CN]$^-$ (Figure 68) and 342.0(5)°-344.6(5)° for [**36**-μ_2-CN]$^-$ (Figure 69). The accuracy of the crystallographic measurements does not allow for a comparison of the B-C_{CN} and B-N_{CN} bond distances which fall in the 1.54(4) Å-1.62(3) Å for [**33**-μ_2-CN]$^-$ and 1.63(5) Å-1.67(8) Å for [**36**-μ_2-CN]$^-$. The small difference of the B1-B2 separations in [**33**-μ_2-CN]$^-$ (4.187 (4) Å) and **33** (4.566(5) Å) reflects the rigidity of the molecule. Compared to **33**, the large variation of the B1-B2 separation on going from **36** (B1-B2 5.559(4) Å) to [**36**-μ_2-CN]$^-$

(B1-B2 4.321(5) Å) speaks to the flexibility of the triptycene backbone and its pincer ability toward the cyanide anion.

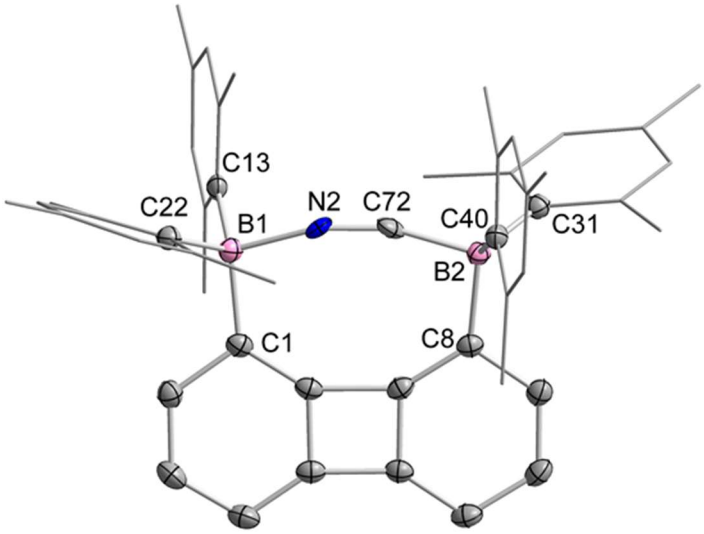

Figure 68. Solid-state structure of [K(dibenzo-18-crown-6)][**33**-μ_2-CN]-(CH_2Cl_2). Thermal ellipsoids are drawn at the 50% probability level. The $[K(dibenzo\text{-}18\text{-}crown\text{-}6)]^+$, the solvate molecules and the hydrogen atoms are omitted for clarity. The cyanide anions shown correspond to that with the higher positional occupancy. Selected bond lengths [Å] and angles [°]: B1-C1 1.635(4), B1-C13 1.649(4), B1-C22 1.639(4), B1-N2 1.58(2), B2-C8 1.641(4), B2-C31 1.643(4), B2-C40 1.657(3), B2-C72 1.54(4) C72-N2 1.21(4); C1-B1-C13 121.1(2), C13-B1-C22 113.8(2), C1-B1-C22 108.3(2), C1-B1-N2 100.9(7), C13-B1-N2 98.7(8), C22-B1-N2 112.9(7), B1-N2-C72 157.0(19), C8-B2-C31 108.4(2), C8-B2-C40 118.0(2), C31-B2-C40 115.3(2), C8-B2-C72 99.8(8), C31-B2-C72 115.8(9), C40-B2-C72 98.5(9), B2-C72-N2 163(2)

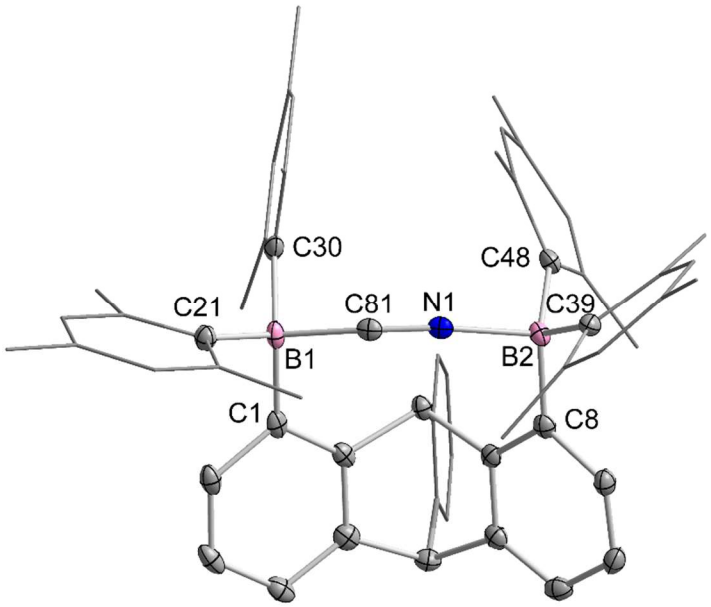

Figure 69. Solid-state structure of [K(dibenzo-18-crown-6)][**36**-μ_2-CN]-$(CH_2Cl_2)_2$. Thermal ellipsoids are drawn at the 50% probability level. The $[K(dibenzo\text{-}18\text{-}crown\text{-}6)]^+$, the solvate molecules and the hydrogen atoms are omitted for clarity. The cyanide anions shown correspond to that with the higher positional occupancy. Selected bond lengths [Å] and angles [º]: C1-B1 1.657(5), C21-B1 1.644(5), C30-B1 1.665(5), C81-B1 1.66(4), C81-N1 1.16(8), C8-B2 1.632(5), C39-B2 1.646(5), C48-B2 1.649(5), N1-B2 1.64(5); C1-B1-C21 109.1(3), C1-B1-C30 120.2(3), C21-B1-C30 112.7(3), C1-B1-C81 102.6(11), C21-B1-C81 111.4(16), C30-B1-C81 99.8(15), B1-C81-N1 158(6), C8-B2-C39 113.5(3), C8-B2-C48 113.1(3), C39-B2-C48 118.0(3), C8-B2-N1 99.8(15), C39-B2-N1 110.6(18), C48-B2-N1 99.1(13), B2-N1-C81 168(6).

The behavior of **33** and **36** and their ability to coordinate to both ends of the cyanide anion is reminiscent of the behavior of dicopper(II) complexes (**37**) which also form μ(1,2) cyanide complexes as described by Krämer (Figure 70).[220-221] This bonding mode differs from that observed for stibonium (**38**) and sulfonium boranes (**39**) in which the cyanide anion interact primarily with the boron atom, with a weak side on contact to the adjacent sulfonium or stibonium cation (Figure 70).[19, 22] Finally, it is important to point out that while [**33**-μ_2-CN]$^-$ and [**36**-μ_2-CN]$^-$ are the first bimolecular μ(1,2) complexes

formed by a diborane and cyanide, their core is reminiscent of that found in termolecular complexes of general formula $[Ar_3B\text{-}CN\text{-}BAr_3]^-$ (Ar = Ph or C_6F_5).[222-225]

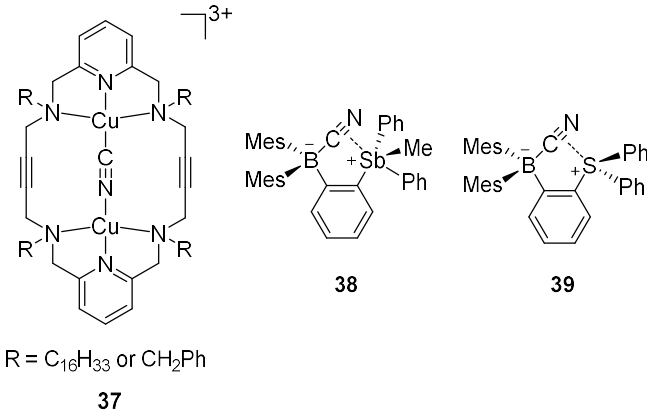

Figure 70. Dicopper(II) complexes (**37**), stibonium (**38**) and sulfonium boranes (**39**).

Since the CV data of **33** and **36** and the IR data of [**33**-μ_2-CN]$^-$ and [**36**-μ_2-CN]$^-$ suggest that **33** is a stronger Lewis acid than **36**, we became eager to experimentally confirm that **33** would indeed outcompete **36** with regard to cyanide binding. In accordance with this prediction, we observed, using ^{1}H NMR spectroscopy, the quantitative transfer of the cyanide anion from **36** to **33** when [^{n}Bu$_4$N][**36**-μ_2-CN] was mixed with an equimolar quantity of **33** in $CDCl_3/CD_3OD$ (1/1 vol.) at 60 °C over the course of 12 h (Figure 71). This observation confirms the higher cyanide ion affinity of **33** in protic solution, which is consistent with the electrochemical and IR measurements described above. Furthermore, a competition experiment was also performed with the monofunctional model borane Mes_2BPh. In these tests, the cyanide anion was transferred from $[Mes_2PhBCN]^-$ to **33** quantitatively in $CDCl_3/CD_3OD$ (1/1 vol.) at 60 °C (Figure 71). However, no transfer was observed between $[Mes_2PhBCN]^-$ and **36**. The absence of a

reaction points to the weaker cyanide affinity of **36** when compared to **33**. The reversibility of the cyanide binding was also investigated by allowing [^{n}Bu$_4$N][**33**-μ_2-CN] and [^{n}Bu$_4$N][**36**-μ_2-CN] to react with one equivalent of $(C_6F_5)_3B$ in $CDCl_3/CD_3OD$ (1/1 vol.).[226] Under these conditions, [**36**-μ_2-CN]$^-$ was readily converted into **36** while [**33**-μ_2-CN]$^-$ remained untouched, again supporting the superior Lewis acidity of **33**.

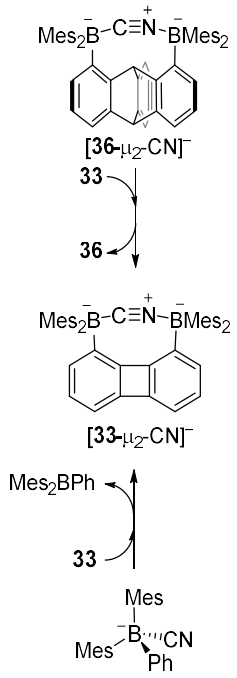

Figure 71. The competition reaction of [^{n}Bu$_4$N][**36**-μ_2-CN] and **33** (top) and [^{n}Bu$_4$N][Mes_2PhBCN] and **33** (bottom). The [^{n}Bu$_4$N]$^+$ cations are not shown for clarity.

4.4 Reactions of the diboranes with neutral diatomic molecules

Next in our survey of the properties of these diboranes, we decided to investigate the behavior of these two compounds in the presence of simple diatomic molecules including hydrogen peroxide, hydroxylamine and hydrazine. While complexes containing doubly coordinated peroxide[91, 133] and hydrazine[227-228] molecules have generated much interest in the context of energy related research, we also note that coordinated hydrazine has been identified as a possible intermediate in nitrogen fixation reactions.[201, 229-233] Because of its acute toxicity, there are also numerous ongoing efforts aimed at developing selective receptors for molecular recognition and sensing applications.[234]

Inspired by the recent discovery that perfluorinated boranes can doubly complex the peroxide and superoxide anion,[235-236] we first tested the reaction of **33** and **36** with 30% $H_2O_{2(aq)}$. Unfortunately, we observed decomposition, illustrating the vulnerability of these non-perfluorinated diboranes under oxidative conditions. We also tested the reaction of **33** and **36** with 50% $NH_2OH_{(aq)}$, which also resulted in decomposition of the hosts. By contrast, reaction of diborane **33** with hydrazine monohydrate ($N_2H_4 \cdot H_2O$) in THF proceeded smoothly to afford the corresponding hydrazine complex **33**-μ_2-N_2H_4 as an air- and moisture-stable off-white solid (Figure 72).

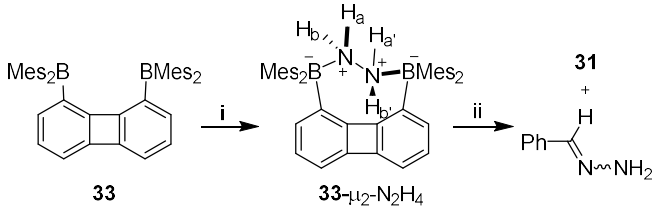

Figure 72. Synthesis of **33**-μ_2-N_2H_4 and the reaction of **33**-μ_2-N_2H_4 with benzaldehyde. i) 2.5 equiv $N_2H_4 \cdot H_2O$, THF, rt. ii) 1 equiv. benzaldehyde, $CDCl_3$, 60 ºC.

This reaction results in a distinct loss of the yellow color indicating coordination of the hydrazine to each boron atoms. The same effect is responsible for the observed quenching of the green fluorescence (Figure 73). In stark contrast, diborane **36** does not complex hydrazine under the same condition, even with a large excess of $N_2H_4 \cdot H_2O$. The lack of reactivity of **36** toward hydrazine may be correlated to its lower Lewis acidity as suggested by the CV measurements. It is also possible that the increased spacing between the two boron atoms, the lower rigidity of the backbone[164] and the presence of a bridgehead methine group interfere with the ability of **36** to bind hydrazine.

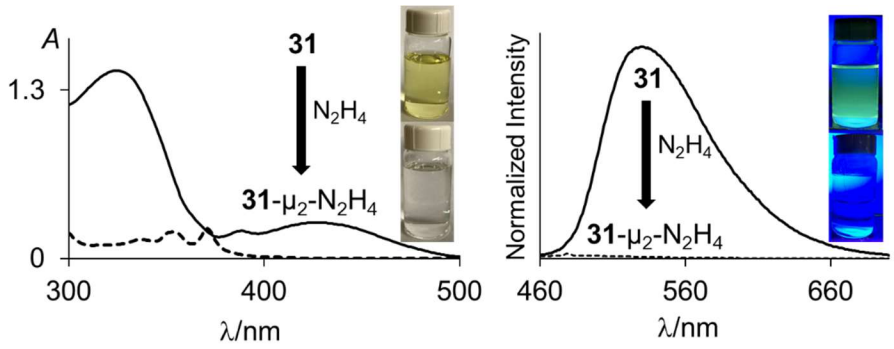

Figure 73. UV-Vis absorption (left) and emission (right) spectra of **33** (solid line) and **33**-μ_2-N_2H_4 (dash line) (4.52×10^{-5} M, λ_{ex} = 370 nm) in THF. The pictures of the solutions were taken at the same concentration and the fluorescent images were illuminated with a hand-held UV lamp.

The ^{1}H NMR spectrum recorded for the resulting hydrazine adduct **33**-μ_2-N_2H_4 in CD_2Cl_2 features six methyl-proton and four *meta*-proton resonances, indicating that the complex adopts C_2 symmetry in solution. The most conspicuous evidence for the formation of a B-NH_2-NH_2-B bridge is the detection of two broad multiplets at 5.15 and 6.29 ppm, indicating that the B-NH_2-NH_2-B unit gives rise to an AA'BB' spin system. These spectroscopic features also indicate that the conformation of the hydrazine molecule

in the diboron pocket is rigidly locked in solution. The solid-state structure of **33**-μ_2-N_2H_4 offers a consistent picture (Figure 74). This neutral complex crystalizes in the monoclinic *C*2/c space group with a half molecule in the asymmetric unit. The hydrazine nitrogen atoms are coordinated to the boron atoms via a B-N bond length of 1.688(2) Å which is longer than that in H_3B-NH_2-NH_2-BH_3 (1.609 Å)[237] but comparable to that recently reported by Szymczak for complex **40**-μ_2-N_2H_4 (1.697(2) Å and 1.698(2) Å) (Figure 75).[201]

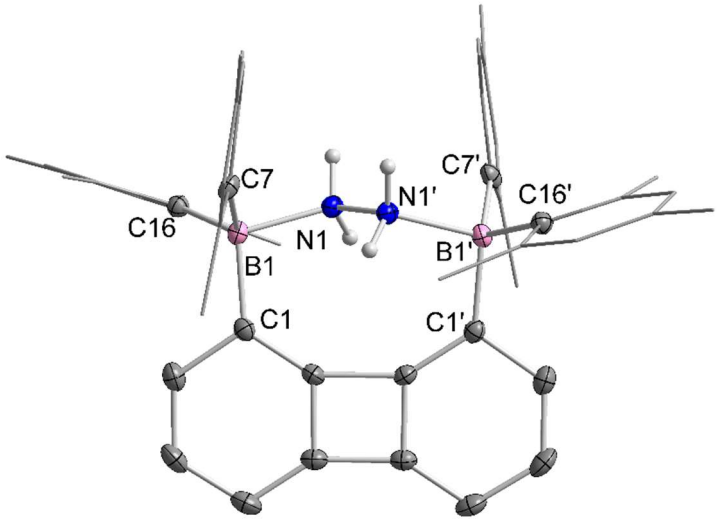

Figure 74. The solid-state structure of **33**-μ_2-N_2H_4. Thermal ellipsoids are drawn at the 50% probability level. The hydrogen atoms, except that bound to the nitrogen atoms, are omitted for clarity. Selected bond lengths [Å] and angles [º]: B1-N1 1.688(2), N1-N1‘ 1.469(2), B1-C1 1.627(2), B1-C7 1.651(2), B1-C16 1.647(2); B1-N1-N1‘ 113.7(1), C7-B1-C16 118.7(1), C1-B1-C7 119.7(1), C1-B1-C16 106.6(1).

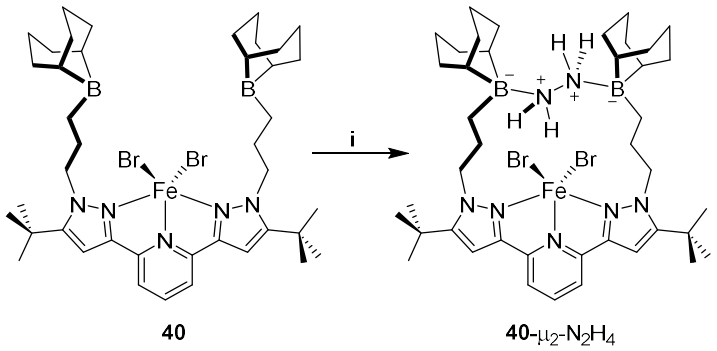

Figure 75. Reaction of Iron complex (**40**) with hydrazine to afford **40**-μ_2-N_2H_4 according to Szymczak et al.[201] i) 1 equiv N_2H_4, THF, rt.

The N-N bond length of 1.469(2) Å is similar to the N-N bond length determined previously in the literature.[238] This observation clearly indicates that diborane **33** is well suited for the chelation of hydrazine molecule. We also note that **D** can bind two hydrazine molecules, one at each boron atom. This is not the case of diborane **33** which only forms a 1:1 complex, even in the presence of an excess of hydrazine. This difference in behaviour illustrates the selectivity imparted by the rigid preorganization of the two boron atoms in **33**.[201]

To further establish the high affinity that **33** displays for hydrazine, we have studied the complexation under dilute conditions. We observed that diborane **33** is capable of capturing N_2H_4 from dilute aqueous solutions under biphasic conditions. Quantitative formation of **33**-μ_2-N_2H_4 was observed by ^{1}H NMR spectrometry when a solution of **33** in CH_2Cl_2 (1 mL, [**33**] = 7.7 mM) was stirred for 24 hours with an aqueous solution (2.5 mL) containing 1 weight% of N_2H_4. Complex **33**-μ_2-N_2H_4 is remarkably stable. It can be stored in air and shows no evidence of decomposition for months. It is also resistant to reactions with aldehydes. For example, **33**-μ_2-N_2H_4 failed to react with benzaldehyde in $CDCl_3$ at

room temperature over the course of 20 h. However, upon heating to 60 ºC, a clean, yet slow reaction is observed leading to the quantitative formation of the free diborane **33** and benzaldehyde hydrazone after 20 h as confirmed by ^{1}H NMR spectroscopy (Figure 72).[239]

4.5 1,8-Bis(methylium)biphenylenediyl dications

In an exploratory part of this work, we synthesized stable triarylmethylium cations, which are the isoelectronic analogues of triarylboranes. Like their boron counterparts, these carbocations constitute powerful Lewis acids which, for example, serve as anionic ligand abstractors in the olefin polymerization.[169, 240]

To obtain symmetrical biphenylene-based dications, we first reacted 1,8-dibromobiphenylene with *n*BuLi (2 equiv) to generate the corresponding dilithium salt *in situ*. The reaction mixture was then treated with xanthone to afford **41**-$(OH)_2$ after aqueous work up (Figure 76). The ^{1}H NMR spectrum of **41**-$(OH)_2$ in $CDCl_3$ displays the hydroxy proton resonance at 5.90 ppm and three proton resonances of the biphenylene backbone. These resonances confirm the formation of symmetrical **41**-$(OH)_2$.

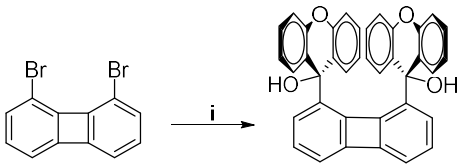

41-$(OH)_2$

Figure 76. Synthesis of **41**-$(OH)_2$. i) 2 equiv *n*BuLi, 2 equiv xanthone, Et_2O, rt.

By following a literature procedure,[241] dehydration of **41**-$(OH)_2$ with HBF_4 in trifluoroacetic anhydride (TFA anhydride) yielded an air- and moisture-stable dicationic species [**41**][BF_4]$_2$ as a dark green solid. The ^{1}H NMR spectrum of [**41**][BF_4]$_2$ in CD_3CN shows three biphenylene proton resonances, confirming the C_2 symmetry of the [**41**]$^{2+}$ in solution. Moreover, the ^{1}H NMR spectrum of [**41**][BF_4]$_2$ shows a distinct downfield shift

of all aromatic resonances with respect to **41**-$(OH)_2$, indicating the formation of the dication.

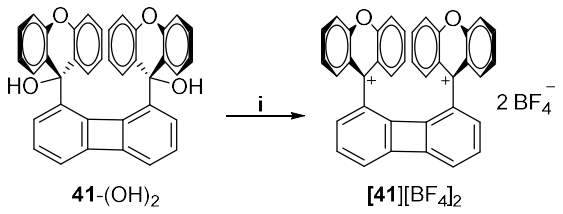

Figure 77. Synthesis of [**41**][BF_4]$_2$. i) excess $HBF_{4(aq)}$, TFA anhydride, rt.

Single crystals of [**41**][BF_4]$_2$ were obtained by slow diffusion of Et_2O into a CH_3CN solution of [**41**][BF_4]$_2$ at room temperature. The solid-state structure of [**41**][BF_4]$_2$ shown in Figure 78 features a C13-C26 separation of 4.065(2) Å which is shorter than that the B1-B2 separation in **33** (4.566(5) Å). This observation shows that two Lewis acidic units in [**41**]$^{2+}$ are not engaged in strong repulsive steric interactions. The cationic carbon atoms adopt a trigonal planar geometry as indicated by the sum of the C_{aryl}-C-C_{aryl} angles ($\sum\angle_{C\text{-}C13\text{-}C} = 360.0^o$, $\sum\angle_{C\text{-}C26\text{-}C} = 360.0^o$).

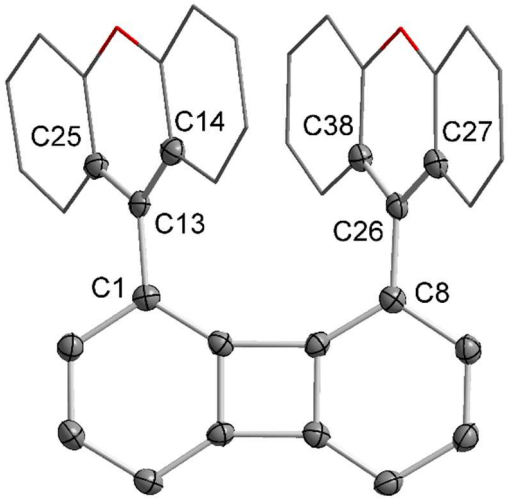

Figure 78. Solid-state structure of [**41**][BF_4]$_2$-(CH_3CN)$_2$. Thermal ellipsoids are drawn at the 50% probability level. The [BF_4]$^-$, the solvate molecules and the hydrogen atoms are omitted for clarity. Selected bond lengths [Å] and angles [°]: C1-C13 1.477(2), C13-C14 1.413(2), C13-C25 1.414(2), C8-C26 1.470(2), C26-C27 1.409(2), C26-C38 1.417(2), C1-C13-C14 121.4(1), C1-C13-C25 120.1(1), C14-C13-C25 118.5(1), C8-C26-C27 121.3(1), C8-C26-C38 119.9(1), C27-C26-C38 118.8(1).

By analogy with the aforementioned method, we also synthesized the dication [**42**][BF_4]$_2$ which features *para*-methoxyphenyl groups (Figure 79). The ^{1}H NMR spectrum of [**42**][BF_4]$_2$ in CD_2Cl_2 shows three proton resonances of the biphenylene backbone, indicating that the molecule adopts a C_2 symmetry in solution. The two broad aromatic resonances correspond to the *para*-methoxyphenyl groups reveal the dynamic movement of these phenyl groups at room temperature.

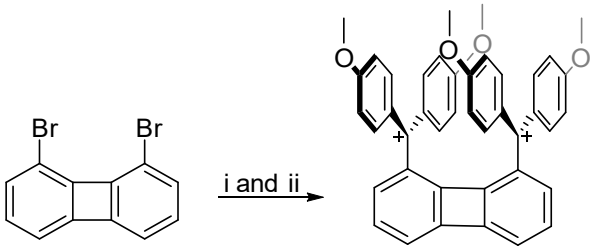

Figure 79. Synthesis of [**42**][BF_4]$_2$. i) 2 equiv *n*BuLi, 2 equiv 4,4'-dimethoxybenzophenone, Et_2O, rt. ii) excess HBF_4, excess TFA anhydride, rt.

The solid-state structure of [**42**][BF_4]$_2$ shows two trigonal planar carbon atoms as indicated by the sum of the C_{aryl}-C-C_{aryl} angles ($\sum_{\angle C\text{-}C13\text{-}C}$ = 360.0°, $\sum_{\angle C\text{-}C28\text{-}C}$ = 360.0°) (Figure 80). The separation between two cationic centers is 4.033(3) Å, comparable to that found in [**41**]$^{2+}$.

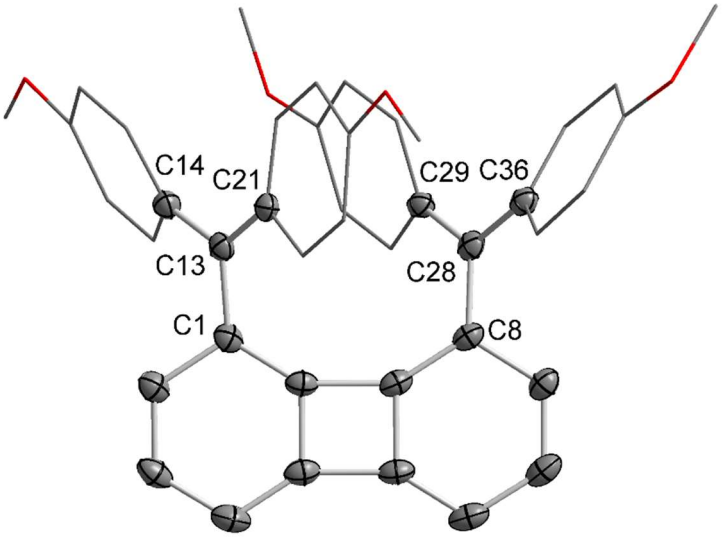

Figure 80. Solid-state structure of [42][BF_4]$_2$-(CH_2Cl_2). Thermal ellipsoids are drawn at the 50% probability level. The [BF_4]$^-$, the solvate molecules and the hydrogen atoms are omitted for clarity. Selected bond lengths [Å] and angles [°]: C1-C13 1.481(3), C13-C14 1.429(3), C13-C21 1.434(3), C8-C28 1.465(3), C28-C29 1.432(3), C28-C36 1.431(3), C1-C13-C14 116.3(2), C1-C13-C21 119.0(2), C14-C13-C21 124.7(2), C8-C28-C29 119.1(2), C8-C28-C36 117.9(2), C29-C28-C36 123.0(2).

4.6 Conclusions

In summary, we describe two "large-bite" diboranes that are ideally suited for the selective μ(1,2) complexation of hydrazine and cyanide, two diatomic molecules that are known for their high toxicity. The high selectivity displayed for these two specific molecules highlights the defining role played by the backbone. The most potent binder is the biphenylene-based diborane which complexes both hydrazine and cyanide while the triptycene derivative only binds cyanide. A similar picture emerges from competition experiments which show that **33** is a better molecular recognition unit for cyanide than **36**. Our results and analyses indicate that the enhanced properties of **33** arise from the electron withdrawing nature of the biphenylene backbone. We also propose that the rigidity of this diborane is a favorable factor that helps sequester hydrazine and the cyanide anion in the diboron pocket. This binding appears to be irreversible in the case of the cyanide anion. In the case of the hydrazine complex, we observe that slow release can triggered upon elevation of the temperature and in the presence of a reaction partner such as benzaldehyde. This last feature shows that such bidentate hosts could be used for the slow release of reactive compounds.

4.7 Experimental section

General considerations. *n*Butyllithium (2.65 M in hexane), $LiHBEt_3$ (1 M in THF) and $TBAF{\cdot}3H_2O$ were purchased from Alfa Aesar and used without further purification. TASF and TBAT were purchased from Sigma-Aldrich and used without further purification. Dimesitylboron fluoride (Mes_2BF) was purchased from TCI and used as received. 1, 8-Dibromobiphenylene and 1, 8-dibromotriptycene were synthesized by following the literature procedures.[105, 165] All preparations were carried out under a dry N_2 atmosphere employing either a glovebox or standard Schlenk techniques. Solvents were dried by passing through an alumina column (*n*-pentane and CH_2Cl_2) or by refluxing under N_2 over Na/K (Et_2O and THF). All other solvents were ACS reagent grade and used as received. NMR spectra were recorded on an Inova 500 FT NMR (499.41 MHz for ^1H) spectrometer, Varian NMRS 500RM NMR spectrometer (499.69 MHz for ^1H) or an Inova 400 FT NMR (399.46 MHz for ^1H) spectrometer at room temperature. Chemical shifts are given in ppm and are referenced to residual ^1H or ^{13}C solvent signals. Elemental analyses were performed by Atlantic Microlab (Norcross, GA).

Computational details. Density functional theory (DFT) structural optimizations were done with the Gaussian 09 program. In all cases, the structures were optimized using the B3LYP functional and the following mixed basis set: C/H, 6-31g; B, 6-31g+(d'). For all optimized structures, frequency calculations were carried out to confirm the absence of imaginary frequencies. The molecular orbitals were visualized and plotted using the Jimp2 program. The TD-DFT and NTO calculations were carried out using the MPW1PW91 functional and the above-mentioned basis sets.

Electrochemistry. Electrochemical experiments were performed with an electrochemical analyzer from CH Instruments (model 610A) with a glassy-carbon working electrode and a platinum auxiliary electrode. The reference electrode was built from a silver wire inserted into a small glass tube fitted with a porous Vycor frit at the tip and filled with a THF solution containing tetrabutylammonium hexafluorophosphate ($TBAPF_6$, 0.1 M) and $AgNO_3$ (0.005 M). All three electrodes were immersed in a deoxygenated THF solution (5 mL) containing $TBAPF_6$ (0.1 M) as a support electrolyte and the diboranes (1 and 2) (0.003 M). Ferrocene was used as an internal standard, and all potentials are reported with respect to $E_{1/2}$ of the Fc/Fc^+ redox couple.

Crystallographic details. The crystallographic measurements were performed at 110(2) K using a Bruker APEX-II CCD area detector diffractometer, with a graphite-monochromated Mo-Kα radiation (λ = 0.71073 Å). A specimen of suitable size and quality was selected and mounted onto a nylon loop. The semi-empirical method SADABS was applied for absorption correction. The structure was solved by direct methods, which successfully located most of the non-hydrogen atoms. Subsequent refinement on F^2 using the SHELXTL/PC package (version 6.1) allowed location of the remaining non-hydrogen atoms.

Table 6. Crystal data, data collection, and structure refinement for **36**.

Identification code	y
Empirical formula	C56 H56 B2
Formula weight	750.62
Temperature	110 K
Wavelength	0.71073 Å
Crystal system	Monoclinic
Space group	P 1 21/c 1
Unit cell dimensions	a = 11.785(3) Å b = 19.051(5) Å c = 19.029(5) Å a= 90°. b= 93.290(4)°. g = 90°.
Volume	4265.4(18) $Å^3$
Z	4
Density (calculated)	1.169 Mg/m^3
Absorption coefficient	0.065 mm^{-1}
F(000)	1608
Crystal size	0.4 x 0.18 x 0.1 mm^3
Theta range for data collection	1.514 to 27.566°.
Index ranges	-15<=h<=15, -24<=k<=24, -24<=l<=24
Reflections collected	48875
Independent reflections	9827 [R(int) = 0.1188]
Completeness to theta = 25.242°	100.00%
Absorption correction	Semi-empirical from equivalents
Max. and min. transmission	0.7456 and 0.6960
Refinement method	Full-matrix least-squares on F^2
Data / restraints / parameters	9827 / 0 / 535
Goodness-of-fit on F^2	1.01
Final R indices [I>2sigma(I)]	R1 = 0.0727, wR2 = 0.1230
R indices (all data)	R1 = 0.1521, wR2 = 0.1540
Largest diff. peak and hole	0.313 and -0.256 $e.Å^{-3}$

Table 7. Crystal data, data collection, and structure refinement for **33**-μ_2-N_2H_4.

Identification code	y_sq
Empirical formula	C48 H54 B2 N2
Formula weight	680.55
Temperature	110 K
Wavelength	0.71073 Å
Crystal system	Monoclinic
Space group	C 1 2/c 1
Unit cell dimensions	a = 18.849(3) Å b = 11.5959(16) Å c = 20.422(3) Å a= 90°. b= 106.9137(18)°. g = 90°.
Volume	4270.7(10) $Å^3$
Z	4
Density (calculated)	1.058 Mg/m^3
Absorption coefficient	0.060 mm^{-1}
F(000)	1464
Crystal size	0.91 x 0.53 x 0.3 mm^3
Theta range for data collection	2.085 to 27.548°.
Index ranges	-24<=h<=24, -15<=k<=15, -26<=l<=26
Reflections collected	46117
Independent reflections	4928 [R(int) = 0.0259]
Completeness to theta = 25.242°	100.00%
Absorption correction	Semi-empirical from equivalents
Max. and min. transmission	0.7456 and 0.6876
Refinement method	Full-matrix least-squares on F^2
Data / restraints / parameters	4928 / 0 / 241
Goodness-of-fit on F^2	1.042
Final R indices [I>2sigma(I)]	R1 = 0.0512, wR2 = 0.1412
R indices (all data)	R1 = 0.0567, wR2 = 0.1471
Largest diff. peak and hole	0.453 and -0.376 $e.Å^{-3}$

Table 8. Crystal data, data collection, and structure refinement for [K(dibenzo-18-crown-6)][**33**-μ_2-CN]-(CH_2Cl_2).

Identification code	d
Empirical formula	C71 H78 B2 Cl4 K N O6
Formula weight	1243.86
Temperature	110 K
Wavelength	0.71073 Å
Crystal system	Monoclinic
Space group	P 1 21/c 1
Unit cell dimensions	a = 15.4096(14) Å b = 23.693(2) Å c = 19.0628(17) Å a= 90°. b= 112.9484(11)°. g = 90°.
Volume	6409.0(10) $Å^3$
Z	4
Density (calculated)	1.289 Mg/m^3
Absorption coefficient	0.303 mm^{-1}
F(000)	2624
Crystal size	0.5 x 0.3 x 0.2 mm^3
Theta range for data collection	2.074 to 27.614°.
Index ranges	-20<=h<=20, -30<=k<=30, -24<=l<=24
Reflections collected	140726
Independent reflections	14800 [R(int) = 0.0670]
Completeness to theta = 25.242°	99.80%
Absorption correction	Semi-empirical from equivalents
Max. and min. transmission	0.7456 and 0.6917
Refinement method	Full-matrix least-squares on F^2
Data / restraints / parameters	14800 / 36 / 801
Goodness-of-fit on F^2	1.074
Final R indices [I>2sigma(I)]	R1 = 0.0543, wR2 = 0.1549
R indices (all data)	R1 = 0.0805, wR2 = 0.1724
Largest diff. peak and hole	0.915 and -1.201 $e.Å^{-3}$

Table 9. Crystal data, data collection, and structure refinement for [K(dibenzo-18-crown-6)][**36** -μ_2-CN]-$(CH_2Cl_2)_2$.

Identification code	y
Empirical formula	C79 H83 B2 Cl4 K N O6
Formula weight	1344.98
Temperature	110 K
Wavelength	0.71073 Å
Crystal system	Monoclinic
Space group	C 1 c 1
Unit cell dimensions	a = 21.407(3) Å b = 13.6932(18) Å c = 23.988(3) Å α = 90°. β = 92.4764(14)°. γ = 90°.
Volume	7025.2(16) $Å^3$
Z	4
Density (calculated)	1.272 Mg/m^3
Absorption coefficient	0.282 mm^{-1}
F(000)	2836
Crystal size	0.49 x 0.36 x 0.22 mm^3
Theta range for data collection	1.942 to 26.507°.
Index ranges	-26<=h<=26, -17<=k<=17, -30<=l<=30
Reflections collected	70236
Independent reflections	14546 [R(int) = 0.0661]
Completeness to theta = 25.242°	100.00%
Absorption correction	Semi-empirical from equivalents
Max. and min. transmission	0.7454 and 0.6939
Refinement method	Full-matrix least-squares on F^2
Data / restraints / parameters	14546 / 2 / 858
Goodness-of-fit on F^2	1.023
Final R indices [I>2sigma(I)]	R1 = 0.0452, wR2 = 0.1119
R indices (all data)	R1 = 0.0538, wR2 = 0.1181
Absolute structure parameter	0.002(16)
Largest diff. peak and hole	0.463 and -0.555 $e.Å^{-3}$

Table 10. Crystal data, data collection, and structure refinement for [**41**][BF_4]$_2$-(CH_3CN)$_2$.

Identification code	y
Empirical formula	C42 H28 B2 F8 N2 O2
Formula weight	766.28
Temperature	110(2) K
Wavelength	0.71073 Å
Crystal system	Triclinic
Space group	P-1
Unit cell dimensions	a = 8.4490(12) Å b = 13.8583(19) Å c = 15.553(2) Å α = 105.774(5)° β = 97.654(5)° γ = 90.195(5)°
Volume	1735.4(4) Å^3
Z	2
Density (calculated)	1.466 Mg/m^3
Absorption coefficient	0.119 mm^{-1}
F(000)	784
Crystal size	1.00 x 0.46 x 0.21 mm^3
Theta range for data collection	1.37 to 27.70°.
Index ranges	-10<=h<=10, -18<=k<=17, 0<=l<=20
Reflections collected	7988
Independent reflections	7988 [R(int) = 0.0000]
Completeness to theta = 27.70°	98.3 %
Absorption correction	Semi-empirical from equivalents
Max. and min. transmission	0.9755 and 0.8905
Refinement method	Full-matrix least-squares on F^2
Data / restraints / parameters	7988 / 0 / 571
Goodness-of-fit on F^2	1.018
Final R indices [I>2sigma(I)]	R1 = 0.0385, wR2 = 0.1003
R indices (all data)	R1 = 0.0479, wR2 = 0.1091
Largest diff. peak and hole	0.706 and -0.444 e.Å^{-3}

Table 11. Crystal data, data collection, and structure refinement for [**42**][BF_4]$_2$-(CH_2Cl_2).

Identification code	y
Empirical formula	C42.25 H34.50 B2 Cl0.50 F8 O4
Formula weight	797.54
Temperature	110(2) K
Wavelength	0.71073 Å
Crystal system	Triclinic
Space group	P-1
Unit cell dimensions	a = 8.320(6) Å b = 18.008(13) Å c = 24.936(18) Å α = 83.776(8)° β = 81.633(8)° γ = 86.698(8)°
Volume	3671(5) $Å^3$
Z	4
Density (calculated)	1.443 Mg/m^3
Absorption coefficient	0.153 mm^{-1}
F(000)	1642
Crystal size	0.39 x 0.30 x 0.15 mm^3
Theta range for data collection	1.66 to 27.54°.
Index ranges	-10<=h<=10, -23<=k<=23, 0<=l<=32
Reflections collected	16661
Independent reflections	16661 [R(int) = 0.0000]
Completeness to theta = 27.54°	98.4 %
Absorption correction	Semi-empirical from equivalents
Max. and min. transmission	0.9775 and 0.9428
Refinement method	Full-matrix least-squares on F^2
Data / restraints / parameters	16661 / 0 / 1035
Goodness-of-fit on F^2	1.024
Final R indices [I>2sigma(I)]	R1 = 0.0505, wR2 = 0.1234
R indices (all data)	R1 = 0.0802, wR2 = 0.1449
Largest diff. peak and hole	0.552 and -1.322 $e.Å^{-3}$

Determinations of quantum yield.[242] Quantum yields were determined relative to fluorescein (λ_{ex} = 470 nm) in 0.1 M NaOH as a standard (Φ=0.91). Absorbance measurements were taken on a Shimadzu UV-2502PC UV-Vis spectrophotometer. Fluorescence measurements were taken on samples in capped quartz cuvettes under air on a PTI QuantaMaster spectrofluorometer with entrance and exit slit widths of 2 nm and an integration time of 1 s. Fluorescence quantum yields were calculated based on the gradients of integrated emission (IE) versus absorbance at λ_{ex} (Abs) for a series of measurements on the sample or fluorescence standard, according to the following equation:[243]

$$\Phi_{sample} = \Phi_{std} \times \frac{IE_{sample}}{IE_{std}} \times \frac{Abs_{std}}{Abs_{sample}} \times \left(\frac{\eta_{sample}}{\eta_{std}}\right)^2$$

$$= \Phi_{std} \times \frac{Grad_{sample}}{Grad_{std}} \times \left(\frac{\eta_{sample}}{\eta_{std}}\right)^2$$

where η was 1.334 for 0.1 M NaOH and 1.407 for THF solutions. The resulting gradient plots obtained are shown in Figure 81 for compound **33** and **36**.

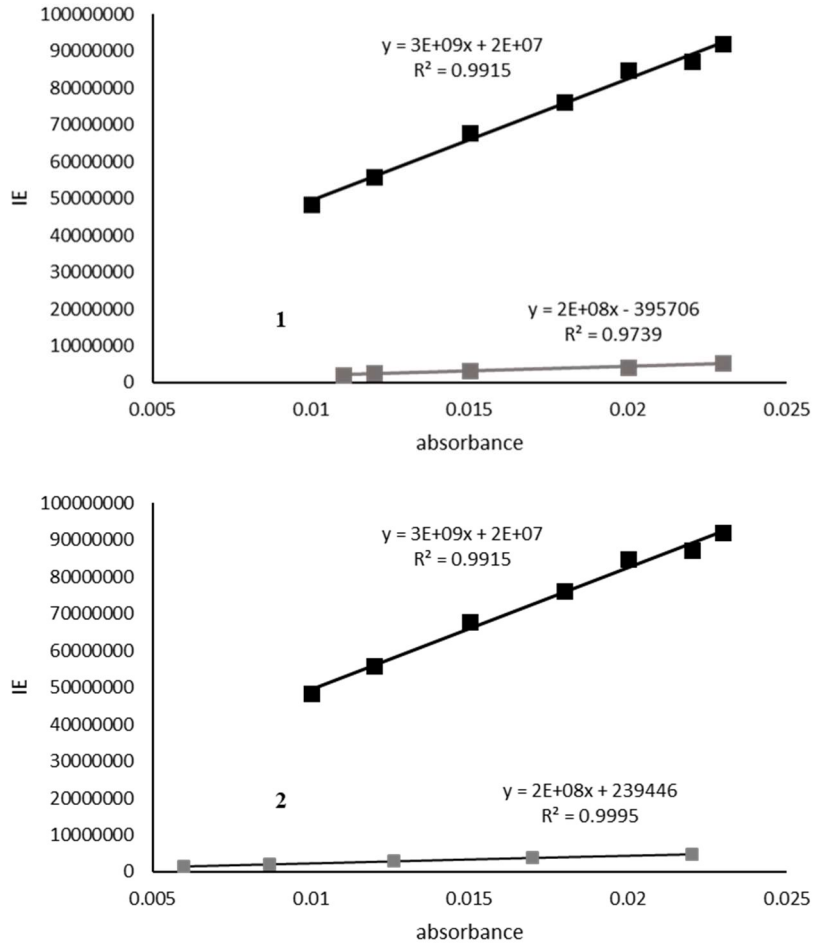

Figure 81. Plots of integrated emission (IE) vs. absorbance at λ_{ex} for **33** (top) and **36** (bottom) and fluorescein.

Synthesis of 36. ^{n}BuLi (2.65 M, 1 mL, 2.65 mmol) was slowly added to a solution of 1,8-dibromotriptycene (500 mg, 1.2 mmol) in dry THF (8 mL) under N_2 at -78 °C. After 30 min of stirring at low temperature, a solution of Mes_2BF (715 mg, 2.6 mmol) in THF (5 mL) was slowly transferred into the reaction flask using a cannula. The resulting solution was stirred for an additional 12 h at room temperature. The solution was then treated with saturated $NH_4Cl_{(aq)}$ (1 mL) and the solvent was removed under vacuum. The resulting white solid was then dissolved in CH_2Cl_2 (5 mL). The resulting solution was filtered and brought to dryness under vacuum. The off-white solid was then washed with MeOH (15 mL) twice and dried under vacuum to afford diborane **36** as a white powder in 60 % yield. ^{1}H NMR (399.50 MHz, 25 °C, $CDCl_3$): δ 7.49 (d, 2 H, $^{3}J_{H-H}$ = 6.6 Hz, triptycene-C*H*), 7.23 (d, 1 H, $^{3}J_{H-H}$ = 7.0 Hz, triptycene-C*H*), 6.97 (pseudo t, 2 H, $^{3}J_{H-H}$ = 7.4 Hz, triptycene-C*H*), 6.90 – 6.86 (m, 3 H, triptycene-C*H*), 6.82 (s, 2 H, mes-C*H*), 6.77 (s, 2 H, mes-C*H*), 6.73 (s, 2 H, mes-C*H*), 6.61 (pseudo t, 1 H, $^{3}J_{H-H}$ = 7.4 Hz, triptycene-C*H*), 6.35 (s, 2 H, mes-C*H*), 5.40 (s, 1 H, triptycene-C*H*), 5.30 (d, 1 H, $^{3}J_{H-H}$ = 7.4 Hz, triptycene-C*H*), 5.16 (s, 1 H, triptycene-C*H*), 2.34 (s, 6 H, -C*H*$_3$), 2.30 (s, 6 H, -C*H*$_3$), 2.17 (s, 6 H, -C*H*$_3$), 2.13 (s, 6 H, -C*H*$_3$), 1.79 (s, 6 H, -C*H*$_3$), 0.60 (s, 6 H, -C*H*$_3$) ppm. ^{13}C NMR (100.46 MHz, 25 °C, $CDCl_3$): δ 150.86, 145.50, 145.23, 144.42, 144.27, 143.12, 141.52, 141.17, 140.90, 140.77, 139.89, 138.58, 138.57, 131.21, 129.92, 129.90, 128.47, 128.14, 127.90, 126.58, 126.17, 125.05, 124.16, 123.50, 121.60, 55.45 (triptycene-*C*H), 54.26 (triptycene-*C*H), 25.20 (-*C*H$_3$), 24.96 (-*C*H$_3$), 22.37 (-*C*H$_3$), 22.03 (-*C*H$_3$), 21.39 (-*C*H$_3$), 21.25 (-*C*H$_3$) ppm. ^{11}B (128.16 MHz, 25 °C, $CDCl_3$): δ 73.0 (br) ppm. Elemental analysis calculated (%) for $C_{56}H_{56}B_2$: C, 89.60; H, 7.52; found C, 89.62; H, 7.47.

Synthesis of 33-μ$_2$-N$_2$H$_4$. A solution of $N_2H_4 \cdot H_2O$ (20 mg, 0.4 mmol) in THF (2 mL) was combined with a solution of diborane **33** (100 mg, 0.154 mmol) in THF (5 mL) at room temperature. The resulting solution was stirred for an additional hour and brought to dryness under vacuum. The resulting solid was washed twice with MeOH (5 mL) to afford **33**-μ$_2$-N_2H_4 as a off-white powder in 90 % yield. ^{1}H NMR (499.48 MHz, 25 ºC, CD_2Cl_2): δ 6.85 (s, 2 H, mes-C*H*), 6.80 (s, 2 H, mes-C*H*), 6.68 (s, 2 H, mes-C*H*), 6.57 (s, 2 H, mes-C*H*), 6.55 - 6.50 (m, 6 H, biphenylene-C*H*), 6.31 – 6.28 (m, 2 H, -N*H*$_2$-), 5.17 – 5.13 (m, 2 H, -N*H*$_2$-), 2.25 (s, 6 H, -C*H*$_3$), 2.24 (s, 6 H, -C*H*$_3$), 2.15 (s, 6 H, -C*H*$_3$), 1.80 (s, 6 H, -C*H*$_3$), 1.74 (s, 6 H, -C*H*$_3$), 1.67 (s, 6 H, -C*H*$_3$) ppm. ^{13}C NMR (125.61 MHz, 25 ºC, CD_2Cl_2): δ 151.26, 149.80, 143.94, 141.61, 139.50, 137.63, 137.42, 136.01, 135.58, 132.50, 131.24, 130.65, 130.60, 128.00, 115.17, 26.77(-*C*H$_3$), 25.72(-*C*H$_3$), 23.61(-*C*H$_3$), 23.21(-*C*H$_3$), 21.07(-*C*H$_3$), 20.87(-*C*H$_3$) ppm. ^{11}B (128.16 MHz, 25 ºC, $CDCl_3$): not observed. Elemental analysis calculated (%) for $C_{48}H_{54}B_2N_2 \bullet 0.93 \times CHCl_3$: C, 74.24; H, 6.99; found C, 74.22; H, 7.03. This EA result indicates the crystal sample obtain from $CHCl_3$/MeOH contains interstitial solvent molecules. This view is consistent with result of the crystallographic measurements which show the presence of disordered interstitial solvents equivalent to an electron count of 59 as indicated by application of the SQUEEZE protocol.[244] This electron count corresponds exactly to the number of electrons of a chloroform molecule (58). The EA results suggest partial loss of the interstitial chloroform molecule.

Synthesis of [K(dibenzo-18-crown-6)][33-μ$_2$-CN]. A solution of KCN (10 mg, 0.15 mmol) in MeOH (2 mL) was slowly added at room temperature into a CH_2Cl_2

solution (10 mL) containing **33** (100 mg, 0.15 mmol) and dibenzo-18-crown-6 (56 mg, 0.15 mmol). The resulting colorless solution was stirred for an additional 1 h at room temperature. The solvent was removed under vacuum and the resulting solid was washed by Et_2O (10 mL) twice to afford [K(dibenzo-18-crown-6)][**33**-μ_2-CN] as a white powder in 90 % yield. ^{1}H NMR (499.53 MHz, 25 ^{o}C, $CDCl_3$): δ 7.00-6.97 (m, 4 H, -C_6H_4-), 6.84-6.79 (m, 4 H, -C_6H_4-), 6.66 (t, 2 H, ^{3}J = 8.78 Hz, biphenylene-C*H*), 6.50 (br, 8 H, mes-C*H*), 6.20-6.16 (m, 2 H, biphenylene-C*H*), 6.10 (d, ^{3}J = 6.34 Hz, biphenylene-C*H*), 4.03-4.01 (m, 8 H, -CH_2-), 3.76-3.74 (m, 8 H, -CH_2-), 2.13 (br, 12 H, -CH_3), 1.84 (br, 24 H, -CH_3) ppm. ^{1}H NMR (399.46 MHz, -50 ^{o}C, $CDCl_3$): δ 6.95-6.94 (m, 4 H, -C_6H_4-), 6.77-6.74 (m, 4 H, -C_6H_4-), 6.67 (t, 2 H, ^{3}J = 9.34 Hz, biphenylene-C*H*), 6.58-6.52 (m, 6 H, mes-C*H*), 6.41 (s, 1 H, mes-C*H*), 6.39 (s, 1 H, mes-C*H*), 6.19-6.12 (m, 4 H, biphenylene-C*H*), 3.94 (br, 8 H, -CH_2-), 3.37 (br, 8 H, -CH_2-), 2.18 (s, 6 H, -CH_3), 2.14 (s, 3 H, -CH_3), 2.11 (s, 3 H, -CH_3), 2.05 (s, 6 H, -CH_3), 1.84-1.80 (m, 12 H, -CH_3), 1.70 (s, 6 H, -CH_3) ppm. ^{13}C NMR (125.62 MHz, 25 ^{o}C, $CDCl_3$): δ 158.33, 157.36, 150.05, 146.14, 137.01, 136.28, 132.48, 132.37, 128.55, 124.36, 122.25, 112.02, 111.77, 80.29, 68.97 (-*C*H_2-), 66.59 (-*C*H_2-), 24.44 (-*C*H_3), 20.82 (-*C*H_3) ppm. ^{11}B (128.16 MHz, 25 ^{o}C, $CDCl_3$): δ -15.8 ppm. IR ν_{CN} = 2229 cm^{-1}. Elemental analysis calculated (%) for $C_{69}H_{74}B_2KO_6 \cdot 0.55 \times CH_2Cl_2$: C, 75.48; H, 6.84; found C, 75.49; H, 6.78. These EA results indicate partial loss of the interstitial solvent molecules.

Synthesis of [K(dibenzo-18-crown-6)][36-μ_2-CN]. A solution of KCN (10 mg, 0.15 mmol) in MeOH (2 mL) was slowly added at room temperature into a CH_2Cl_2 solution (10 mL) containing **36** (116 mg, 0.15 mmol) and dibenzo-18-crown-6 (56 mg,

0.15 mmol). The resulting colorless solution was stirred for an additional 1 h at room temperature. The solvent was removed under vacuum and the resulting solid was washed by Et_2O (10 mL) twice to afford [K(dibenzo-18-crown-6)][**36**-μ_2-CN] as a white powder in 88 % yield. ^{1}H NMR (499.49 MHz, 25 ^{o}C, CD_2Cl_2): δ 7.32 (d, 1 H, $^3J_{H-H}$ = 7.3 Hz, triptycene-C*H*), 7.09 (d, 2 H, $^3J_{H-H}$ = 7.3 Hz, triptycene-C*H*), 7.04 – 6.98 (m, 5 H), 6.93 – 6.88 (m, 6 H), 6.84 (d, 1 H. $^3J_{H-H}$ = 7.3 Hz, triptycene-C*H*), 6.66 (s, 2 H, mes-C*H*), 6.58 (pseudo t, 2 H, $^3J_{H-H}$ = 7.3 Hz, triptycene-C*H*), 6.53 (s, 1 H, mes-C*H*), 6.52 (s, 2 H, mes-C*H*), 6.48 (s, 1 H, mes-C*H*), 6.41 (d, 1 H, $^3J_{H-H}$ = 7.8 Hz, triptycene-C*H*), 6.37 (d, 1 H, $^3J_{H-H}$ = 7.8 Hz, triptycene-C*H*), 6.31 (s, 1 H, mes-C*H*), 6.27 (s, 1 H, mes-C*H*), 5.74 (s, 1 H, triptycene-C*H*), 5.26 (s, 1 H, triptycene-C*H*), 4.18 – 4.16 (m, 8 H, -C*H*$_2$-), 3.93 – 3.91 (m, 8 H, -C*H*$_2$-), 2.25 (s, 3 H, -C*H*$_3$), 2.23 (s, 3 H, -C*H*$_3$), 2.19 (s, 6 H, -C*H*$_3$), 2.14 (s, 3 H, -C*H*$_3$), 2.02 (s, 3 H, -C*H*$_3$), 2.00 (s, 3 H, -C*H*$_3$), 1.95 (s, 3 H, -C*H*$_3$), 1.63 (s, 3 H, -C*H*$_3$), 1.62 (s, 3 H, -C*H*$_3$), 1.18 (s, 3 H, -C*H*$_3$), 1.13 (s, 3 H, -C*H*$_3$) ppm. ^{13}C NMR (125.61 MHz, 25 ^{o}C, CD_2Cl_2): δ 151.30, 150.72, 147.52, 146.65, 146.59, 144.42, 144.27, 143.19, 142.76, 142.53, 142.21, 141.89, 141.66, 140.88, 133.17, 130.01, 132.75, 132.63, 131.47, 131.34, 129.29, 129.12, 129.02, 128.90, 128.73, 128.60, 128.15, 126.69, 124.49, 123.46, 122.85, 122.57, 122.48, 121.56, 120.50, 120.40, 111.95, 69.85 (-*C*H$_2$-), 67.21 (-*C*H$_2$-), 56.15 (triptycene-*C*H), 51.86 (triptycene-*C*H), 26.87 (-*C*H$_3$), 25.97 (-*C*H$_3$), 25.91 (-*C*H$_3$), 25.77 (-*C*H$_3$), 25.55 (-*C*H$_3$), 25.48 (-*C*H$_3$), 24.79 (-*C*H$_3$), 24.48 (-*C*H$_3$), 21.24 (-*C*H$_3$), 20.86 (-*C*H$_3$) ppm. ^{11}B (128.16 MHz, 25 ^{o}C, $CDCl_3$): δ -11.7 ppm. IR ν_{CN} = 2184 cm^{-1}. Elemental analysis calculated (%) for $C_{77}H_{80}B_2KNO_6 \cdot 0.43 \times CH_2Cl_2$: C, 76.69; H, 6.72; found C, 76.70; H, 6.71. These EA results indicate partial loss of the interstitial solvent molecules.

Stability test for 33-μ_2-N_2H_4 in the presence of benzaldehyde. A solution of **33**-μ_2-N_2H_4 (5 mg,7.3 μmol) in $CDCl_3$ (0.25 ml) was combined in an NMR tube with a solution of benzaldehyde (1 mg, 9.0 μmol) in $CDCl_3$ (0.25 ml). The mixture was allowed to react at room temperature for 24 h, at which point no reaction was observed by ^{1}H NMR spectrometry. The same reaction mixture was then warmed to 60 ºC for 20 h. The quantitative formation of diborane **33** and benzaldehyde hydrazone was confirmed by ^{1}H NMR spectroscopy.

Reactivity of 33 toward ^{n}Bu$_4$NF. Diborane **33** (3.5 mg, 5.4 μmol) was added into a solution of tetrabutylammonium fluoride trihydrate (1.7 mg, 5.4 μmol, TBAF·3H_2O) in $CDCl_3$/CD_3OD (0.25 ml/0.25 ml) in an NMR tube at room temperature. No reaction was observed by ^{1}H NMR spectroscopy after 1 h and 12 h.

Reactivity of 36 toward ^{n}Bu$_4$NF. Diborane **36** (3.0 mg, 4.0 μmol) was added into a solution of tetrabutylammonium fluoride trihydrate (1.3 mg, 4.0 μmol, TBAF·3H_2O) in $CDCl_3$/CD_3OD (0.25 ml/0.25 ml) in an NMR tube at room temperature. No reaction was observed by ^{1}H NMR spectroscopy after 1 h and 12 h.

Reactivity of 33 toward [^{n}Bu$_4$N][Ph$_3$SiF$_2$]. [^{n}Bu$_4$N][Ph_3SiF_2] (4.2 mg, 7.7 μmol) was added into a solution of diborane **33** (5.0 mg, 7.7 μmol) in dry $CDCl_3$ (0.5 ml) in an NMR tube at room temperature. No reaction was observed by ^{1}H NMR spectroscopy after 5 h.

Reactivity of 36 toward [^{n}Bu$_4$N][Ph$_3$SiF$_2$]. [^{n}Bu$_4$N][Ph_3SiF_2] (4.0 mg, 6.7 μmol) was added into a solution of diborane **36** (5.0 mg, .6.7 μmol) in dry $CDCl_3$ (0.5 ml) in an

NMR tube at room temperature. No reaction was observed by ^{1}H NMR spectroscopy after 5 h.

Reactivity of 36 toward [(Me$_2$N)$_3$S][Me$_3$SiF$_2$]. [(Me$_2$N)$_3$S][Me$_3$SiF$_2$] (1.9 mg, 6.7 μmol) was added into a solution of diborane **36** (5.0 mg, 6.7 μmol) in dry $CDCl_3$ (0.5 ml) in an NMR tube at room temperature. No reaction was observed by ^{1}H NMR spectroscopy after 5 h.

Reactivity of 33 toward LiHBEt$_3$. A solution of diborane **33** (3.0 mg, 4.6 μmol) in dry $CDCl_3$ (0.5 ml) was added a solution of $LiHBEt_3$ in THF (1 M, 20 μL, 20 μmol) in an NMR tube at room temperature. No reaction was observed by ^{1}H NMR spectroscopy after 1 h.

Reactivity of 36 toward LiHBEt$_3$. A solution of diborane **36** (5.0 mg, 4.0 μmol) in dry $CDCl_3$ (0.5 ml) was added a solution of $LiHBEt_3$ in THF (1 M, 20 μL, 20 μmol) in an NMR tube at room temperature. No reaction was observed by ^{1}H NMR spectroscopy after 1 h.

Reactivity of 33 toward HCO_3^-, HSO_4^-, $H_2PO_4^-$, CH_3COO^-, Cl^-, Br^-, I^-, and N_3^-. A solution of **33** (6.2×10^{-5} M, 3 ml) in $CHCl_3$/CH_3OH (v/v =1/1) was allowed to react with excess amount of [^{n}Bu$_4$N][Cl] (1 mg), [^{n}Bu$_4$N][Br] (1 mg), [^{n}Bu$_4$N][I] (1 mg), [^{n}Bu$_4$N][CH_3COO] (1 mg) and [^{n}Bu$_4$N][N_3] (1 mg) sequentially in a cuvette. UV-Vis spectra were taken after each addition and no reaction was observed. To the same solution, the saturated aqueous solution of $NaHCO_3$ (20 μL), NaH_2PO_4 (20 μL) and $NaHSO_4$ (20 μL) were added sequentially into the cuvette. No reaction was observed after each addition by UV-Vis spectrometry.

Reactivity of 36 toward HCO_3^-, HSO_4^-, $H_2PO_4^-$, CH_3COO^-, Cl^-, Br^-, I^-, and N_3^-. A solution of **36** (4.2×10^{-5} M, 3 ml) in $CHCl_3/CH_3OH$ (v/v =1/1) was allowed to react with excess amount of $[^nBu_4N][Cl]$ (1 mg), $[^nBu_4N][Br]$ (1 mg), $[^nBu_4N][I]$ (1 mg), $[^nBu_4N][CH_3COO]$ (1 mg) and $[^nBu_4N][N_3]$ (1 mg) sequentially in a cuvette. UV-Vis spectra were taken after each addition and no reaction was observed. To the same solution, the saturated aqueous solution of $NaHCO_3$ (20 μL), NaH_2PO_4 (20 μL) and $NaHSO_4$ (20 μL) were added sequentially into the cuvette. No reaction was observed after each addition by UV-Vis spectrometry.

Reaction of 33 with [^{n}Bu$_4$N][36-μ$_2$-CN]. Diborane **36** (2.8 mg, 3.7 μmol) was added to a solution of tetrabutylammonium cyanide (1.0 mg, 3.7 μmol, TBACN) in $CDCl_3$/CD_3OD (0.25 ml/0.25 ml) in an NMR tube at room temperature. The quantitative formation of [^{n}Bu$_4$N][**36**-μ$_2$-CN] was confirmed by ^{1}H NMR spectroscopy after 5 h. At this point, a slight excess of diborane **33** (3 mg, 4.6 μmol) was directly added into the tube as a solid and the resulting mixture was warmed to 60 ºC for an addition 12 h. During this time, **33** which formed a suspension in the solvent was slowly consumed. Formation of free diborane **36** and [**33**-μ$_2$-CN]$^-$ was confirmed by ^{1}H NMR spectroscopy.

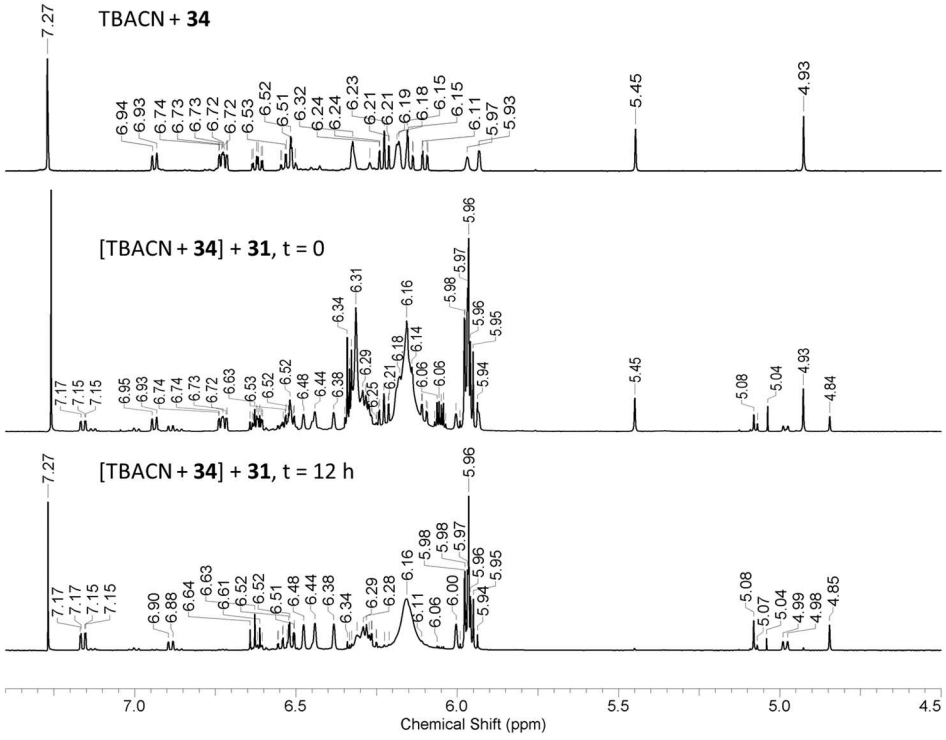

Figure 82. ^{1}H NMR monitoring of the reaction of **33** with [^{n}Bu$_4$N][**36**-μ$_2$-CN] in $CDCl_3$.

Reaction of 33 with [^{n}Bu$_4$N][Mes$_2$PhBCN]. Mes$_2$BPh (3.2 mg, 9.7 μmol) was added to a solution of tetrabutylammonium cyanide (2.6 mg, 9.7 μmol, TBACN) in $CDCl_3$/CD_3OD (0.25 ml/0.25 ml) in an NMR tube at room temperature. The formation of [^{n}Bu$_4$N][Mes$_2$PhBCN] was confirmed by ^{1}H NMR spectroscopy after 1 h. At this point, diborane **33** (6.3 mg, 9.7 μmol) was directly added into the tube as a solid and the resulting mixture was warmed to 60 ºC for an addition 12 h. During this time, **33** which formed a suspension in the solvent was slowly consumed. Formation of Mes$_2$BPh and [**33**-μ_2-CN]$^-$ was confirmed by ^{1}H NMR spectroscopy.

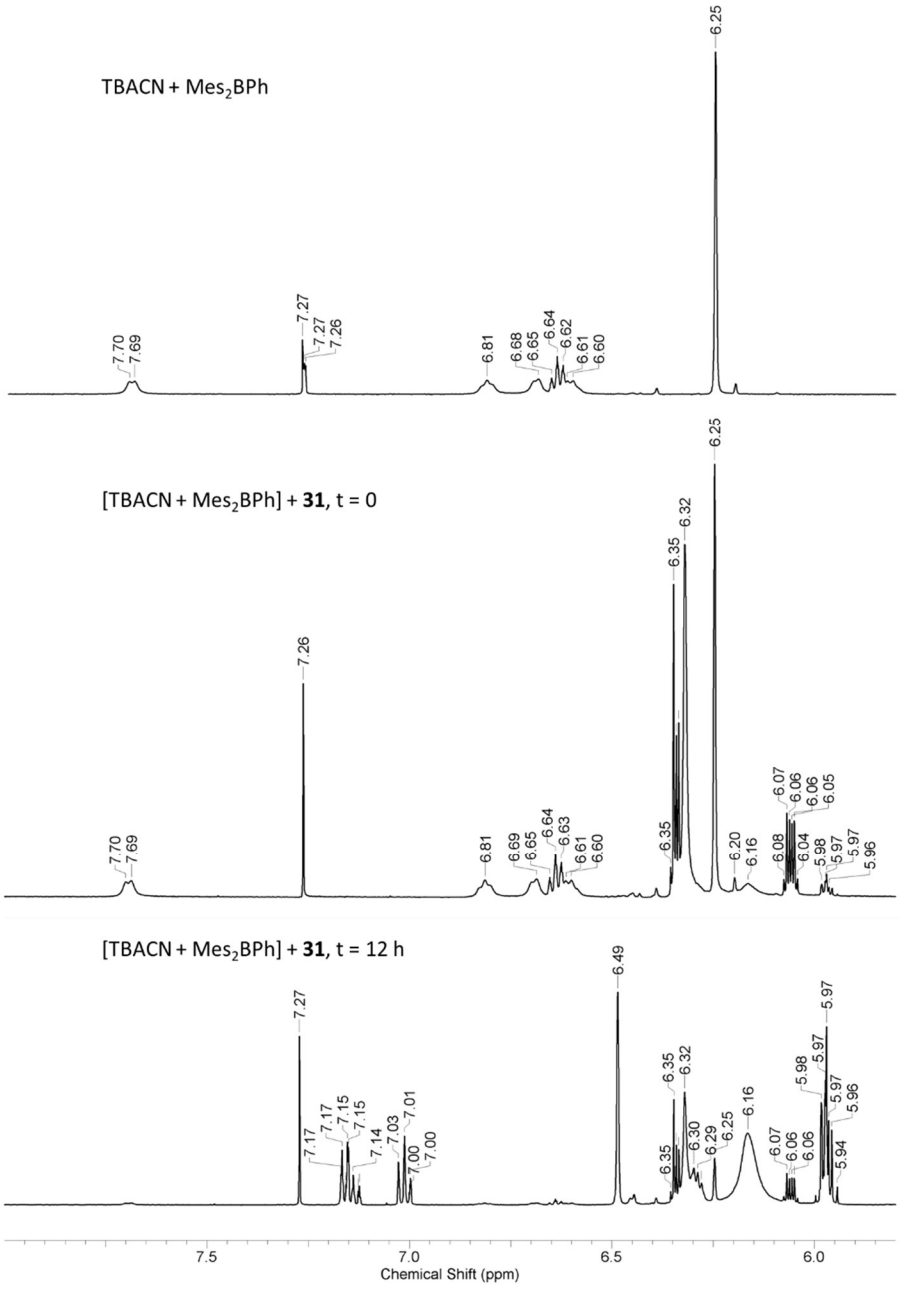

Figure 83. ^{1}H NMR monitoring of the reaction of **33** with [^{n}Bu$_4$N][Mes$_2$PhBCN] in $CDCl_3$.

Reaction of $(C_6F_5)_3B$ with $[^nBu_4N][33\text{-}\mu_2\text{-}CN]$. Diborane **33** (3.0 mg, 4.6 μmol) was added to a solution of tetrabutylammonium cyanide (1.2 mg, 4.6 μmol, TBACN) in $CDCl_3/CD_3OD$ (0.25 ml/0.25 ml) in an NMR tube at room temperature. The quantitative formation of $[^nBu_4N][1\text{-}\mu_2\text{-}CN]$ was confirmed by ^1H NMR spectroscopy after 5 h. At this point, a slight excess of $(C_6F_5)_3B$ (3 mg, 5.9 μmol) was directly added into the tube and the mixture was sonicated for an additional hour. No reaction was observed by ^1H NMR spectroscopy after 1 h and 12 h.

Reaction of $(C_6F_5)_3B$ with [^{n}Bu$_4$N][36-μ_2-CN]. Diborane **36** (2.6 mg, 3.5 μmol) was added to a solution of tetrabutylammonium cyanide (1.0 mg, 3.7 μmol, TBACN) in $CDCl_3/CD_3OD$ (0.25 ml /0.25 ml) in an NMR tube at room temperature. The quantitative formation of [^{n}Bu$_4$N][**36**-μ_2-CN] was confirmed by ^{1}H NMR spectroscopy after 5 h. At this point, a slight excess of $(C_6F_5)_3B$ (2 mg, 3.9 μmol) was directly added into the tube and the mixture was sonicated for an additional hour. Formation of free diborane **36** was confirmed by ^{1}H NMR spectroscopy.

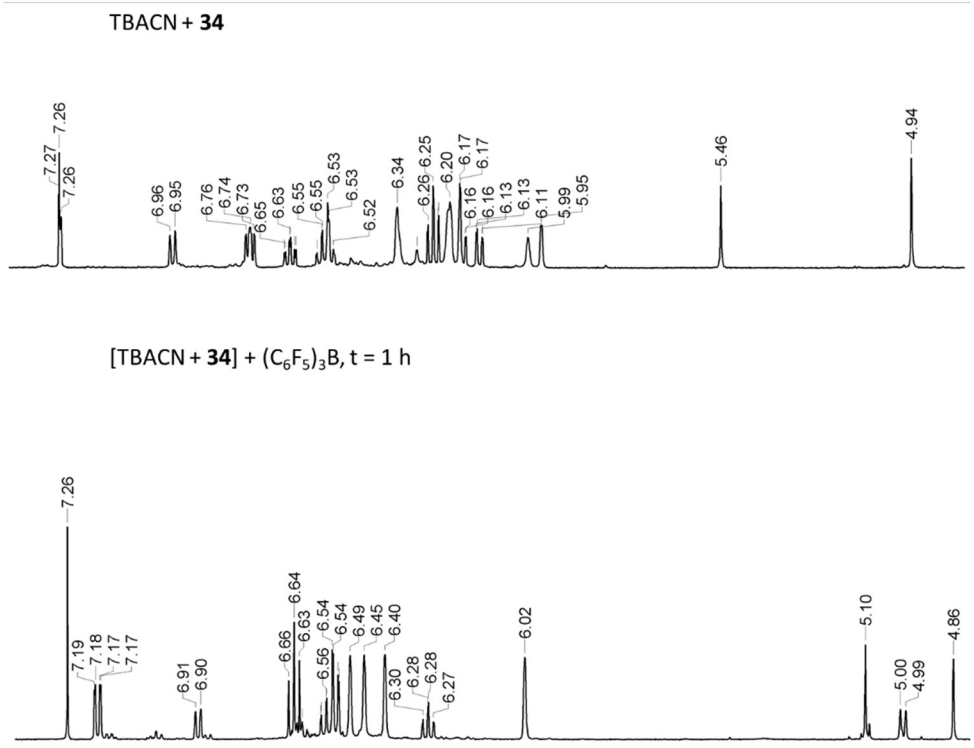

Figure 84. ^{1}H NMR monitoring of the reaction of $(C_6F_5)_3B$ with [^{n}Bu$_4$N][**36**-μ_2-CN] in $CDCl_3$.

Synthesis of 41-$(OH)_2$. ^{n}BuLi (2.65 M, 1.1 mL, 2.92 mmol) was slowly added to a solution of 1,8-dibromobiphenylene (370 mg, 1.2 mmol) in dry Et_2O (5 mL) under N_2 at room temperature. After 30 min of stirring, a solution of xanthone (540 mg, 2.8 mmol) in Et_2O (5 mL) was slowly transferred into the reaction flask using a cannula. The resulting solution was stirred for an additional 12 h at room temperature. The solution was then treated with saturated $NH_4Cl_{(aq)}$ (1 mL) and the solvent was removed under vacuum. The resulting white solid was then dissolved in CH_2Cl_2 (5 mL). The resulting solution was filtered and brought to dryness under vacuum. The off-white solid was then washed with Et_2O (15 mL) twice and dried under vacuum to afford diborane **41**-$(OH)_2$ as a white powder in 81 % yield. ^{1}H NMR (499.55 MHz, 25 ^{o}C, $CDCl_3$, Figure 85): δ 7.69 (dd, 4 H, $^{3}J_{H\text{-}H}$ = 7.8 Hz, $^{4}J_{H\text{-}H}$ = 1.5 Hz), 7.30 (pseudo t, 4 H, $^{3}J_{H\text{-}H}$ = 6.3 Hz), 7.16 (d, 4 H, $^{3}J_{H\text{-}H}$ = 7.3 Hz),7.11 (t, 4 H, $^{3}J_{H\text{-}H}$ = 7.3 Hz), 6.63-6.58 (m, 4 H, biphenylene-C*H*), 6.13 (d, 2 H, $^{3}J_{H\text{-}H}$ = 7.3 Hz, biphenylene-C*H*), 5.67 (s, 2 H, -O*H*) ppm. ^{13}C NMR (125.62 MHz, 25 ^{o}C, $CDCl_3$, Figure 86): δ 150.21, 149.79, 147.70, 140.69, 131.28, 130.19, 129.28, 128.15, 125.56, 123.43, 116.47, 114.31, 71.78 ppm.

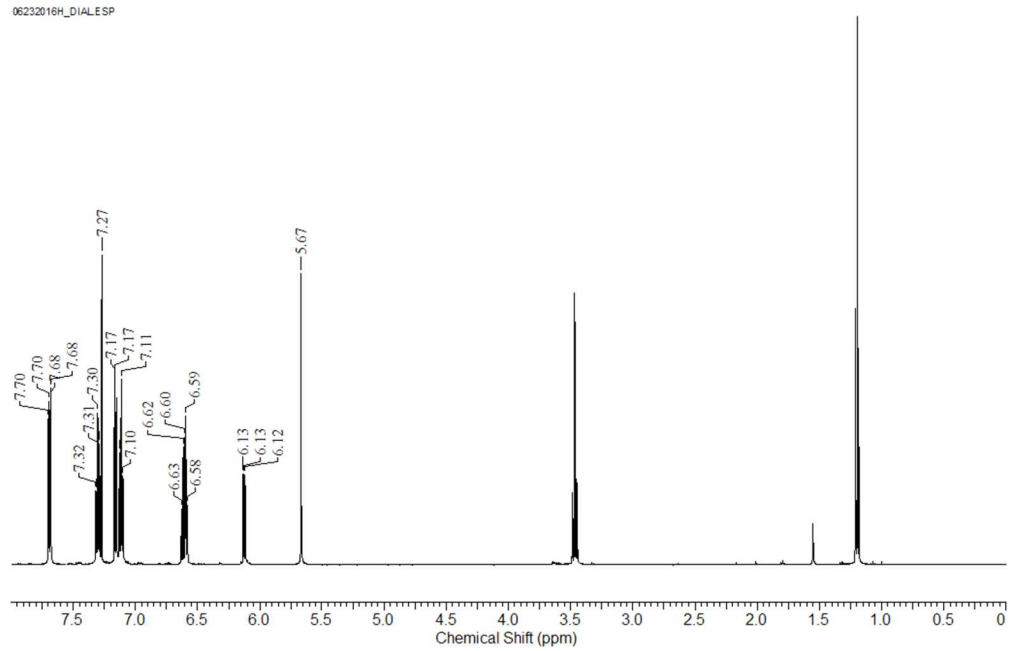

Figure 85. ^{1}H NMR spectrum of 41-$(OH)_2$ in $CDCl_3$.

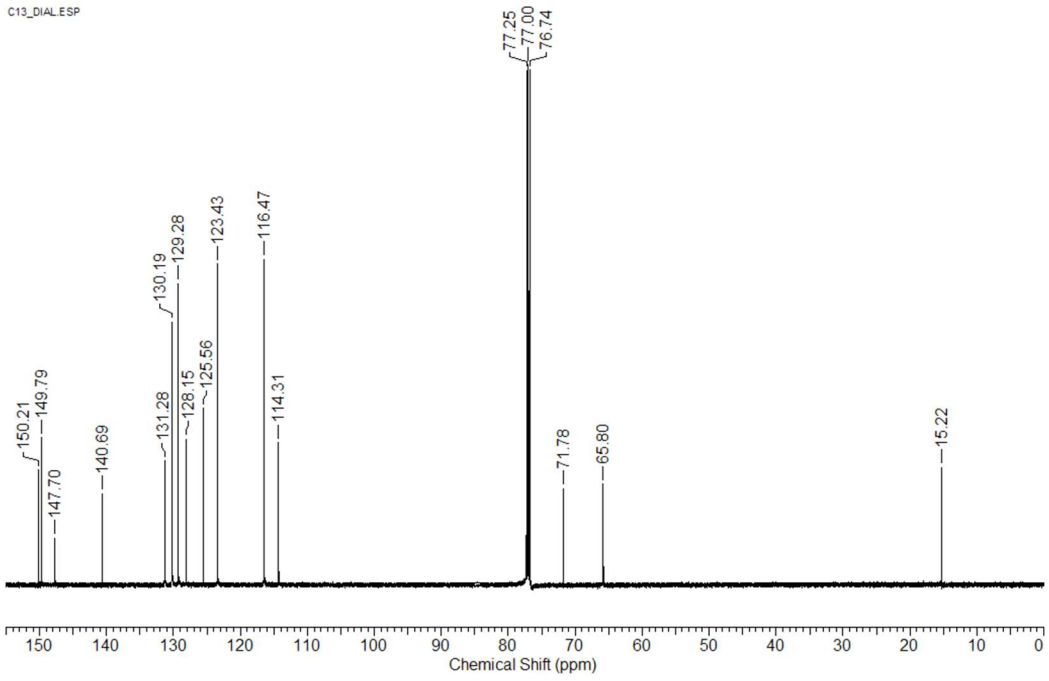

Figure 86. ^{13}C NMR spectrum of **41**-$(OH)_2$ in $CDCl_3$.

Synthesis of [41][BF_4]$_2$. A suspension of **41**-$(OH)_2$ (150 mg, 0.27 mmol) in TFA anhydride (4.5 ml) was treated with 48 % $HBF_{4(aq)}$ (0.25 ml) at room temperature. The reaction mixture was stirred for 2 h before Et_2O (10 ml) was added to the mixture. The resulting suspension was then filtered, and the dark green powder was further washed with Et_2O (10 ml) twice to afford [**41**][BF_4]$_2$ in 80 % yield. ^{1}H NMR (499.55 MHz, 25 ^{o}C, CD_3CN, Figure 87): δ 8.21 (br, 4 H), 8.12-8.09 (m, 8 H), 7.58 (t, 4 H, $^3J_{H-H}$ = 7.8 Hz), 7.42-7.35 (m, 4 H, biphenylene-C*H*), 6.98 (d, 2 H, $^3J_{H-H}$ = 7.8 Hz, biphenylene-C*H*) ppm. ^{13}C NMR (125.62 MHz, 25 ^{o}C, $CDCl_3$,): δ 156.92, 152.06, 145.10, 131.50, 130.83, 130.38, 129.92, 121.62, 119.73 ppm. Due to the poor solubility of [**41**][BF_4]$_2$ in CD_3CN, few peaks were not observed.

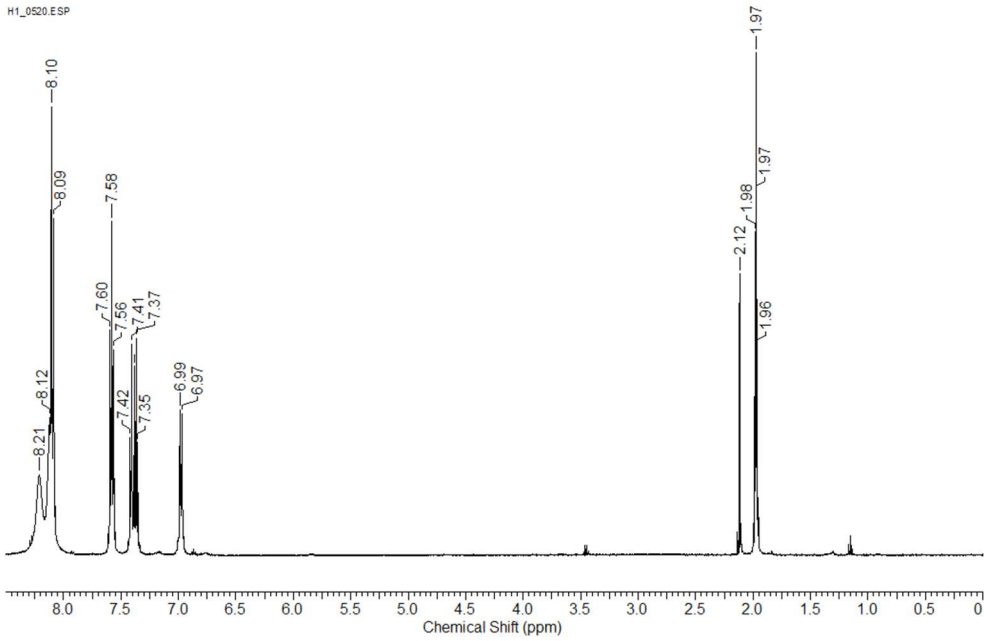

Figure 87. ^{1}H NMR spectrum of [**41**][BF_4]$_2$ in CD_3CN.

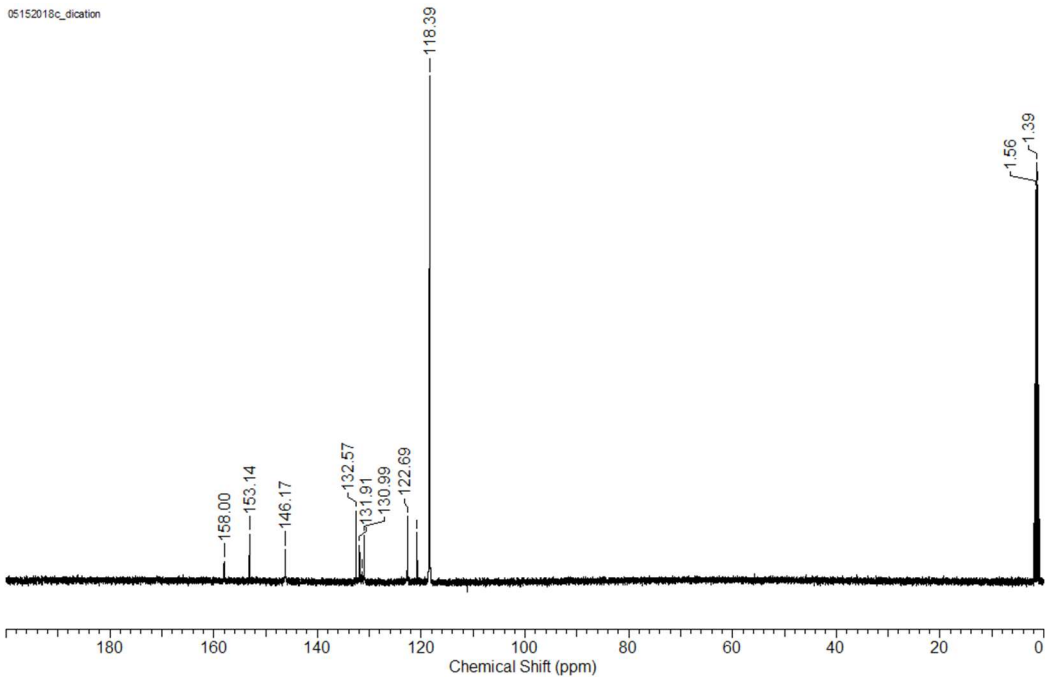

Figure 88. ^{13}C NMR spectrum of [**41**][BF_4]$_2$ in CD_3CN.

Synthesis of 42-$(OH)_2$. *n*BuLi (2.65 M, 1 mL, 2.65 mmol) was slowly added to a solution of 1,8-dibromobiphenylene (326 mg, 1.05 mmol) in dry Et_2O (5 mL) under N_2 at room temperature. After 30 min of stirring, a solution of 4,4'-dimethoxybenzophenone (560 mg, 2.3 mmol) in Et_2O (5 mL) was slowly transferred into the reaction flask using a cannula. The resulting solution was stirred for an additional 12 h at room temperature. The solution was then treated with saturated $NH_4Cl_{(aq)}$ (1 mL) and the solvent was removed under vacuum. The resulting white solid was then dissolved in CH_2Cl_2 (5 mL). The resulting solution was filtered and brought to dryness under vacuum. The off-white solid was then washed with Et_2O (15 mL) twice and dried under vacuum to afford diborane **42**-$(OH)_2$ as a white powder in 65 % yield. ^{1}H NMR (399.49 MHz, 25 ºC, $CDCl_3$, Figure 89): δ 7.07 (d, 8 H, $^3J_{H-H}$ = 7.8 Hz), 6.76 (d, 8 H, $^3J_{H-H}$ = 8.2 Hz), 6.59-6.56 (m, 4 H, biphenylene-C*H*),6.03 (d, 2 H, $^3J_{H-H}$ = 7.0 Hz, biphenylene-C*H*), 4.44 (s, 2 H, -O*H*), 3.78 (s, 12 H, -C*H*$_3$) ppm. ^{13}C NMR (100.46 MHz, 25 ºC, $CDCl_3$, Figure 90): δ 158.61, 151.41, 149.40, 139.87, 138.91, 130.43, 129.20, 127.59, 114.68, 113.11, 80.53, 55.13 ppm.

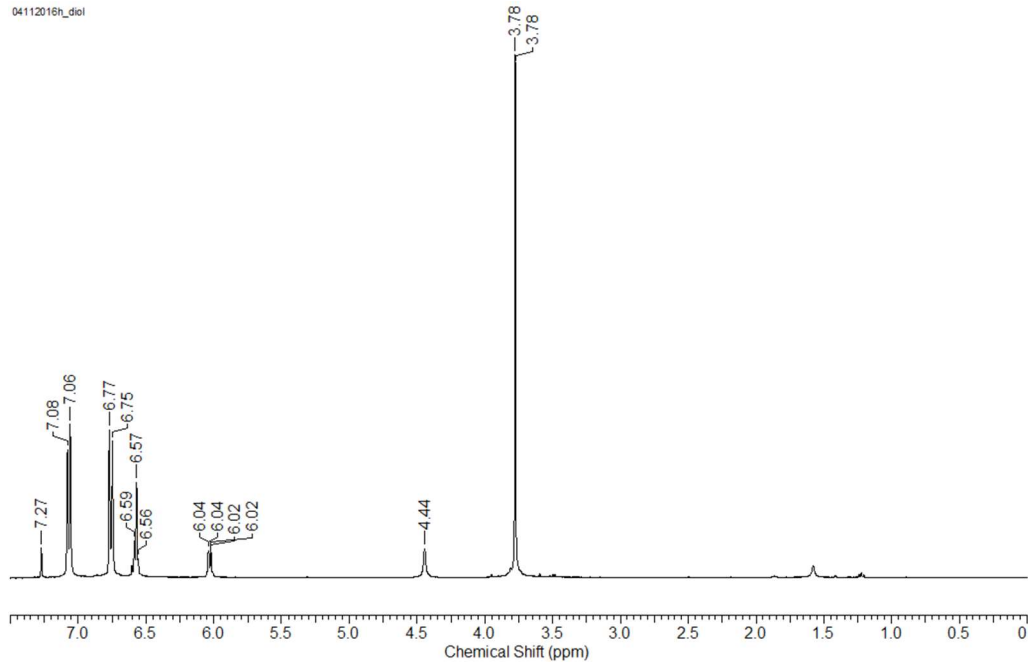

Figure 89. ^{1}H NMR spectrum of **42**-$(OH)_2$ in $CDCl_3$.

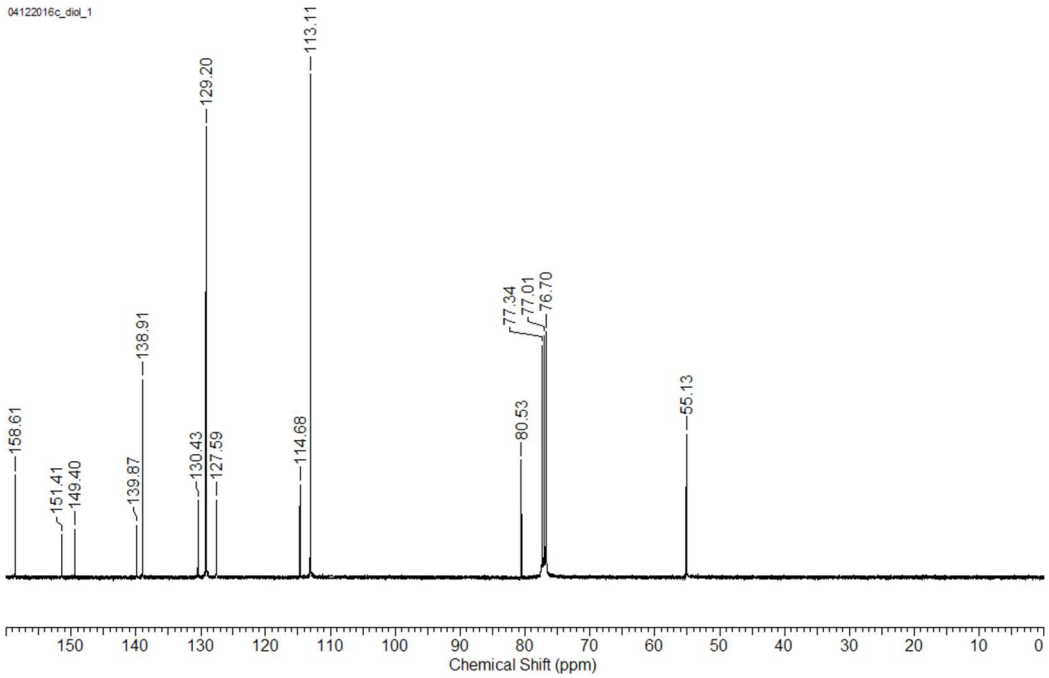

Figure 90. ^{13}C NMR spectrum of **42**-$(OH)_2$ in $CDCl_3$.

Synthesis of [42][BF_4]$_2$. A suspension of **42**-$(OH)_2$ (100 mg, 0.16 mmol) in TFA anhydride (2.0 ml) was treated with 48 % $HBF_{4(aq)}$ (0.1 ml) at room temperature. The reaction mixture was stirred for 2 h before Et_2O (8 ml) was added to the mixture. The resulting suspension was then filtered and the dark green powder was further washed with Et_2O (10 ml) twice to afford [**42**][BF_4]$_2$ in 88 % yield. ^{1}H NMR (399.49 MHz, 25 ºC, CD_2Cl_2, Figure 91): δ 7.56 (br, 8 H), 7.25-7.09 (m, 12 H), 6.48 (d, 2 H, $^3J_{H\text{-}H}$ = 8.2 Hz, biphenylene-C*H*), 4.04 (s, 12 H, -C*H*$_3$) ppm. ^{13}C NMR (100.46 MHz, 25 ºC, CD_2Cl_2, Figure 92): δ 185.79, 173.21, 155.49, 151.82, 146.27 (br), 142.71 (br), 134.56, 131.21, 130.56, 129.83, 122.71, 118.70 (br), 117.01 (br), 57.78 ppm.

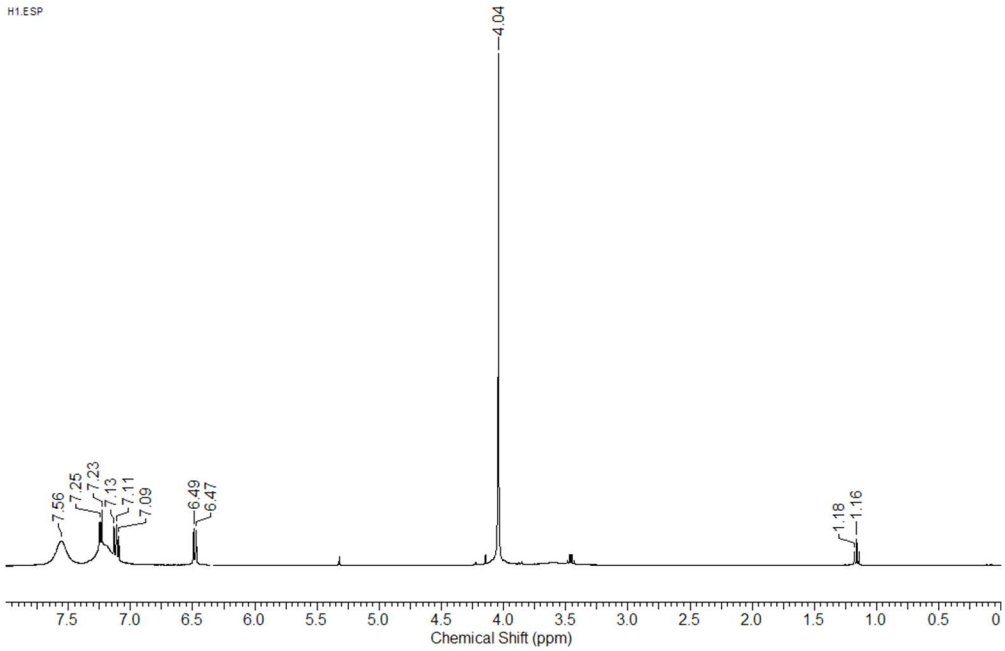

Figure 91. ^{1}H NMR spectrum of [**42**][BF_4]$_2$ in CD_2Cl_2.

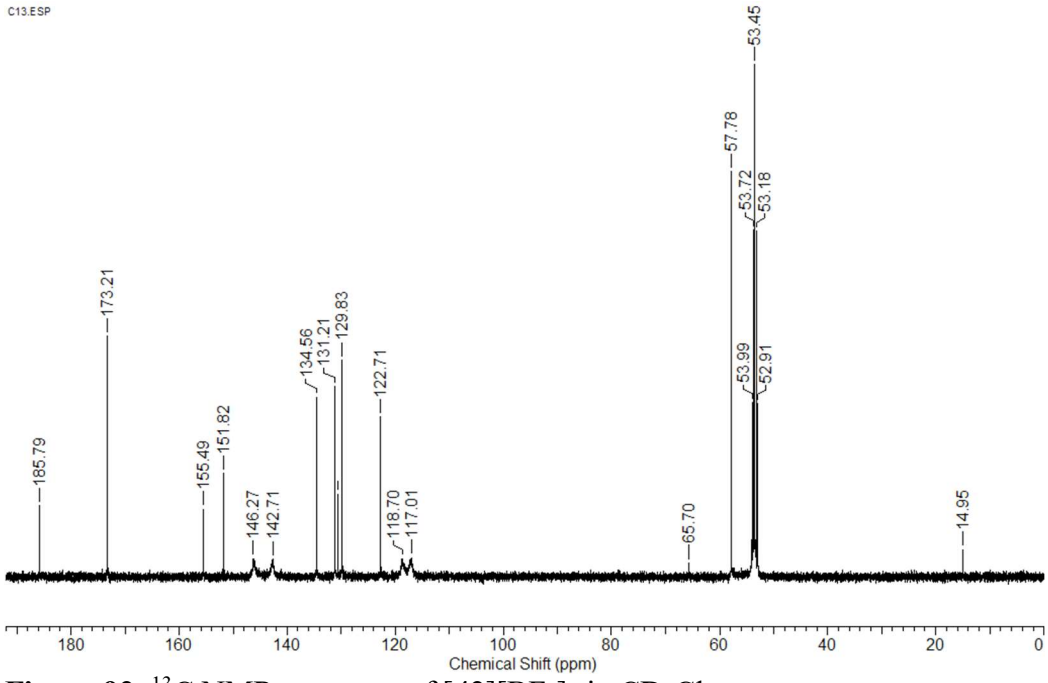

Figure 92. ^{13}C NMR spectrum of [**42**][BF_4]$_2$ in CD_2Cl_2.

CHAPTER V

SYNTHESIS AND CHARACTERIZATION OF BIFUNCTIONAL BIPHENYLENE-BASED DIORGANOANTIMONY (V) COMPOUND

5.1 Introduction

As part of our interest in the chemistry of antimony-based Lewis acids,[18, 24, 26-27, 93-97, 99, 102] we have recently developed a class of bidentate systems in which two antimony (V) moieties are positioned next to one another and connected by an organic backbone. Examples of such compounds include the dimethylxanthene-based[28] (**4**) and triptycene-based[164] (**30**) system (Figure 93). We found that these derivatives are well suited for the complexation of fluoride anions; however, we also observed some important differences. The first one is that the triptycene-based system displays higher fluoride ion affinity than the dimethylxanthene-based system. Using a series of structural and computational studies, we assigned the origin of this difference to the structure of the backbone and the absence of an oxygen atom in the case of the triptycene backbone.

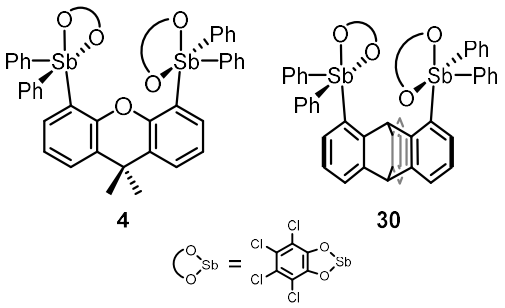

Figure 93. Dimethylxanthene- (**4**) and triptycene-based (**30**) distiboranes.

With the view of discovering other platforms that also lack an electron rich atom positioned below the anion binding pocket. Our attention was drawn by the 1,8-biphenylenediyl linker.[165, 203] We have investigated the construction of bifunctional Lewis acid using this linker and were able to successfully introduce boron atoms at C1 and C8 positions. It occurred to us that analogous antimony-based system may also possess attractive properties because of the absence of an electron rich atom in the backbone, as well as a clear depression below the anion pocket. In this chapter, we report a series of reactions and efforts in which we have investigated the synthesis of such system and we report the discovery of a stibine oxide stabilized by an adjacent stiborane.

5.2 Synthesis of the biphenylene-based distibine

It occurred to us that the target distiborane could be prepared by oxidative addition of *o*-chloranil to 1,8-bis(diphenylstibino)biphenylene (**43**). We first attempted to obtain distibine **43** by dilithiation of 1,8-dibromobiphenylene followed by metathesis with Ph_2SbCl. Unfortunately, these efforts proved unsuccessful. The reaction was accompanied by the formation of a black precipitate suggesting partial reduction of the antimony reagent. Faced with these difficulties, we decided to adopt an alternative approach based on the use of 1,8-bis(trimethylstannyl)biphenylene (**44**) which has been previously employed by Jordan et al to produce biphenylene gallium derivatives. We found that **44** reacted with Ph_2SbCl in refluxing toluene to afford the desired distibine **43** (Figure 94).

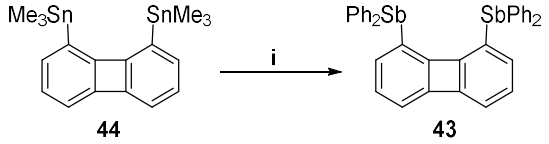

Figure 94. Synthesis of distibine **43**. i) Ph_2SbCl, 2 equiv, toluene, reflux.

Although the product was formed only in low yield, it could be effectively separated, purified and characterized. Compound **43** was obtained as a pale-yellow air-stable solid in an overall 20 % yield. This compound has been fully characterized. The ^1H NMR spectrum of **43** in $CDCl_3$ indicates that all four phenyl groups are equivalent. Its ^1H NMR spectrum also shows the expected symmetrical biphenylene backbone resonances including three individual resonances consistent with an ABC spin system. Single crystals suitable for X-ray diffraction of **43** were obtained from slow evaporation of a solution of

compound **43** in hexanes. In the solid-state structure of **43**, the two antimony atoms are separated by 4.099(2) Å (Figure 95).

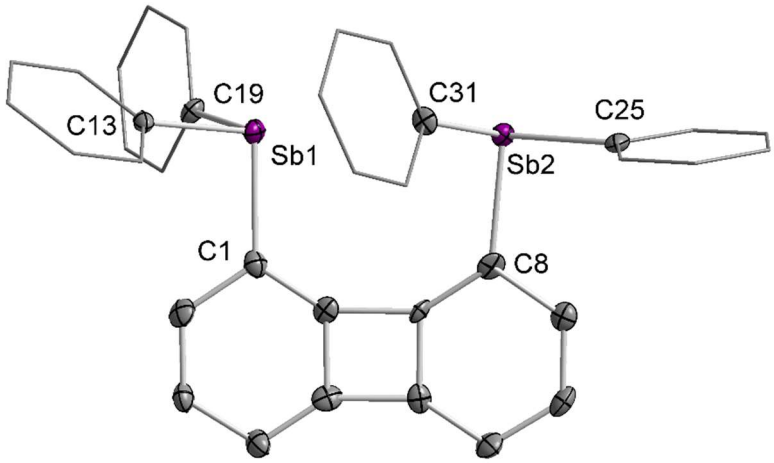

Figure 95. Solid-state structure of **43**. Thermal ellipsoids are drawn at the 50% probability level. The hydrogen atoms are omitted for clarity. Selected bond lengths [Å] and angles [º]: Sb1-C1 2.15(1), Sb1-C13 2.17(1), Sb1-C19 2.154(9), Sb2-C8 2.15(1), Sb2-C25 2.16(1), Sb2-C31 2.159(9); C1-Sb1-C13 95.2(3), C1-Sb1-C19 98.2(4), C13-Sb1-C19 95.2(4), C8-Sb2-C25 93.7(4), C8-Sb2-C31 97.4(4), C25-Sb2-C31 95.9(4).

5.3 Oxidation of the biphenylene-based distibine

Next, we attempted to generate the corresponding distiborane **45** by oxidation of **43** with *o*-chloranil (Figure 96). Such reactions are well precedented and have been used to obtain **4** and **30**. In the present case, we monitored the reaction by ^{1}H NMR spectroscopy. Direct addition of *o*-chloranil in to a solution of **43** in $CDCl_3$ under dry condition results in uncharacterizable broad peaks. Interestingly, the same reaction performed under ambient condition with unpurified $CDCl_3$ afforded compound **46** , a hydrolyzed diantimony (V) derivative. The ^{1}H NMR spectrum of **46** in $CDCl_3$ shows five resonances arising from the phenyl groups, indicating the asymmetry of the molecule.

Compound **46** can be formulated as a diantimony (V) species which features a stibine oxide coordinated to and adjacent stiborane (Figure 96). We attribute the formation of this hydrolyzed product to the highly Lewis acidic pocket formed between two antimony (V) centers. The ^{1}H NMR spectrum in $CDCl_3$ indicates two different sets of phenyl proton resonances revealing the asymmetrical structure of compound **46**. By comparison, triphenylstibine oxide forms a dimeric complex,[245] the formation of Sb=O→Sb moiety in compound **46** points to the suited spacing of the biphenylene backbone for the formation of the intramolecular oxo-bridge.

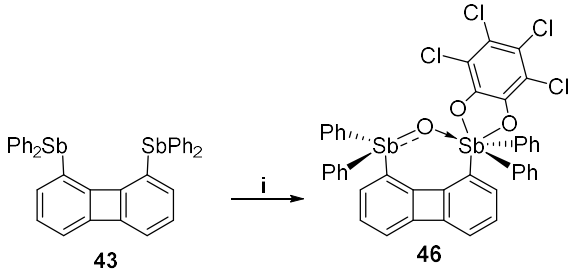

Figure 96. Synthesis of **46**. i) *o*-chloranil, $CHCl_3$ (not purified), rt.

X-ray diffraction analysis confirmed the asymmetry of this derivative. In the solid-state structure of **46** (Figure 97), the two antimony atoms are separated by a distance of 3.6281 Å which is shorter than that in **43**. This shortening reflects the strong Sb=O→Sb interaction connecting the two Lewis acids. Accordingly, the antimony center of the stiborane functionality assumes an octahedral geometry as expected for a hexacoordinate antimony(V) species. The asymmetrical oxo-bridge features Sb1-O1 bond length of 1.880(4) Å, Sb2-O1 bond length of 2.084(4) Å and Sb1-O1-Sb2 bond angle of 132.4(2)º. These observations point to the presence of a donor-acceptor interaction involving an oxygen lone pair as a donor and a Sb(V)-CPh σ* orbital as an acceptor.

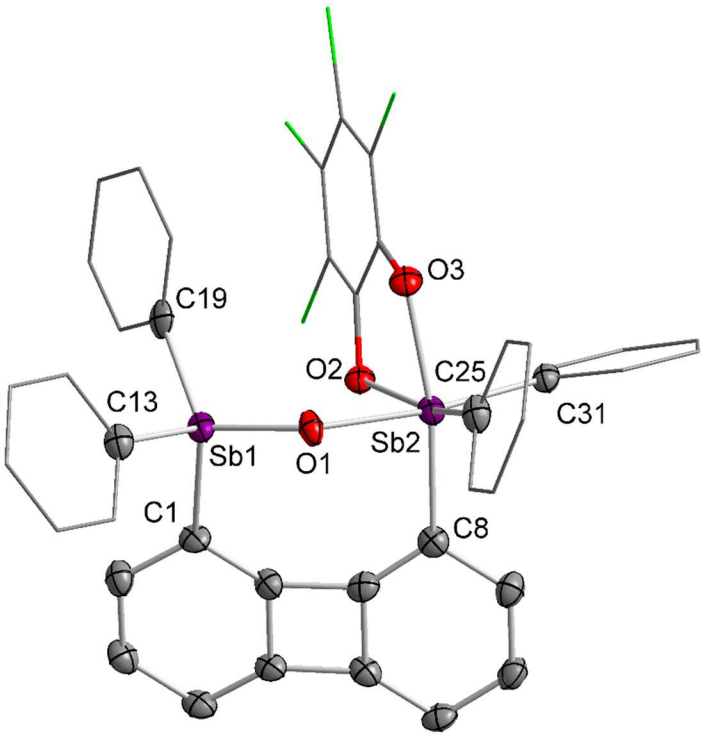

Figure 97. The solid-state structure of **46**-$(CHCl_3)_2$. Thermal ellipsoids are drawn at the 50% probability level. The hydrogen atoms and $CHCl_3$ molecules are omitted for clarity. Selected bond lengths [Å] and angles [°]: Sb1-O1 1.880(4), Sb1-C1 2.087(6), Sb1-C13 2.100(6), Sb1-C19 2.086(7), Sb2-O1 2.084(4), Sb2-O2 2.107(4), Sb2-O3 2.088(4), Sb2-C8 2.139(6), Sb2-C25 2.137(6), Sb2-C31 2.150(6); Sb1-O1-Sb2 132.4(2), C1-Sb1-C13 107.7(2), C1-Sb1-C19 113.5(2), C13-Sb1-C19 107.2(2), O1-Sb1-C1 104.5(2), O1-Sb1-C13 104.9(2), O1-Sb1-C19 118.4(2), C8-Sb2-C25 102.2(2), C8-Sb2-C31 95.0(2), C25-Sb2-C31 101.1(2), O1-Sb2-O2 82.8(2), O1-Sb2-O3 84.2(2), O2-Sb2-O3 78.3(2), O2-Sb2-C25 162.1(2), O3-Sb2-C8 168.2(2), O1-Sb2-C31 171.3(2).

To further investigate the O → Sb (V) interaction, compound **46** has been computationally optimized using DFT methods and analyzed using the NBO methods. The O-Sb2 distance in the DFT optimized structure is 2.1277 Å which is close to the O1-Sb2 separation found in the solid-state structure. The NBO calculation confirms a donor-acceptor interaction from a lone pair of O1 to the Sb2(V)-C_{Ph} σ* orbital. The donor-acceptor interaction in Figure 98 was also investigated by the NBO deletion method in which the stabilization energy of 208.8 kJ/mol was calculated.

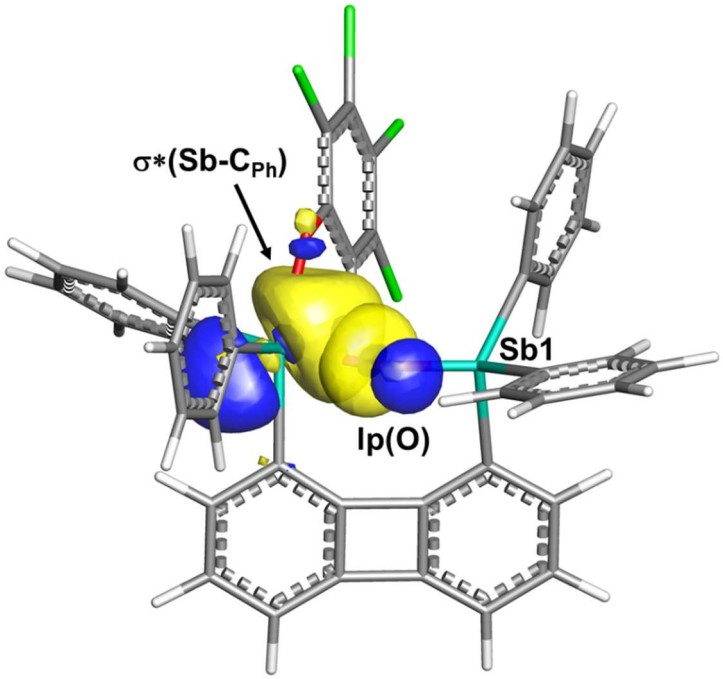

Figure 98. The NBO lp(O)→σ*(Sb-C_{Ph}) donor-acceptor interaction of 208.8 kJ/mol.

5.4 Conclusion

In summary, we describe the reaction of 1,8-bis(trimethylstannyl)biphenylene (**44**) with Ph_2SbCl producing the distibine **43**. This distibine reacts with *o*-chloranil to afford the unstable distiborane which undergoes hydrolysis to afford a stable oxo-bridge complex **46**. This derivative features a Sb=O→Sb donor-acceptor interaction, which was further studied by computational methods. A donor-acceptor interaction of 208.8 kJ/mol was identified using the NBO method. These results show that the biphenylene backbone is well suited for the Lewis acid stabilized by a Sb=O bond. This result is noteworthy because stibine oxides are usually dimeric.

5.5 Experimental section

General considerations. *n*Butyllithium (2.65 M in hexane), 1, 8-Dibromobiphenylene was synthesized by following the literature procedures.[165] Antimony trichloride ($SbCl_3$) and triphenyl stibine (Ph_3Sb) were purchased from Alfa Aesar and used without further purification. Ph_2SbCl was obtained by directly reacting $SbCl_3$ (1 equiv) with Ph_3Sb (2 equiv) at room temperature under N_2 for 3 days. The resulting solid was recrystallized from CH_2Cl_2 at -40 ºC. Tetrachloro-*o*-benzoquinone (*o*-chloranil) was purchased from Acros Organics and used without further purification. Trimethyltin chloride (Me_3SnCl) was purchased from TCI chemical and used as received. All preparations were carried out under a dry N_2 atmosphere employing either a glovebox or standard Schlenk techniques. Solvents were dried by passing through an alumina column (*n*-pentane and CH_2Cl_2) or by refluxing under N_2 over Na/K (Et_2O and THF). All other solvents were ACS reagent grade and used as received. NMR spectra were recorded on an Inova 500 FT NMR (499.41 MHz for ^1H) spectrometer, Varian NMRS 500RM NMR spectrometer (499.69 MHz for ^1H) or an Inova 400 FT NMR (399.46 MHz for ^1H) spectrometer at room temperature. Chemical shifts are given in ppm and are referenced to residual ^1H or ^{13}C solvent signals.

Computational details. Computational details. Density functional theory (DFT) structural optimizations were done with the Gaussian 09 program. In all cases, the structures were optimized using the B3LYP functional and the following mixed basis set: Sb, cc-pVTZ-PP; C/O/H, 6-31g; Cl, 6-311g(d). For all optimized structures, frequency calculations were carried out to confirm the absence of imaginary frequencies. The NBO

analysis was performed using the NBO 5.9 program. The energy of the Sb=O→Sb interaction was derived from the second order perturbation energy associated to the donor-acceptor interaction shown in Figure 98. The molecular orbitals were visualized and plotted using the Jimp2 program.[122]

Crystallographic details. The crystallographic measurements were performed at 110(2) K using a Bruker APEX-II CCD area detector diffractometer, with a graphite-monochromated Mo-Kα radiation (λ = 0.71073 Å). A specimen of suitable size and quality was selected and mounted onto a nylon loop. The semi-empirical method SADABS was applied for absorption correction. The structure was solved by direct methods, which successfully located most of the non-hydrogen atoms. Subsequent refinement on F^2 using the SHELXTL/PC package (version 6.1) allowed location of the remaining non-hydrogen atoms.

Table 12. Crystal data, data collection, and structure refinement for **43**.

Identification code	y
Empirical formula	C36 H26 Sb2
Formula weight	702.07
Temperature	110 K
Wavelength	0.71073 Å
Crystal system	Monoclinic
Space group	P 1 21 1
Unit cell dimensions	a = 6.205(3) Å b = 17.811(9) Å c = 12.643(6) Å α = 90°. β = 96.512(6)°. γ = 90°.
Volume	1388.2(12) $Å^3$
Z	2
Density (calculated)	1.680 Mg/m^3
Absorption coefficient	1.969 mm^{-1}
F(000)	688
Crystal size	0.18 x 0.05 x 0.04 mm^3
Theta range for data collection	1.621 to 26.782°.
Index ranges	-7<=h<=7, -22<=k<=22, -14<=l<=15
Reflections collected	13087
Independent reflections	5877 [R(int) = 0.0630]
Completeness to theta = 25.242°	100.00%
Absorption correction	Semi-empirical from equivalents
Max. and min. transmission	0.7454 and 0.5998
Refinement method	Full-matrix least-squares on F^2
Data / restraints / parameters	5877 / 1 / 343
Goodness-of-fit on F^2	0.997
Final R indices [I>2sigma(I)]	R1 = 0.0433, wR2 = 0.0946
R indices (all data)	R1 = 0.0511, wR2 = 0.0986
Absolute structure parameter	0.05(3)
Largest diff. peak and hole	0.705 and -1.619 $e.Å^{-3}$

Table 13. Crystal data, data collection, and structure refinement for **46**-$(CHCl_3)_2$.

Identification code	y
Empirical formula	C43.43 H27.43 Cl8.30 O3 Sb2
Formula weight	1134.83
Temperature	110 K
Wavelength	0.71073 Å
Crystal system	Monoclinic
Space group	$P12_1/c1$
Unit cell dimensions	a = 16.192(2) Å b = 17.205(3) Å c = 16.316(2) Å α = 90°. β = 90.4177(19)°. γ = 90°.
Volume	4545.0(12) $Å^3$
Z	4
Density (calculated)	1.658 Mg/m^3
Absorption coefficient	1.714 mm^{-1}
F(000)	2220
Crystal size	0.15 x 0.06 x 0.05 mm3
Theta range for data collection	1.720 to 26.449°.
Index ranges	-20<=h<=20, -21<=k<=21, -20<=l<=20
Reflections collected	49072
Independent reflections	9353 [R(int) = 0.0878]
Completeness to theta = 25.242°	100.00%
Absorption correction	Semi-empirical from equivalents
Max. and min. transmission	0.7454 and 0.6494
Refinement method	Full-matrix least-squares on F^2
Data / restraints / parameters	9353 / 0 / 527
Goodness-of-fit on F^2	1.064
Final R indices [I>2sigma(I)]	R1 = 0.0543, wR2 = 0.1514
R indices (all data)	R1 = 0.0670, wR2 = 0.1637
Largest diff. peak and hole	2.211 and -2.214 $e.Å^{-3}$

Synthesis of 43. A suspension of 1,8-bis(trimethylstannyl)biphenylene (**44**, 500 mg, 1.05 mmol) and Ph2SbCl (2 g, 6.4 mmol) in toluene (15 ml) was refluxed in a sealed Schlenk tube for 24 h. After cooled to room temperature, the solvent was removed under vacuum. The resulting brown solid was firstly washed by MeOH (20 ml) and then hexanes (20 ml) to afford **43** as a pale-yellow solid in 22 % yield. ^{1}H NMR (499.46 MHz, 25 ^{o}C, $CDCl_3$, Figure 99): δ 7.38-7.37 (m, 8 H, Sb-*Ph*), 7.29-7.27 (m, 12 H, Sb-*Ph*), 6.63-6.58 (m, 4 H, biphenylene-C*H*), 6.49 (d, 2 H, $^{3}J_{H\text{-}H}$ = 7.8 Hz,) ppm. ^{13}C NMR (125.61 MHz, 25 ^{o}C, $CDCl_3$, Figure 100): δ 160.83, 151.53, 138.26, 136.26, 135.05, 128.85, 128.84, 128.43, 128.34,116.94 ppm.

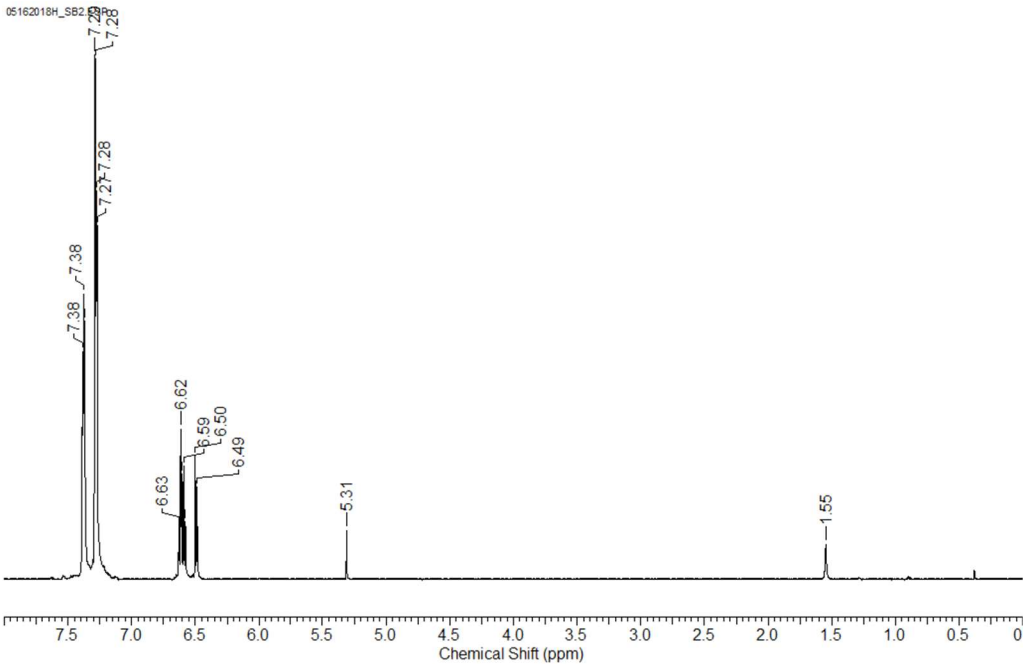

Figure 99. ^{1}H NMR spectrum of **43** in $CDCl_3$.

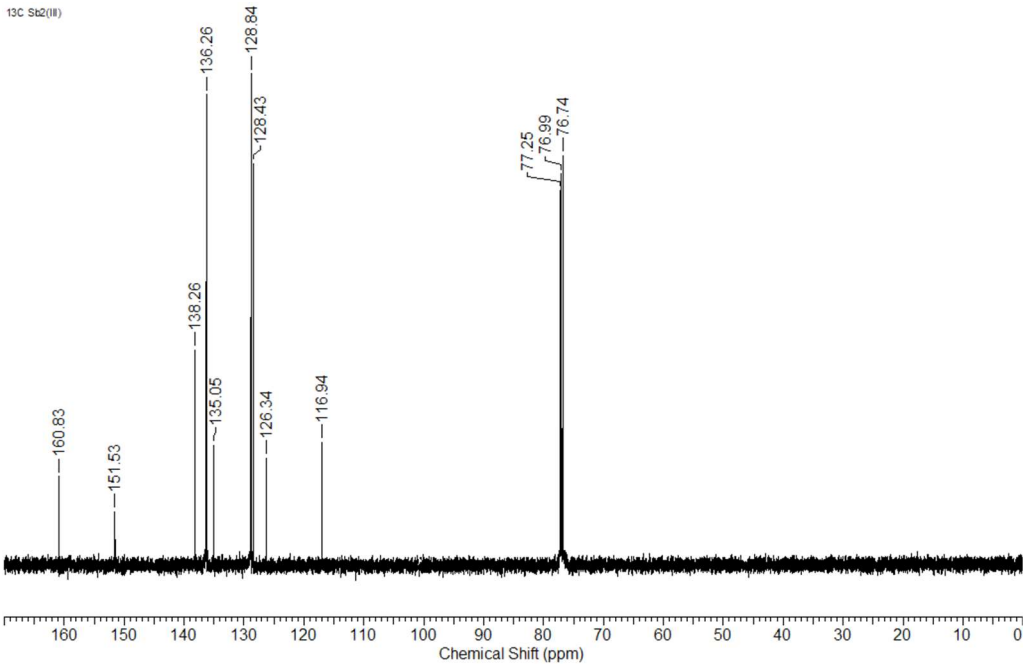

Figure 100. ^{13}C NMR spectrum of **43** in $CDCl_3$.

Synthesis of **46.** A solution of *o*-chloranil (92 mg, 0.38 mmol, 2 equiv) in CH_2Cl_2 (3 mL) was slowly transferred via cannula into a flask containing a solution of **43** (150 mg, 0.19 mmol, 1 equiv) in CH_2Cl_2 (5 mL) in an open flask at room temperature. The oxidation of the distibine was observed by the disappearing of the bright red color of *o*-chloranil. After stirring for 5 h at room temperature, the solvent was removed under vacuum. The resulting yellow solid was washed by MeOH (20 mL) twice to afford **46** as a yellow solid in 61 % yield. ^{1}H NMR (499.47 MHz, $CDCl_3$,): δ 7.81 (d, 4 H, $^3J_{H-H}$ = 6.8 Hz, Sb-*Ph*), 7.49-7.44 (m, 6 H, Sb-*Ph*), 7.34 (d, 4 H, $^3J_{H-H}$ = 6.8 Hz, Sb-*Ph*), 7.24 (d, 2 H, Sb-*Ph*), 7.17 (t, 4 H, $^3J_{H-H}$ = 7.8 Hz, Sb-*Ph*), 6.84 (dd, 2 H, $^3J_{H-H}$ = 6.8 Hz, $^4J_{H-H}$ = 1.0 Hz biphenylene-C*H*), 6.80 (pseudo t, 2 H, $^3J_{H-H}$ = 6.8 Hz, biphenylene-C*H*), 6.70 (d, 2 H, $^3J_{H-H}$ = 7.3 Hz, biphenylene-C*H*) ppm. $^{13}C\{^1H\}$ NMR (125.60 MHz, $CDCl_3$,): δ 152.68, 147.72, 145.17, 134.87, 134.13, 134.03, 133.84, 133.53, 132.95, 132.22, 131.05, 130.70, 130.60, 129.93, 129.69, 129.67, 129.36, 129.28, 128.68, 128.56, 119.63, 119.55, 119.15, 118.61, 117.67, 117.54, 116.91 ppm.

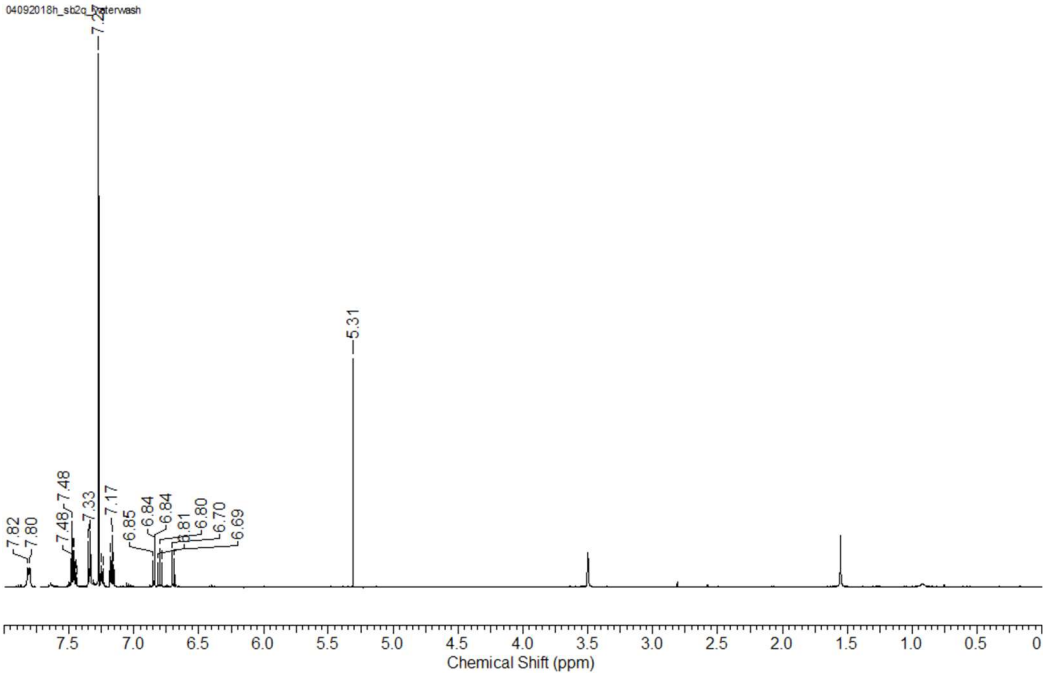

Figure 101. ^{1}H NMR spectrum of **46** in $CDCl_3$.

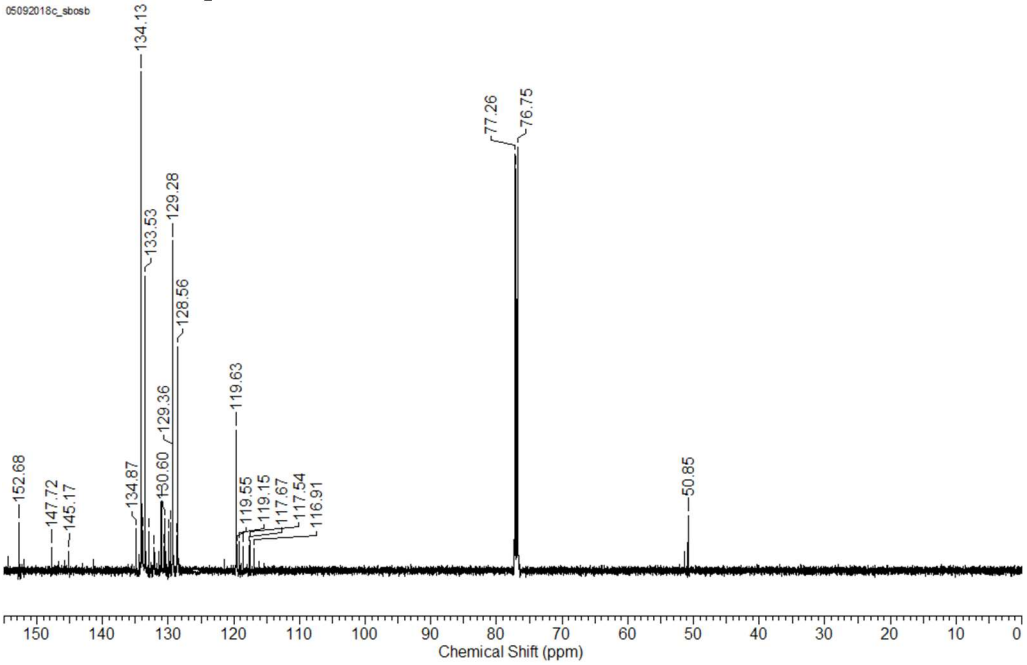

Figure 102. ^{13}C NMR spectrum of **46** in $CDCl_3$.

CHAPTER VI

SUMMARY

6.1 Bidentate distiborane for fluoride anion chelation

Previous studies in our group show that polyfunctional Lewis acids can greatly enhance the stability of the Lewis base adducts via chelation effect. Previously in our group, we have successfully synthesized dimethylxanthene-based distiborane (**4**) which displays elevated Lewis acidity toward fluoride in aqueous media. However, dimethylxanthene backbone features an electron-rich oxygen atom pointing into the binding pocket of **4**, which presumably decreases the overall fluoride ion affinity of **4**. To further increase the Lewis acidity of the distiborane system, we synthesized the triptycene-based distiborane **30**. The triptycene backbone adopts a barrelene-type structure and features a neutral methine group at the bridgehead. The solid-state structure of **30** features two square pyramidal stiborane units which are oriented in a face-to-face fashion. Compound **30** features an extended Sb-Sb separation of ~5.2 Å, which depends on the conformation of **30**. The computational studies indicate the LUMO of **30** bears large contribution from the σ*-orbitals on both antimony (V) atoms.

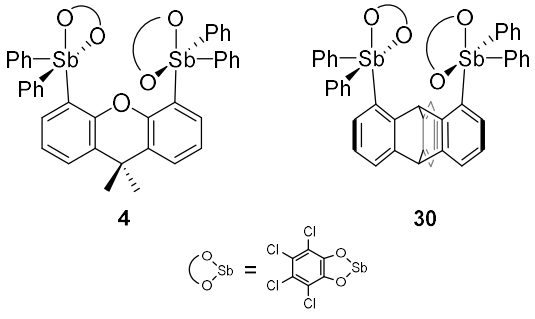

4 **30**

The reaction of **30** with TBAT in CH_2Cl_2 afforded a bridging fluoroantimonate complex [**30**-μ_2-F]$^-$. Examination of the solid-state structure of [**30**-μ_2-F]$^-$ indicates a short separation of 2.915(4) Å between fluorine atom and the central carbon atom of triptycene backbone, pointing to the existence hydrogen-bonding interaction. This view is further supported by the $^1H\{^{19}F\}$ and $^{13}C\{^{19}F/^1H\}$ NMR spectra in which the coupling constants, J_{HF} = 4.9 Hz and J_{CF} = 7.4 Hz, were observed. Meanwhile, the NBO analysis of [**30**-μ_2-F]$^-$ shows a weak donor-acceptor interaction of 5.9 kJ/mol between the fluorine lone pair electrons and σ*(C-H) orbital.

The Lewis acidity of distiborane **30** was further investigated by rigorous fluoride competition experiments, in which [**4**-μ_2-F]$^-$ was allowed to react with **30**. By monitoring the reaction by ^{19}F NMR spectrometry, we observed that the fluoride anions were transferred from **4** to **30** quantitatively. This observation clearly indicates that the higher fluoride ion affinity of **30** in the solution than the dimethylxanthene-based distiborane **4**. This experimental result also reveals the better suitability of the triptycene backbone in supporting Lewis acidic stiborane functionalities for fluoride anion complexation.

6.2 Borane-borinic acid bidentate Lewis acid for fluoride complexation

Hydrogen bond donor derivatives that bind small halide anions are of increasing importance in anion sensing. In search of new hydrogen bond donors for fluoride complexation, we synthesized a borane-borinic acid **35** which is stable and resists condensation. The borane-borinic acid **35** was obtained from the fluoride-promoted hydrolysis of a B-C_{Mes} bond of diborane **33**.

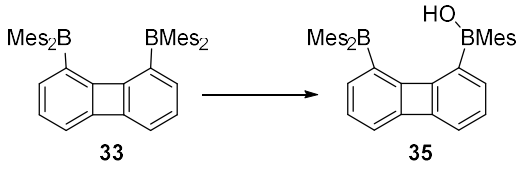

The reaction of **35** with TASF in a mixture of CH_2Cl_2/THF (1/1 vol.) afforded [TAS][**35**-F] which has been fully characterized. The ^1H NMR resonance observed for the borinic acid hydroxy group is largely shifted from $\delta = 5.25$ in **35** to 11.12 ppm in [**35**-F]$^-$. The formation of [**35**-F]$^-$ is further supported by the fact that the hydroxy ^1H NMR signal in [**35**-F]$^-$ is coupled to the ^{19}F nucleus by a value of $^1J_{HF} = 57.2$ Hz as confirmed by the $^1H\{^{19}F\}$ NMR experiment. A weakening of the O-H stretching frequency from $\nu_{O\text{-}H}$ = 3503 cm^{-1} in **35** to $\nu_{O\text{-}H}$ = 3193 cm^{-1} in [TAS][**35**-F] was also observed, pointing to the lp(F)→ σ*(O-H) donor-acceptor interaction. Moreover, the titration of **35** with TBAF in THF/H_2O mixture (v/v = 4/1) confirmed a fluoride binding constant of $K = 1.4\ (\pm 0.1) \times 10^4$ M^{-1}. In stark contrast, monofunctional borane **34** does not complex fluoride under the same aqueous condition pointing to the crucial role played by the borinic acid functionality. Finally, the NBO analysis provides a complementary picture with a strong donor-acceptor

lp(F)→σ*(O-H) interaction ($E^{(2)}$ = 118.3 kJ/mol) connecting the fluorine and hydrogen atom.

6.3 Large-bite diboranes for μ(1,2) chelation of hydrazine and cyanide

Many recent studies indicate that bifunctional boranes may display a different selectivity and may become well adapted to the μ(1,2) chelation of diatomic molecules through increasing the separation of two boron centers. In this project, we synthesized the triptycene-based diborane **36** featuring a boron-boron separation of 5.559(4) Å and compared it with the biphenylene-based diborane **33** which features a boron-boron separation of 4.566(5) Å. The CV measurements of these two diboranes show that diborane **33** is significantly more electron deficient than **36**, pointing to the higher Lewis acidity of diborane **33**.

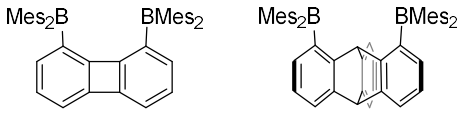

33 **36**

First, we tried to react the large-bite diboranes with KCN in the presence of dibenzo-18-crown-6. Interestingly, both diboranes reacted with KCN in $CHCl_3$/MeOH quickly in the presence of one equivalent of 18-dibenzo-crown-6 to afford the 1:1 cyanide complex [**33**-μ_2-CN]$^-$ and [**36**-μ_2-CN]$^-$. Examination of the solid-state structures of both cyanide complexes indicate the formation of intramolecular μ(1,2) cyanide bridge. The IR spectrum of [**33**-μ_2-CN]$^-$ shows a C≡N stretching frequency of 2229 cm^{-1} which is higher than that observed for [**36**-μ_2-CN]$^-$ (2184 cm^{-1}), suggesting the higher cyanide ion affinity of **33**. This view is also confirmed by the reaction of [**36**-μ_2-CN]$^-$ with **33**, in which cyanide anion was quantitatively transferred from [**36**-μ_2-CN]$^-$ to **33**.

In addition to cyanide complexation, the reaction of these two diboranes with neutral diatomic molecules were also investigated. Both **33** and **36** formed uncharacterizable mixture when reacting with H_2O_2 and NH_2OH. However, diborane **33** reacts with $N_2H_4{\cdot}H_2O$ cleanly to afford the corresponding μ(1,2) hydrazine complex **33**-μ_2-N_2H_4. In stark contrast, diborane **36** shows no reactivity toward $N_2H_4{\cdot}H_2O$, again pointing to the lower Lewis acidity of **36**.

6.4 Synthesis and characterization of bifunctional biphenylene-based diorganoantimony (V) compound

Given the fact that biphenylene shows greater electron withdrawing ability than triptycene in the diborane studies in Chapter IV, we became interested in the synthesis of the biphenylene-based antimony (V) Lewis acids. To this end, we have synthesized the biphenylene-based distibine **43** by the reaction of 1,8-bis(trimethylstannyl)biphenylene (**44**) with Ph_2SbCl. This distibine reacts with *o*-chloranil under ambient condition to afford a diantimony (V) derivative **46**, which features a Sb=O→Sb interaction. In the computational studies, a donor-acceptor interaction of 208.8 kJ/mol from an oxygen lone pair on the stibine oxide to the σ* of the stiborane was confirmed by the NBO method. These results show that the biphenylene backbone is well suited for the formation of stibine oxide stabilized by a neighbor stiborane functionality. Given the fact that stibine oxides are usually dimeric, this intramolecular Sb=O→Sb interaction is noteworthy.

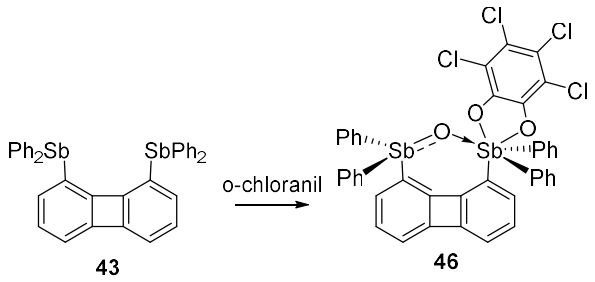

43 46

6.5 Future work

In this dissertation, we report the triptycene- and biphenylene-based diboranes as large-bite bidentate Lewis acids for the μ(1,2) complexation of the cyanide anion as well as hydrazine. The results demonstrate that the biphenylene platform can be used as a support for hybrid ditopic Lewis acids containing both borane and borinic acid moieties. An investigation of this unusual bifunctional Lewis acid reveals that this is well for the complexation of the fluoride anion in aqueous media. Finally, this thesis shows that these platforms can also be incorporated in antimony-based bifunctional derivatives. The most interesting results have been obtained with a triptycene-based distiborane which shows a remarkable affinity for fluoride anions. Overall, these results indicate that changes in the nature of the backbone have a defining influence on the binding selectivity of bidentate Lewis acids.

Although many triptycene- and biphenylene-based derivatives have been synthesized and investigated, the studies of main-group derivatives of these backbones remain limited. Given the fact that the chemistry of the bidentate Lewis acids can be extended by using these novel backbones, three future directions for triptycene- and biphenylene-based bidentate Lewis acids are suggested. Firstly, the development of new triptycene- and biphenylene-based main group derivatives. For example, tellurium and bismuth derivatives known for their Lewis acidity are suitable candidates for this chemistry. Secondly, the enhancement of the Lewis acidity of the boron and antimony derivatives by incorporation of the electron-withdrawing substituents, such as pentafluorophenyl groups. Finally, with the ability of tuning the pocket sizes and the

electronic properties of the bidentate Lewis acids, innovative applications, such as anion transport and organocatalysis should also be considered as future direction for these novel bidentate Lewis acids.

REFERENCES

(1) Hudnall, T. W.; Chiu, C.-W.; Gabbaï, F. P., *Acc. Chem. Res.* **2009,** *42* (2), 388-397.

(2) Galbraith, E.; James, T. D., *Chem. Soc. Rev.* **2010,** *39* (10), 3831-3842.

(3) Wade, C. R.; Broomsgrove, A. E. J.; Aldridge, S.; Gabbaï, F. P., *Chem. Rev.* **2010,** *110* (7), 3958-3984.

(4) Zhao, H.; Leamer, L. A.; Gabbaï, F. P., *Dalton Trans.* **2013,** *42* (23), 8164-8178.

(5) Yamaguchi, S.; Akiyama, S.; Tamao, K., *J. Am. Chem. Soc.* **2001,** *123* (46), 11372-11375.

(6) Katz, H. E., *J. Am. Chem. Soc.* **1985,** *107* (5), 1420-1421.

(7) Katz, H. E., *J. Org. Chem.* **1985,** *50* (25), 5027-5032.

(8) Solé, S.; Gabbaï, F. P., *Chem. Commun.* **2004,** (11), 1284-1285.

(9) Zhao, H.; Gabbaï, F. P., *Organometallics* **2012,** *31* (6), 2327-2335.

(10) Melaïmi, M.; Sole, S.; Chiu, C.-W.; Wang, H.; Gabbaï, F. P., *Inorg. Chem.* **2006,** *45* (20), 8136-8143.

(11) Williams, V. C.; Piers, W. E.; Clegg, W.; Elsegood, M. R. J.; Collins, S.; Marder, T. B., *J. Am. Chem. Soc.* **1999,** *121* (13), 3244-3245.

(12) Lewis, S. P.; Taylor, N. J.; Piers, W. E.; Collins, S., *J. Am. Chem. Soc.* **2003,** *125* (48), 14686-7.

(13) Chai, J.; Lewis, S. P.; Collins, S.; Sciarone, T. J. J.; Henderson, L. D.; Chase, P. A.; Irvine, G. J.; Piers, W. E.; Elsegood, M. R. J.; Clegg, W., *Organometallics* **2007,** *26* (23), 5667-5679.

(14) Day, J. K.; Bresner, C.; Coombs, N. D.; Fallis, I. A.; Ooi, L.-L.; Aldridge, S., *Inorg. Chem.* **2008,** *47* (3), 793-804.

(15) Lee, M. H.; Gabbaï, F. P., *Inorg. Chem.* **2007,** *46* (20), 8132-8138.

(16) Melaïmi, M.; Gabbaï, F. P., *J. Am. Chem. Soc.* **2005,** *127* (27), 9680-9681.

(17) Zhao, H. Y.; Gabbai, F. P., *Nat. Chem.* **2010,** *2* (11), 984-990.

(18) Wade, C. R.; Gabbaï, F. P., *Organometallics* **2011,** *30*, 4479-4481.

(19) Wade, C. R.; Gabbaï, F. P., *Z. Naturforsch. B Chem. Sci.* **2014,** *69* (11-12), 1199-1205.

(20) Hudnall, T. W.; Kim, Y.-M.; Bebbington, M. W. P.; Bourissou, D.; Gabbaï, F. P., *J. Am. Chem. Soc.* **2008,** *130* (33), 10890-10891.

(21) Kim, Y.; Hudnall, T. W.; Bouhadir, G.; Bourissou, D.; Gabbaï, F. P., *Chem. Commun.* **2009**, 3729-3731.

(22) Kim, Y.; Zhao, H.; Gabbaï, F. P., *Angew. Chem. Int. Ed.* **2009,** *48*, 4957-4960.

(23) Ke, I.-S.; Myahkostupov, M.; Castellano, F. N.; Gabbaï, F. P., *J. Am. Chem. Soc.* **2012,** *134* (37), 15309-15311.

(24) Bowen, L. H.; Rood, R. T., *J. Inorg. Nucl. Chem.* **1966,** *28* (9), 1985-1990.

(25) Hall, M.; Sowerby, D. B., *J. Am. Chem. Soc.* **1980,** *102* (2), 628-632.

(26) Robertson, A. P. M.; Burford, N.; McDonald, R.; Ferguson, M. J., *Angew. Chem. Int. Ed.* **2014,** *53* (13), 3480-3483.

(27) Pan, B.; Gabbaï, F. P., *J. Am. Chem. Soc.* **2014,** *136* (27), 9564-9567.

(28) Hirai, M.; Gabbaï, F. P., *Angew. Chem. Int. Ed.* **2015,** *54* (4), 1205-1209.

(29) Chen, P.; Jäkle, F., *J. Am. Chem. Soc.* **2011,** *133* (50), 20142-20145.

(30) Chen, P.; Marshall, A. S.; Chi, S.-H.; Yin, X.; Perry, J. W.; Jäkle, F., *Chem. Eur. J.* **2015,** *21* (50), 18237-18247.

(31) Ashcroft, F. M., *Ion Channels and Disease*. Academic Press: 2000.

(32) Gale, P. A.; Davis, J. T.; Quesada, R., *Chem. Soc. Rev.* **2017,** *46* (9), 2497-2519.

(33) Jung, M. E.; Xia, H., *Tetrahedron Lett.* **1988,** *29* (3), 297-300.

(34) Tschinkl, M.; Schier, A.; Riede, J.; Gabbaï, F. P., *Organometallics* **1999,** *18* (10), 2040-2042.

(35) Tschinkl, M.; Schier, A.; Riede, J.; Gabbaï, F. P., *Organometallics* **1999,** *18* (9), 1747-1753.

(36) Tikhonova, I. A.; Shubina, E. S.; Dolgushin, F. M.; Tugashov, K. I.; Teplitskaya, L. N.; Filin, A. M.; Sivaev, I. B.; Petrovskii, P. V.; Furin, G. G.; Bregadze, V. I.; Epstein, L. M.; Shur, V. B., *Russ. Chem. Bull.* **2003,** *52* (3), 594-600.

(37) Chistyakov, A. L.; Stankevich, I. V.; Gambaryan, N. P.; Tikhonova, I. A.; Shur, V. B., *Russ. Chem. Bull.* **1995,** *44* (6), 997-1004.

(38) Shubina, E. S.; Tikhonova, I. A.; Bakhmutova, E. V.; Dolgushin, F. M.; Antipin, M. Y.; Bakhmutov, V. I.; Sivaev, I. B.; Teplitskaya, L. N.; Chizhevsky, I. T.; Pisareva, I. V.; Bregadze, V. I.; Epstein, L. M.; Shur, V. B., *Chem. Eur. J.* **2001,** *7* (17), 3783-3790.

(39) Tikhonova, I. A.; Tugashov, K. I.; Dolgushin, F. M.; Yakovenko, A. A.; Strunin, B. N.; Petrovskii, P. V.; Furin, G. G.; Shur, V. B., *Inorg. Chim. Acta* **2006,** *359* (9), 2728-2735.

(40) Yan, Z.; Zhou, Z.; Wu, Y.; Tikhonova, I. A.; Shur, V. B., *Anal. Lett.* **2005,** *38* (3), 377-388.

(41) Zaraisky, A. P.; Kachurin, O. I.; Velichko, L. I.; Tikhonova, I. A.; Furin, G. G.; Shur, V. B., *J. Mol. Catal. A: Chem.* **2005,** *231* (1-2), 103-111.

(42) Rothmaier, M.; Simon, W., *Anal. Chim. Acta* **1993,** *271* (1), 135-141.

(43) Dakternieks, D.; Jurkschat, K.; Zhu, H.; Tiekink, E. R. T., *Organometallics* **1995,** *14* (5), 2512-2521.

(44) Altmann, R.; Jurkschat, K.; Schürmann, M.; Dakternieks, D.; Duthie, A., *Organometallics* **1998,** *17* (26), 5858-5866.

(45) Chaniotakis, N.; Jurkschat, K.; Mueller, D.; Perdikaki, K.; Reeske, G., *Eur. J. Inorg. Chem.* **2004,** (11), 2283-2288.

(46) Jentzsch, A. V.; Emery, D.; Mareda, J.; Nayak, S. K.; Metrangolo, P.; Resnati, G.; Sakai, N.; Matile, S., *Nat. Commun.* **2012,** *3*, 905.

(47) Vargas Jentzsch, A.; Emery, D.; Mareda, J.; Metrangolo, P.; Resnati, G.; Matile, S., *Angew. Chem. Int. Ed.* **2011,** *50* (49), 11675-11678.

(48) Benz, S.; Macchione, M.; Verolet, Q.; Mareda, J.; Sakai, N.; Matile, S., *J. Am. Chem. Soc.* **2016,** *138* (29), 9093-9096.

(49) Gilday, L. C.; Robinson, S. W.; Barendt, T. A.; Langton, M. J.; Mullaney, B. R.; Beer, P. D., *Chem. Rev.* **2015,** *115* (15), 7118-7195.

(50) Lu, Y.; Li, H.; Zhu, X.; Zhu, W.; Liu, H., *J. Phys. Chem. A* **2011,** *115* (17), 4467-4475.

(51) Metrangolo, P.; Meyer, F.; Pilati, T.; Resnati, G.; Terraneo, G., *Angew. Chem. Int. Ed.* **2008,** *47* (33), 6114-6127.

(52) Getmanenko, Y. A.; Risko, C.; Tongwa, P.; Kim, E.-G.; Li, H.; Sandhu, B.; Timofeeva, T.; Brédas, J.-L.; Marder, S. R., *J. Org. Chem.* **2011,** *76* (8), 2660-2671.

(53) Garrett, G. E.; Gibson, G. L.; Straus, R. N.; Seferos, D. S.; Taylor, M. S., *J. Am. Chem. Soc.* **2015,** *137* (12), 4126-4133.

(54) Semenov, N. A.; Lonchakov, A. V.; Pushkarevsky, N. A.; Suturina, E. A.; Korolev, V. V.; Lork, E.; Vasiliev, V. G.; Konchenko, S. N.; Beckmann, J.; Gritsan, N. P.; Zibarev, A. V., *Organometallics* **2014,** *33* (16), 4302-4314.

(55) Prakash, G. K. S.; Mathew, T.; Marinez, E. R.; Esteves, P. M.; Rasul, G.; Olah, G. A., *J. Org. Chem.* **2006,** *71* (10), 3952-3958.

(56) Olah, G. A.; Parker, D. G.; Yoneda, N.; Pelizza, F., *J. Am. Chem. Soc.* **1976,** *98* (8), 2245-2250.

(57) Piers, W. E.; Chivers, T., *Chem. Soc. Rev.* **1997,** *26* (5), 345-354.

(58) Jiang, C.; Blacque, O.; Berke, H., *Chem. Commun.* **2009,** (37), 5518-5520.

(59) Kessler, S. N.; Neuburger, M.; Wegner, H. A., *J. Am. Chem. Soc.* **2012,** *134* (43), 17885-17888.

(60) Kessler, S. N.; Neuburger, M.; Wegner, H. A., *Eur. J. Org. Chem.* **2011,** *2011* (17), 3238-3245.

(61) Kessler, S. N.; Wegner, H. A., *Org. Lett.* **2010,** *12* (18), 4062-4065.

(62) Hirai, M.; Cho, J.; Gabbaï, F. P., *Chem. Eur. J.* **2016,** *22* (19), 6537-6541.

(63) Jungbauer, S. H.; Walter, S. M.; Schindler, S.; Rout, L.; Kniep, F.; Huber, S. M., *Chem. Commun.* **2014,** *50* (47), 6281-6284.

(64) Gliese, J.-P.; Jungbauer, S. H.; Huber, S. M., *Chem. Commun.* **2017,** *53* (88), 12052-12055.

(65) Jungbauer, S. H.; Huber, S. M., *J. Am. Chem. Soc.* **2015,** *137* (37), 12110-20.

(66) Kniep, F.; Jungbauer, S. H.; Zhang, Q.; Walter, S. M.; Schindler, S.; Schnapperelle, I.; Herdtweck, E.; Huber, S. M., *Angew. Chem. Int. Ed.* **2013,** *52* (27), 7028-7032.

(67) Wonner, P.; Vogel, L.; Kniep, F.; Huber, S. M., *Chem. Eur. J.* **2017,** *23* (67), 16972-16975.

(68) Jäkle, F., *Chem. Rev.* **2010,** *110* (7), 3985-4022.

(69) Hertz, V. M.; Michael, B.; Hans-Wolfram, L.; Matthias, W., *Angew. Chem. Int. Ed.* **2015,** *54* (30), 8800-8804.

(70) Reus, C.; Weidlich, S.; Bolte, M.; Lerner, H.-W.; Wagner, M., *J. Am. Chem. Soc.* **2013,** *135* (34), 12892-12907.

(71) von Grotthuss, E.; Diefenbach, M.; Bolte, M.; Lerner, H.-W.; Holthausen, M. C.; Wagner, M., *Angew. Chem. Int. Ed.* **2016,** *55* (45), 14067-14071.

(72) Taylor, J. W.; McSkimming, A.; Guzman, C. F.; Harman, W. H., *J. Am. Chem. Soc.* **2017,** *139* (32), 11032-11035.

(73) Caputo, C. B.; Hounjet, L. J.; Dobrovetsky, R.; Stephan, D. W., *Science* **2013,** *341* (6152), 1374-1377.

(74) Holthausen, M. H.; Mehta, M.; Stephan, D. W., *Angew. Chem. Int. Ed.* **2014,** *53* (25), 6538-6541.

(75) Hounjet, L. J.; Caputo, C. B.; Stephan, D. W., *Dalton Trans.* **2013,** *42* (7), 2629-2635.

(76) Holthausen, M. H.; Hiranandani, R. R.; Stephan, D. W., *Chem. Sci.* **2015,** *6* (3), 2016-2021.

(77) Holthausen, M. H.; Bayne, J. M.; Mallov, I.; Dobrovetsky, R.; Stephan, D. W., *J. Am. Chem. Soc.* **2015,** *137* (23), 7298-7301.

(78) Wonner, P.; Vogel, L.; Düser, M.; Gomes, L.; Kniep, F.; Mallick, B.; Werz Daniel, B.; Huber Stefan, M., *Angew. Chem. Int. Ed.* **2017,** *56* (39), 12009-12012.

(79) Walter, S. M.; Kniep, F.; Herdtweck, E.; Huber, S. M., *Angew. Chem. Int. Ed.* **2011,** *50* (31), 7187-7191.

(80) Broomsgrove, A. E. J.; A. Addy, D.; Di Paolo, A.; Morgan, I. R.; Bresner, C.; Chislett, V.; Fallis, I. A.; Thompson, A. L.; Vidovic, D.; Aldridge, S., *Inorg. Chem.* **2010,** *49* (1), 157-173.

(81) Xu, Z.; Chen, X.; Kim, H. N.; Yoon, J., *Chem. Soc. Rev.* **2010,** *39* (1), 127-137.

(82) Hudson, Z. M.; Wang, S., *Dalton Trans.* **2011,** *40* (31), 7805-7816.

(83) Guo, Z.; Shin, I.; Yoon, J., *Chem. Commun.* **2012,** *48*, 5956-5967.

(84) Lamm, J.-H.; Niermeier, P.; Mix, A.; Chmiel, J.; Neumann, B.; Stammler, H.-G.; Mitzel, N. W., *Angew. Chem. Int. Ed.* **2014,** *53* (30), 7938-7942.

(85) Busschaert, N.; Caltagirone, C.; Van Rossom, W.; Gale, P. A., *Chem. Rev.* **2015,** *115* (15), 8038-8155.

(86) Lee, M. H.; Kim, J. S.; Sessler, J. L., *Chem. Soc. Rev.* **2015,** *44* (13), 4185-4191.

(87) Chang, K.-C.; Sun, S.-S.; Odago, M. O.; Lees, A. J., *Coord. Chem. Rev.* **2015,** *284*, 111-123.

(88) Schafer, A. G.; Wieting, J. M.; Fisher, T. J.; Mattson, A. E., *Angew. Chem. Int. Ed.* **2013,** *52* (43), 11321-11324.

(89) Reisman, S. E.; Doyle, A. G.; Jacobsen, E. N., *J. Am. Chem. Soc.* **2008,** *130* (23), 7198-9.

(90) Malerich, J. P.; Hagihara, K.; Rawal, V. H., *J. Am. Chem. Soc.* **2008,** *130* (44), 14416-7.

(91) Lopez, N.; Graham, D. J.; McGuire, R.; Alliger, G. E.; Shao-Horn, Y.; Cummins, C. C.; Nocera, D. G., *Science* **2012,** *335* (6067), 450-453.

(92) Henderson, L. D.; Piers, W. E., *J. Organomet. Chem.* **2007,** *692* (21), 4661-4668.

(93) Olah, G. A.; Baker, E. B.; Evans, J. C.; Tolgyesi, W. S.; McIntyre, J. S.; Bastien, I. J., *J. Am. Chem. Soc.* **1964,** *86* (7), 1360-73.

(94) Jean, M., *Anal. Chim. Acta* **1971,** *57* (2), 438-439.

(95) Robertson, A. P. M.; Gray, P. A.; Burford, N., *Angew. Chem. Int. Ed.* **2014,** *53* (24), 6050-6069.

(96) Hirai, M.; Gabbaï, F. P., *Chem. Sci.* **2014,** *5* (5), 1886-1893.

(97) Robertson, A. P. M.; Chitnis, S. S.; Jenkins, H. A.; McDonald, R.; Ferguson, M. J.; Burford, N., *Chem. Eur. J.* **2015,** *21* (21), 7902-7913.

(98) Bayne, J. M.; Stephan, D. W., *Chem. Soc. Rev.* **2016,** *45* (4), 765-774.

(99) Hirai, M.; Myahkostupov, M.; Castellano, F. N.; Gabbaï, F. P., *Organometallics* **2016,** *35* (11), 1854-1860.

(100) Tan, C.; Wang, P.; Liu, H.; Zhao, X.-L.; Lu, Y.; Liu, Y., *Chem. Commun.* **2015,** *51* (54), 10871-10874.

(101) Li, Y.-Q.; Wang, P.; Liu, H.; Lu, Y.; Zhao, X.-L.; Liu, Y., *Green Chem.* **2016,** *18* (6), 1798-1806.

(102) Arias Ugarte, R.; Devarajan, D.; Mushinski, R. M.; Hudnall, T. W., *Dalton Trans.* **2016,** *45* (27), 11150-11161.

(103) Mehta, M.; Holthausen, M. H.; Mallov, I.; Pérez, M.; Qu, Z.-W.; Grimme, S.; Stephan, D. W., *Angew. Chem. Int. Ed.* **2015,** *54* (28), 8250-8254.

(104) Li, N.; Qiu, R.; Zhang, X.; Chen, Y.; Yin, S.-F.; Xu, X., *Tetrahedron* **2015,** *71* (25), 4275-4281.

(105) Grossman, O.; Azerraf, C.; Gelman, D., *Organometallics* **2006,** *25* (2), 375-381.

(106) Azerraf, C.; Gelman, D., *Organometallics* **2009,** *28* (22), 6578-6584.

(107) Tauchert, M. E.; Warth, D. C. M.; Braun, S. M.; Gruber, I.; Ziesak, A.; Rominger, F.; Hofmann, P., *Organometallics* **2011,** *30* (10), 2790-2809.

(108) Smith, S. E.; Rosendahl, T.; Hofmann, P., *Organometallics* **2011,** *30* (13), 3643-3651.

(109) Musa, S.; Shpruhman, A.; Gelman, D., *J. Organomet. Chem.* **2012,** *699* (0), 92-95.

(110) Silantyev, G. A.; Filippov, O. A.; Musa, S.; Gelman, D.; Belkova, N. V.; Weisz, K.; Epstein, L. M.; Shubina, E. S., *Organometallics* **2014,** *33* (21), 5964-5973.

(111) Bézier, D.; Brookhart, M., *ACS Catal.* **2014,** *4* (10), 3411-3420.

(112) Chiu, C.-W.; Gabbaï, F. P., *J. Am. Chem. Soc.* **2006,** *128* (44), 14248-14249.

(113) Schneider, H.-J., *Chem. Sci.* **2012,** *3* (5), 1381-1394.

(114) Wang, L.; Zhao, L.; Hu, Y.; Wang, W.; Chen, R.; Yang, Y., *CrystEngComm* **2013,** *15* (15), 2835-2852.

(115) Loader, J. R.; Libri, S.; Meijer, A. J. H. M.; Perutz, R. N.; Brammer, L., *CrystEngComm* **2014,** *16* (41), 9711-9720.

(116) Addison, A. W.; Rao, T. N.; Reedijk, J.; van Rijn, J.; Verschoor, G. C., *J. Chem. Soc., Dalton Trans.* **1984,** (7), 1349-1356.

(117) Isaev, A. N., *Russ. J. Phys. Chem. A* **2016,** *90* (3), 601-609.

(118) Kolandaivel, P.; Nirmala, V., *J. Mol. Struct.* **2004,** *694* (1-3), 33-38.

(119) Timoshkin, A. Y.; Frenking, G., *Organometallics* **2008,** *27* (3), 371-380.

(120) Krossing, I.; Raabe, I., *Chem. Eur. J.* **2004,** *10* (20), 5017-5030.

(121) Zhao, H.; Reibenspies, J. H.; Gabbaï, F. P., *Dalton Trans.* **2013,** *42* (3), 608-610.

(122) Manson, J.; Webster, C. E.; Pérez, L. M.; Hall, M. B., http://www.chem.tamu.edu/jimp2/index.html.

(123) Peterson, K. A., *J. Chem. Phys.* **2003,** *119* (21), 11099-11112.

(124) Metz, B.; Stoll, H.; Dolg, M., *J. Chem. Phys.* **2000,** *113* (7), 2563-2569.

(125) Bowman-James, K.; Bianchi, A.; Garcia-Espana, E.; Editors, *Anion Coordination Chemistry*. Wiley-VCH Verlag GmbH & Co. KGaA: 2012; p 559 pp.

(126) Zhou, Y.; Zhang, J. F.; Yoon, J., *Chem. Rev.* **2014,** *114* (10), 5511-5571.

(127) Gale, P. A.; Howe, E. N. W.; Wu, X., *Chem* **2016,** *1* (3), 351-422.

(128) Molina, P.; Zapata, F.; Caballero, A., *Chem. Rev.* **2017,** *117* (15), 9907-9972.

(129) Zhang, Z.; Schreiner, P. R., *Chem. Soc. Rev.* **2009,** *38* (4), 1187-1198.

(130) Phipps, R. J.; Hamilton, G. L.; Toste, F. D., *Nat. Chem.* **2012,** *4* (8), 603-614.

(131) Beckendorf, S.; Asmus, S.; Mancheño, O. G., *ChemCatChem* **2012,** *4* (7), 926-936.

(132) Brak, K.; Jacobsen, E. N., *Angew. Chem. Int. Ed.* **2013,** *52* (2), 534-561.

(133) Nava, M.; Lopez, N.; Müller, P.; Wu, G.; Nocera, D. G.; Cummins, C. C., *J. Am. Chem. Soc.* **2015,** *137* (46), 14562-14565.

(134) Kim, D. W.; Ahn, D. S.; Oh, Y. H.; Lee, S.; Kil, H. S.; Oh, S. J.; Lee, S. J.; Kim, J. S.; Ryu, J. S.; Moon, D. H.; Chi, D. Y., *J. Am. Chem. Soc.* **2006,** *128* (50), 16394-16397.

(135) Kim, D. W.; Jeong, H.-J.; Lim, S. T.; Sohn, M.-H., *Angew. Chem. Int. Ed.* **2008,** *47* (44), 8404-8406.

(136) Kim, D. W.; Jeong; Lim, S. T.; Sohn, M.-H.; Katzenellenbogen, J. A.; Chi, D. Y., *J. Org. Chem.* **2008,** *73* (3), 957-962.

(137) Engle, K. M.; Pfeifer, L.; Pidgeon, G. W.; Giuffredi, G. T.; Thompson, A. L.; Paton, R. S.; Brown, J. M.; Gouverneur, V., *Chem. Sci.* **2015,** *6* (9), 5293-5302.

(138) Carvalho, N. F.; Pliego, J. R., *J. Org. Chem.* **2016,** *81* (18), 8455-8463.

(139) Jadhav, V. H.; Choi, W.; Lee, S.-S.; Lee, S.; Kim, D. W., *Chem. Eur. J.* **2016,** *22* (13), 4515-4520.

(140) Yamamura, M.; Kondo, S.-i.; Unno, M., *Tetrahedron Lett.* **2014,** *55* (3), 646-649.

(141) Diemoz, K. M.; Wilson, S. O.; Franz, A. K., *Chem. Eur. J.* **2016,** *22* (51), 18349-18353.

(142) Gillespie, R. J.; Johnson, S. A., *Inorg. Chem.* **1997,** *36* (14), 3031-3039.

(143) Chandrasekhar, V.; Boomishankar, R.; Nagendran, S., *Chem. Rev.* **2004,** *104* (12), 5847-5910.

(144) Grabowsky, S.; Hesse, M. F.; Paulmann, C.; Luger, P.; Beckmann, J., *Inorg. Chem.* **2009,** *48* (10), 4384-4393.

(145) Weinhold, F.; West, R., *Organometallics* **2011,** *30* (21), 5815-5824.

(146) Weinhold, F.; West, R., *J. Am. Chem. Soc.* **2013,** *135* (15), 5762-5767.

(147) Vidovic, D.; Moore, J. A.; Jones, J. N.; Cowley, A. H., *J. Am. Chem. Soc.* **2005,** *127* (13), 4566-4567.

(148) Bettinger, H. F., *Organometallics* **2007,** *26* (25), 6263-6267.

(149) Braunschweig, H.; Radacki, K.; Schneider, A., *Science* **2010,** *328* (5976), 345-347.

(150) Wang, Y.; Hu, H.; Zhang, J.; Cui, C., *Angew. Chem. Int. Ed.* **2011,** *50* (12), 2816-2819.

(151) Solovyev, A.; Geib, S. J.; Lacôte, E.; Curran, D. P., *Organometallics* **2012,** *31* (1), 54-56.

(152) Del Grosso, A.; Clark, E. R.; Montoute, N.; Ingleson, M. J., *Chem. Commun.* **2012,** *48* (61), 7589-7591.

(153) Miyada, T.; Yamashita, M., *Organometallics* **2013,** *32* (19), 5281-5284.

(154) Loh, Y. K.; Chong, C. C.; Ganguly, R.; Li, Y.; Vidovic, D.; Kinjo, R., *Chem. Commun.* **2014,** *50* (62), 8561-8564.

(155) Franz, D.; Inoue, S., *Dalton Trans.* **2016,** *45* (23), 9385-9397.

(156) Swarnakar, A. K.; Hering-Junghans, C.; Ferguson, M. J.; McDonald, R.; Rivard, E., *Chem. Eur. J.* **2017,** *23* (36), 8628-8631.

(157) Son, J.-H.; Pudenz, M. A.; Hoefelmeyer, J. D., *Dalton Trans.* **2010,** *39* (45), 11081-11090.

(158) Heiden, Z. M.; Schedler, M.; Stephan, D. W., *Inorg. Chem.* **2011,** *50* (4), 1470-1479.

(159) Siewert, I.; Vidovic, D.; Aldridge, S., *J. Organomet. Chem.* **2011,** *696* (13), 2528-2532.

(160) Chen, J.; Lalancette, R. A.; Jäkle, F., *Chem. Eur. J.* **2014,** *20* (29), 9120-9129.

(161) Tsurusaki, A.; Sasamori, T.; Tokitoh, N., *Chem. Eur. J.* **2014,** *20* (13), 3752-3758.

(162) Pla, D.; Sadek, O.; Cadet, S.; Mestre-Voegtle, B.; Gras, E., *Dalton Trans.* **2015,** *44* (42), 18340-18346.

(163) Chansaenpak, K.; Wang, M.; Wu, Z.; Zaman, R.; Li, Z.; Gabbaï, F. P., *Chem. Commun.* **2015,** *51* (62), 12439-42.

(164) Chen, C.-H.; Gabbaï, F. P., *Angew. Chem. Int. Ed.* **2017,** *56* (7), 1799-1804.

(165) Kilyanek, S. M.; Fang, X.; Jordan, R. F., *Organometallics* **2009,** *28* (1), 300-305.

(166) Cummings, S. A.; Iimura, M.; Harlan, C. J.; Kwaan, R. J.; Trieu, I. V.; Norton, J. R.; Bridgewater, B. M.; Jäkle, F.; Sundararaman, A.; Tilset, M., *Organometallics* **2006,** *25* (7), 1565-1568.

(167) Kirschner, S.; Mewes, J.-M.; Bolte, M.; Lerner, H.-W.; Dreuw, A.; Wagner, M., *Chem. Eur. J.* **2017,** *23* (21), 5104-5116.

(168) Moebs-Sanchez, S.; Saffon, N.; Bouhadir, G.; Maron, L.; Bourissou, D., *Dalton Trans.* **2010,** *39* (18), 4417-4420.

(169) Chen, E. Y.-X.; Marks, T. J., *Chem. Rev.* **2000,** *100* (4), 1391-1434.

(170) Yamaguchi, S.; Akiyama, S.; Tamao, K., *J. Organomet. Chem.* **2002,** *652* (1-2), 3-9.

(171) Piers, W. E., *Adv. Organomet. Chem.* **2004,** *52*, 1-76.

(172) Entwistle, C. D.; Marder, T. B., *Chem. Mater.* **2004,** *16* (23), 4574-4585.

(173) Melaïmi, M.; Gabbaï, F. P., *Adv. Organomet. Chem.* **2005,** *53*, 61-99.

(174) Jäkle, F., *Coord. Chem. Rev.* **2006,** *250*, 1107-1121.

(175) Hudson, Z. M.; Wang, S., *Acc. Chem. Res.* **2009,** *42*, 1584-1596.

(176) Stephan, D. W., *Acc. Chem. Res.* **2015,** *48* (2), 306-316.

(177) Cardenas, A. J. P.; Hasegawa, Y.; Kehr, G.; Warren, T. H.; Erker, G., *Coord. Chem. Rev.* **2016,** *306, Part 2*, 468-482.

(178) Yamaguchi, S.; Akiyama, S.; Tamao, K., *J. Am. Chem. Soc.* **2000,** *122* (26), 6335-6336.

(179) Grenie, Y.; Cornut, J.-C.; Lassegues, J.-C., *J. Chem. Phys.* **1971,** *55* (12), 5844-5846.

(180) Bresner, C.; Aldridge, S.; Fallis, I. A.; Jones, C.; Ooi, L.-L., *Angew. Chem. Int. Ed.* **2005,** *44* (23), 3606-3609.

(181) Kubo, Y.; Ishida, T.; Minami, T.; James, T. D., *Chem. Lett.* **2006,** *35* (9), 996-997.

(182) Hudnall, T. W.; Melaïmi, M.; Gabbaï, F. P., *Org. Lett.* **2006,** *8* (13), 2747-2749.

(183) Swamy, K. M. K.; Lee, Y. J.; Lee, H. N.; Chun, J.; Kim, Y.; Kim, S.-J.; Yoon, J., *J. Org. Chem.* **2006,** *71* (22), 8626-8628.

(184) Xu, Z.; Kim, S. K.; Han, S. J.; Lee, C.; Kociok-Kohn, G.; James, T. D.; Yoon, J., *Eur. J. Org. Chem.* **2009,** *2009* (18), 3058-3065.

(185) Bader, R. F. W., *Atoms in Molecules: A Quantum Theory*. Clarendon Press: Oxford, 1994; p 438 pp.

(186) Reed, A. E.; Weinhold, F.; Curtiss, L. A.; Pochatko, D. J., *J. Chem. Phys.* **1986,** *84* (10), 5687-5705.

(187) Chegini, H.; Ali Beyramabadi, S.; Morsali, A.; Saberi, M.; Lotfi, M., *J. Mol. Struct.* **2015,** *1083*, 1-9.

(188) Keith, T. A. *AIMAll (Version 14.06.21)*, TK Gristmill Software: Overland Park KS, USA, 2014.

(189) Gale, P. A.; Howe, E. N. W.; Wu, X.; Spooner, M. J., *Coord. Chem. Rev.* **2018**.

(190) Badr, I. H. A.; Diaz, M.; Hawthorne, M. F.; Bachas, L. G., *Anal. Chem.* **1999,** *71* (7), 1371-1377.

(191) Benz, S.; López-Andarias, J.; Mareda, J.; Sakai, N.; Matile, S., *Angew. Chem. Int. Ed.* **2017,** *56* (3), 812-815.

(192) Wang, L.; Zhang, S.; Hasegawa, Y.; Daniliuc, C. G.; Kehr, G.; Erker, G., *Chem. Commun.* **2017,** *53* (40), 5499-5502.

(193) Benz, S.; Mareda, J.; Besnard, C.; Sakai, N.; Matile, S., *Chem. Sci.* **2017,** *8* (12), 8164-8169.

(194) Chen, D.; Xu, G.; Zhou, Q.; Chung, L. W.; Tang, W., *J. Am. Chem. Soc.* **2017,** *139* (29), 9767-9770.

(195) Katz, H. E., *Organometallics* **1987,** *6* (5), 1134-1136.

(196) Reilly, M.; Oh, T., *Tetrahedron Lett.* **1994,** *35* (39), 7209-7212.

(197) Metz, M. V.; Schwartz, D. J.; Stern, C. L.; Nickias, P. N.; Marks, T. J., *Angew. Chem. Int. Ed.* **2000,** *39* (7), 1312-1316.

(198) Williams, V. C.; Irvine, G. J.; Piers, W. E.; Li, Z.; Collins, S.; Clegg, W.; Elsegood, M. R. J.; Marder, T. B., *Organometallics* **2000,** *19* (9), 1619-1621.

(199) Schweighauser, L.; Wegner, H. A., *Chem. Eur. J.* **2016,** *22* (40), 14094-14103.

(200) Emslie, D. J. H.; Piers, W. E.; Parvez, M., *Angew. Chem. Int. Ed.* **2003,** *42* (11), 1252-1255.

(201) Kiernicki, J. J.; Zeller, M.; Szymczak, N. K., *J. Am. Chem. Soc.* **2017,** *139* (50), 18194-18197.

(202) Dahl, E. W.; Dong, H. T.; Szymczak, N. K., *Chem. Commun.* **2018,** *54* (8), 892-895.

(203) Chen, C.-H.; Gabbaï, F. P., *Angew. Chem. Int. Ed.* **2018,** *57* (2), 521-525.

(204) Hoefelmeyer, J. D.; Gabbaï, F. P., *J. Am. Chem. Soc.* **2000,** *122* (37), 9054-9055.

(205) Hoefelmeyer, J. D.; Solé, S.; Gabbaï, F. P., *Dalton Trans.* **2004,** (8), 1254-1258.

(206) Parab, K.; Venkatasubbaiah, K.; Jäkle, F., *J. Am. Chem. Soc.* **2006,** *128* (39), 12879-12885.

(207) Yamaguchi, S.; Wakamiya, A., *Pure Appl. Chem.* **2006,** *78* (7), 1413-1424.

(208) Brazeau, A. L.; Yuan, K.; Ko, S.-B.; Wyman, I.; Wang, S., *ACS Omega* **2017,** *2* (12), 8625-8632.

(209) Matsumoto, T.; Wade, C. R.; Gabbaï, F. P., *Organometallics* **2010,** *29* (21), 5490-5495.

(210) Song, K. C.; Lee, K. M.; Nghia, N. V.; Sung, W. Y.; Do, Y.; Lee, M. H., *Organometallics* **2013,** *32* (3), 817-823.

(211) Liu, Z.; He, W.; Guo, Z., *Chem. Soc. Rev.* **2013,** *42* (4), 1568-1600.

(212) Wang, F.; Wang, L.; Chen, X.; Yoon, J., *Chem. Soc. Rev.* **2014,** *43* (13), 4312-4324.

(213) Ashton, T. D.; Jolliffe, K. A.; Pfeffer, F. M., *Chem. Soc. Rev.* **2015,** *44* (14), 4547-4595.

(214) Hudnall, T. W.; Gabbaï, F. P., *J. Am. Chem. Soc.* **2007,** *129* (39), 11978-11986.

(215) Chiu, C.-W.; Gabbaï, F. P., *Dalton Trans.* **2008,** (6), 814-817.

(216) Chiu, C.-W.; Kim, Y.; Gabbaï, F. P., *J. Am. Chem. Soc.* **2009,** *131* (1), 60-61.

(217) Wade, C. R.; Gabbaï, F. P., *Inorg. Chem.* **2010,** *49* (2), 714-720.

(218) Kim, Y.; Huh, H.-S.; Lee, M. H.; Lenov, I. L.; Zhao, H.; Gabbaï, F. P., *Chem. Eur. J.* **2011,** *17* (7), 2057-2062.

(219) Shriver, D. F.; Posner, J., *J. Am. Chem. Soc.* **1966,** *88* (8), 1672-1677.

(220) Ahlers, B.; Cammann, K.; Warzeska, S.; Krämer, R., *Angew. Chem. Int. Ed.* **1996,** *35* (18), 2141-2143.

(221) Warzeska, S.; Krämer, R., *Chem. Commun.* **1996,** (4), 499-500.

(222) Giandomenico, C. M.; Dewan, J. C.; Lippard, S. J., *J. Am. Chem. Soc.* **1981,** *103* (6), 1407-1412.

(223) J. Lancaster, S.; A. Walker, D.; Thornton-Pett, M.; Bochmann, M., *Chem. Commun.* **1999,** (16), 1533-1534.

(224) Zhou, J.; Lancaster, S. J.; Walker, D. A.; Beck, S.; Thornton-Pett, M.; Bochmann, M., *J. Am. Chem. Soc.* **2001,** *123* (2), 223-237.

(225) Brunkan, N. M.; Brestensky, D. M.; Jones, W. D., *J. Am. Chem. Soc.* **2004,** *126* (11), 3627-3641.

(226) Bergquist, C.; Bridgewater, B. M.; Harlan, C. J.; Norton, J. R.; Friesner, R. A.; Parkin, G., *J. Am. Chem. Soc.* **2000,** *122* (43), 10581-10590.

(227) Pylypko, S.; Petit, E.; Yot, P. G.; Salles, F.; Cretin, M.; Miele, P.; Demirci, U. B., *Inorg. Chem.* **2015,** *54* (9), 4574-4583.

(228) Qi, G.; Wang, K.; Yang, K.; Zou, B., *J. Phys. Chem. C* **2016,** *120* (38), 21293-21298.

(229) Yu, Y.; Brennessel, W. W.; Holland, P. L., *Organometallics* **2007,** *26* (13), 3217-3226.

(230) Lee, Y.; Mankad, N. P.; Peters, J. C., *Nat. Chem.* **2010,** *2*, 558-565.

(231) Saouma, C. T.; Lu, C. C.; Peters, J. C., *Inorg. Chem.* **2012,** *51* (18), 10043-54.

(232) Umehara, K.; Kuwata, S.; Ikariya, T., *J. Am. Chem. Soc.* **2013,** *135* (18), 6754-6757.

(233) Li, Y.; Li, Y.; Wang, B.; Luo, Y.; Yang, D.; Tong, P.; Zhao, J.; Luo, L.; Zhou, Y.; Chen, S.; Cheng, F.; Qu, J., *Nat. Chem.* **2013,** *5*, 320-326.

(234) Roy, B.; Bandyopadhyay, S., *Anal. Methods* **2018,** *10* (10), 1117-1139.

(235) Henthorn, J. T.; Agapie, T., *Angew. Chem. Int. Ed.* **2014,** *53* (47), 12893-12896.

(236) Tao, X.; Daniliuc, C. G.; Janka, O.; Pöttgen, R.; Knitsch, R.; Hansen, M. R.; Eckert, H.; Lübbesmeyer, M.; Studer, A.; Kehr, G.; Erker, G., *Angew. Chem. Int. Ed.* **2017,** *56* (52), 16641-16644.

(237) Mebs, S.; Grabowsky, S.; Förster, D.; Kickbusch, R.; Hartl, M.; Daemen, L. L.; Morgenroth, W.; Luger, P.; Paulus, B.; Lentz, D., *J. Phys. Chem. A* **2010,** *114* (37), 10185-10196.

(238) Kohata, K.; Fukuyama, T.; Kuchitsu, K., *J. Phys. Chem.* **1982,** *86* (5), 602-606.

(239) Leusmann, E.; Schneck, F.; Dehnen, S., *Organometallics* **2015,** *34* (13), 3264-3271.

(240) Piers, W. E.; Irvine, G. J.; Williams, V. C., *Eur. J. Inorg. Chem.* **2000,** *2000* (10), 2131-2142.

(241) Wang, H.; Gabbaï, F. P., *Angew. Chem. Int. Ed.* **2004,** *43* (2), 184-187.

(242) Christianson, A. M.; Gabbaï, F. P., *Chem. Commun.* **2017,** *53* (16), 2471-2474.

(243) Würth, C.; Grabolle, M.; Pauli, J.; Spieles, M.; Resch-Genger, U., *Nat. Protoc.* **2013,** *8*, 1535.

(244) Spek, A., *Acta Cryst. C* **2015,** *71* (1), 9-18.

(245) Kather, R.; Svoboda, T.; Wehrhahn, M.; Rychagova, E.; Lork, E.; Dostal, L.; Ketkov, S.; Beckmann, J., *Chem. Commun.* **2015,** *51* (27), 5932-5935.

APPENDIX

VITA

Chang-Hong Chen
Advisor: François P. Gabbaï
Department of Chemistry
Texas A&M University
College Station, TX

EDUCATION

- Ph. D., Chemistry, Texas A&M University, College Station, Texas August 2018
- M. Sc., Chemistry, National Taiwan University, Taipei, Taiwan, June 2011
- B. Sc., Chemistry, National Taiwan University, Taipei, Taiwan, June 2009

HONORS/AWARDS

- 2018 Dow Chemical Scholar Award
- 2017 A. E. Martell Graduate Student Enrichment Fund Travel Award in Chemistry
- 2017 Invited Speaker of Physical Organic Chemistry Gordon Research Seminar

PUBLICATIONS

1. Chang-Hong Chen, François P. Gabbaï, "Large-bite diboranes for the μ(1,2) complexation of hydrazine and cyanide", *Chem.Sci*. **2018,** *in press.*
2. Chang-Hong Chen, François P. Gabbaï, "Exploiting the Strong Hydrogen Bond Donor Properties of a Borinic Acid Functionality for Fluoride Anion Recognition", *Angew. Chem. Int. Ed.* **2018,** *57,* 521.
3. Chang-Hong Chen, François P. Gabbaï, "Fluoride Anion Complexation by a Triptycene-Based Distiborane: Taking Advantage of a Weak but Observable C−H···F Interaction", *Angew. Chem. Int. Ed.* **2017,** *56,* 1799.
4. Chang-Hong Chen, Yi-Hung Liu, Shie-Ming Peng, Jwu-Ting Chen and Shiuh-Tzung Liu, "Synthesis of N-heterocyclic carbene rhenium(I) carbonyl complexes", *Dalton Trans.,* **2012,** *41,* 2747.
5. Shiuh-Tzung Liu, Chun-I Lee, Ching-Feng Fu, Chang-Hong Chen, Yi-Hung Liu, Cornelis J. Elsevier, Shei-Ming Peng, and Jwu-Ting Chen, "N-Heterocyclic Carbene Transfer from Gold(I) to Palladium(II)", *Organometallics,* **2009,** *28,* 6957.